# A COMPUTATIONAL AND SYNTHETIC STUDY OF POLY(BENZYL PHENYL ETHER) DENDRIMERS

A thesis submitted to the

**UNIVERSITY OF CAPE TOWN**

in fulfillment of the requirements for the degree of

**MASTER OF SCIENCE**



by

**SAMANTHA JAYNE HUGHES**

**B.Sc. (HONS.)**

Department of Chemistry

University of Cape Town

Rondebosch 7701

South Africa

March 1998

# ACKNOWLEDGEMENTS

My sincere thanks and appreciation are extended to:

My supervisors, Prof. John R. Moss and Dr Kevin J. Naidoo, for their advice, encouragement, interest and enthusiasm throughout the entire project.

Dr Pieter de Koning, for countless helpful discussions and advice, and also for proof-reading this thesis.

My family and close friends for their support and shelter during the last month of the thesis preparation.

AECI and the FRD for financial support.

Mrs. Karol Cameron, my mentor at AECI R&DD, for her invaluable advice and interest in the project.

Dr Susan Bourne and Dr Anita Coetzee for their time and advice on crystallographic issues.

Friends and colleagues past and present, from the Organometallic research group, especially Paul Galatolo, Fiona Hess, Meredith Hearshaw, Oliver Hill, Jacques Marè, Reinout Meijboom, Earl Starr and Xiaolong Yin for their input during this project.

Dr Alan Hutton, for attending many presentations, and giving helpful advice.

Dr Bette Davidowitz, for her efficient ordering of laboratory supplies.

Dr Anita Coetzee (UCT), Prof. Judith Howard, Dr Christian Lehmann and Janet Kelly (all Durham University) for the crystal structure determinations.

# ACKNOWLEDGEMENTS

Dr Krassi Dimitrova and Mr. Noel Hendricks for recording the NMR spectra.

Mr. Piero Benincasa for the microanalyses and recording the EI mass spectra.

Dr Phillip Boschoff (Cape Technikon) for the FAB and EI mass spectra.

# ABSTRACT

Organic and organochromium poly(benzyl phenyl ether) dendrimers have been investigated by synthetic and computational methods. The first generation organic benzyl alcohol and bromide wedges have been prepared, and a first generation organic dendrimer was synthesised. The preparation of novel organochromium dendrimers has been investigated. Several chromium arene complexes were prepared by different routes, and the halogenation methodology was thoroughly explored with various reagents. The target compound, a chromium complexed first generation dendritic wedge, was not accessible by any of the methods investigated. The novel compound (dibenzyl ether)bis[tricarbonylchromium(0)] has been prepared by two routes and the crystal structure of this complex was determined. Several other chromium arene complexes were synthesised, and the crystal structure of one of these, (benzyl methyl ether)tricarbonylchromium(0), was determined.

The structure and properties of the organic and organochromium dendrimers have been investigated by molecular mechanics and molecular dynamics techniques. The existing CHARMm polymer force field was extended to include parameters for the tricarbonylchromium moiety. The two crystal structures solved as part of the synthetic effort, were used in this regard. The accuracy of the new parameters was assessed by simulation of the crystal structure of (dibenzyl ether)bis[tricarbonylchromium(0)]. The important ether linkage torsion angle parameter, which plays a significant role in the topology of the dendrimer, was singled out for refinement. The torsion angle was parameterised with the model compound benzyl phenyl ether, by fitting the CHARMm results for rotation about the dihedral, to *ab initio* torsional data.

Molecular dynamics simulations have been performed on generations one through five of the organic and organochromium dendrimers. The radius of gyration and RMS variation were investigated as a function of generation for both dendrimer series. The radius of gyration was found to increase exponentially with generation, whereas the relationship of RMS variation to generation was not as

well defined. Density distributions were calculated for all five generations of the organic and organometallic dendrimers. In addition, the distribution of the monomers from each generation within the dendrimer was analysed. In the later generation dendrimers, the monomers belonging to the earlier generations are extended, while the terminal groups are mobile and found in all regions of the dendrimer. The solvent accessible surface was calculated for the organochromium dendrimers. It was concluded from these results that although the terminal groups are mobile, the majority of these monomers remain on the periphery of the dendrimer, or in solvent accessible areas.

# PRESENTATIONS

Parts of this work have been presented as oral presentations or in poster form at:

- Inorganic '97, held in Port Elizabeth, South Africa, January 1997
- AECI Postgraduate Research Seminar, held at AECI R&DD, South Africa, October 1997

Parts of this work have been accepted for presentation at :

- The 33$^{rd}$ International Conference in Co-ordination Chemistry, Italy, August 1998
- The 34$^{th}$ SACI Convention/7$^{th}$ International Conference on Chemistry in Africa, Durban, South Africa, July 1998

# LIST OF ABBREVIATIONS

| | |
|---|---|
| Å | angstrom |
| CHARMm | Chemistry at Harvard Macromolecular mechanics |
| CI-MS | chemical ionisation mass spectroscopy |
| CORE | 1,1,1-tris(4´-hydroxyphenyl)ethane |
| COSY | correlation spectroscopy |
| CSD | Cambridge structural database |
| FAB-MS | fast atom bombardment mass spectroscopy |
| FT-IR | fourier transform infra-red |
| HMQC | heteronuclear multiple quantum coherence |
| IR | infra-red |
| LALLS | low-angle laser light scattering |
| MALDI-TOF | matrix assisted laser desorption ionisation time of flight |
| mp | melting point |
| MS | mass spectrum |
| NMR | nuclear magnetic resonance |
| NVE | microcanonical ensemble |
| NVT | canonical ensemble |
| PAMAM | poly(amidoamine) |
| RMS | root mean square |
| SAS | solvent accessible surface |
| SEC | size exclusion chromatography |
| SCF | self-consistent fields |

# TABLE OF CONTENTS

**Note: References are valid with each individual chapter only**

# Chapter 1 An introduction to dendrimers

Beauty, symmetry and control – these reasons are why, as chemists, we are so intrigued by dendrimers. These highly branched, beautifully symmetrical molecules appeal to the aesthete in all of us, while through the use of well designed synthetic strategies, we can control their growth and morphologies. In addition to their pleasing forms, dendrimers are expected to have a wide range of applications, from medicinal use as drug carriers and medical diagnostics, to industrial application as catalysts, adhesives and coatings. [1,2] This is undoubtedly why, in a relatively short time, dendrimers have become such a popular topic in the scientific literature. In fact, some of these applications have been demonstrated recently, justifying the enthusiasm of the researchers in this field. [2,3]

The term "dendrimers" is derived from the term "dendritic", meaning treelike and "oligomer" which is essentially what these molecules are – treelike branched analogues of the traditional linear polymers. Other names applied to dendrimers are equally descriptive – "arborols" which is derived from the Latin for tree, and "starburst dendrimer". [4] Figure 1.1 shows several examples of these fascinating macromolecules.

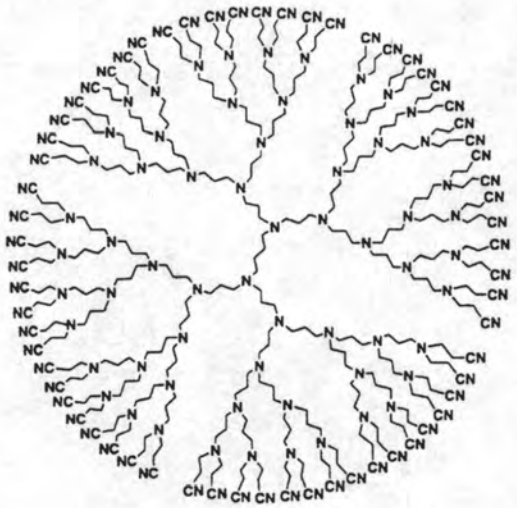

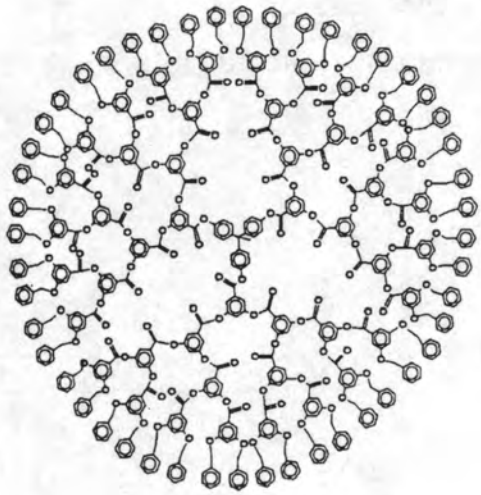

**Figure 1.1**

a) A poly(propylene imine) dendrimer b) A dendritic polyester

**General Synthetic Routes**

The "cascade synthesis" concept - assembling branches upon branches by an iterative protection/deprotection technique – was introduced somewhat quietly by Vögtle *et al* in 1978, [5] but the technique was well developed by Tomalia and co-workers from 1979 to produce, to date, a range of structurally controlled dendrimers. [4] The key constituents of these macromolecules are: a central core molecule, the repeating branched monomers and the terminal groups. The flexibility in the choice of these components allows a host of dendritic molecules to be synthesised, and this is precisely what has occurred. The most widely used of these are the poly(amidoamine) or "PAMAM" dendrimers and the poly(propylene imine) class of dendrimers, both of which are commercially available. [6]

A typical synthesis of such dendrimers begins at the chosen initiator core molecule, which couples with several suitably protected branching monomers, to give a zero generation oligomer or "core cell". The protective groups are then removed to allow further coupling with more branching monomers, to give the first generation dendrimer, having gone through one generation of growth. This process is repeated successively to build up larger generations of dendrimers. This method of synthesis has been termed the "divergent" approach and a schematic diagram of this is shown in Scheme 1.1. [4,7] Scheme 1.2 illustrates the use of the divergent approach for the synthesis of a PAMAM dendrimer. Tomalia has also extensively investigated other aspects of these macromolecules, including their structures, properties and uses, [4,7] and is undoubtedly a leading figure in this field.

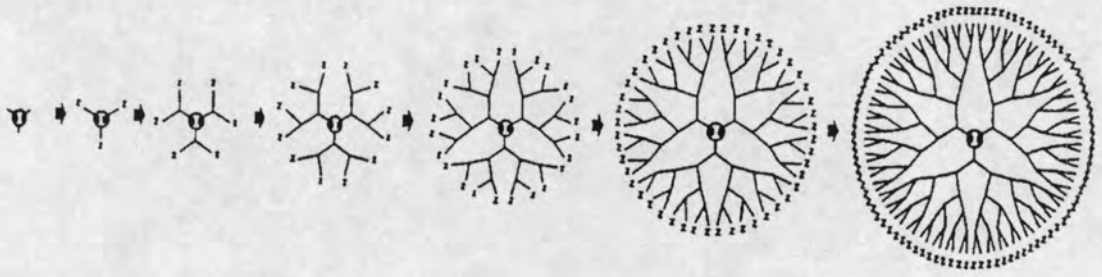

**Scheme 1.1:** A general scheme for dendrimer synthesis via the divergent approach. "I" refers to the initiator core, and "Z" indicates a surface group. [4,7]

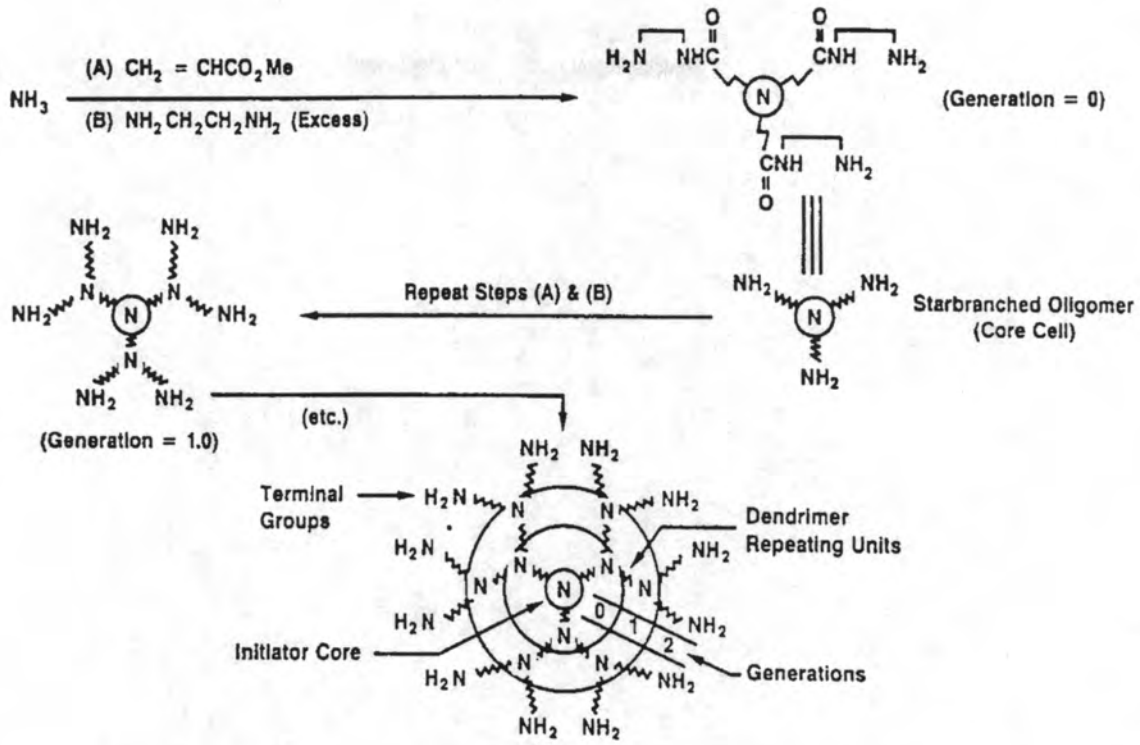


**Scheme 1.2**: The divergent synthesis of a PAMAM dendrimer. [4,7]

Other researchers entered the arena a few years after Tomalia, including Denkewalter *et al* with unsymmetrical dendritic molecules and then Newkome and co-workers with their structurally uncontrolled but highly branched "arborols". [4] Later, researchers Hawker and Fréchet reported several syntheses of poly(benzyl phenyl ether) and related dendrimers, [8] which are also well defined, highly regular branched polymers - see Figure 1.2 for an example of a poly(benzyl phenyl ether) dendrimer.

Interestingly, their approach toward building these molecules was not the "cascade synthesis" or divergent approach utilised by the others up until this point, but was conceptually the reverse. Instead of building the dendrimers from the core outward – they started the synthesis at the periphery of the molecule and built inwards to form a dendritic "wedge", several of which are coupled to the core molecule to form the complete dendrimer. This technique has been termed the "convergent" approach for dendrimer synthesis and was reported by both the Hawker/Fréchet group and Neenan and Miller, [4] almost simultaneously. [9] A schematic of the convergent strategy is shown in Scheme 1.3.

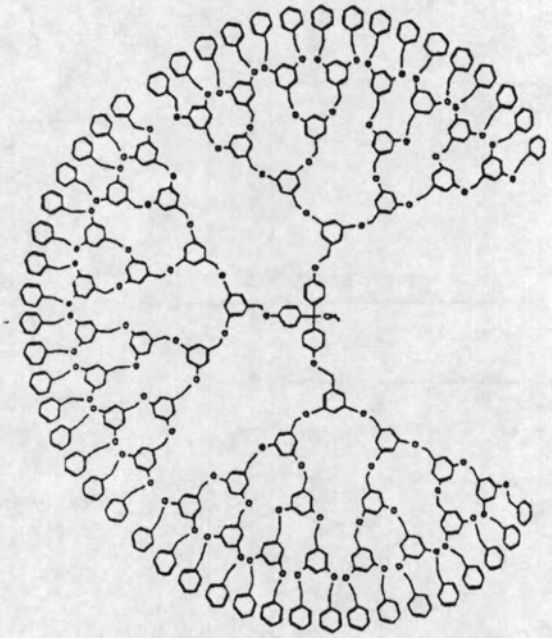

**Figure 1.2**: A poly(benzyl phenyl ether) dendrimer.

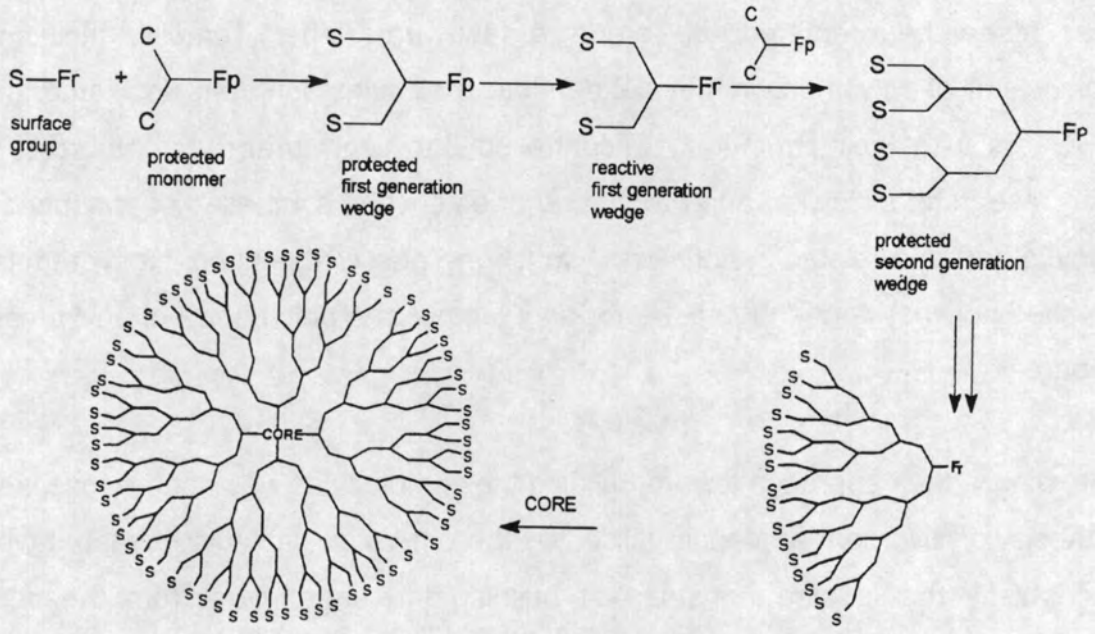


**Scheme 1.3**: A schematic of the convergent approach for dendrimer synthesis.

S = surface group Fp = protected functionality

C = interior group Fr = reactive functionality

This new convergent approach has several advantages over the divergent synthetic strategy. Divergent syntheses require larger excesses of reagents to build the later generations, in order to avoid imperfect growth at the periphery. In the convergent approach, growth reactions are performed on wedges, which are less sterically hindered than the full dendrimer, and so smaller excesses are required to force the reaction to completion. The convergent approach also allows for the incorporation of different wedges, thus enabling the formation of block co-polymers. [10] Surface groups are easily modified or incorporated precisely as desired in this strategy. The approach is limited however, in the size of macromolecule that can be attained, with the molecular weight limit being under 100 000 amu. [10] Much larger molecules can be synthesised with the divergent technique.

Since the convergent synthesis was reported by Hawker and Fréchet, the field of dendrimer research seems to have exploded with new classes of dendrimers, including polyether, polysilane and phenylacetylene dendrimers, and many papers report new methods for their syntheses. [7,11,12] Most of these procedures are variations on the convergent approach, such as the double-stage convergent, [12] double exponential, [13] the branched monomer [14] and the two-step approaches. [15] The logic behind all of these approaches is to "accelerate" the synthesis of large dendrimers by eliminating one or more purification and separation steps. The ultimate dendrimer synthetic strategy would involve the iterative steps required to produce structurally regular and well defined dendrimers, but with the minimum number of purification stages. Such a synthesis has recently been reported where, by a prudent choice of coupling chemistry, dendrimers of up to the third generation have been synthesised in a one-pot procedure with better than 95% purity. [16]

Another interesting recent modification was reported by Zimmerman and Feng. [17] They utilise the traditional convergent approach to build dendritic wedges, then attach each wedge to an organic unit which "self-assembles" with other identically modified wedges, to form a hydrogen bonded hexameric cyclic core with six dendritic wedges attached. Figure 1.3 depicts the self-assembling unit, as well as the dendritic wedge employed.

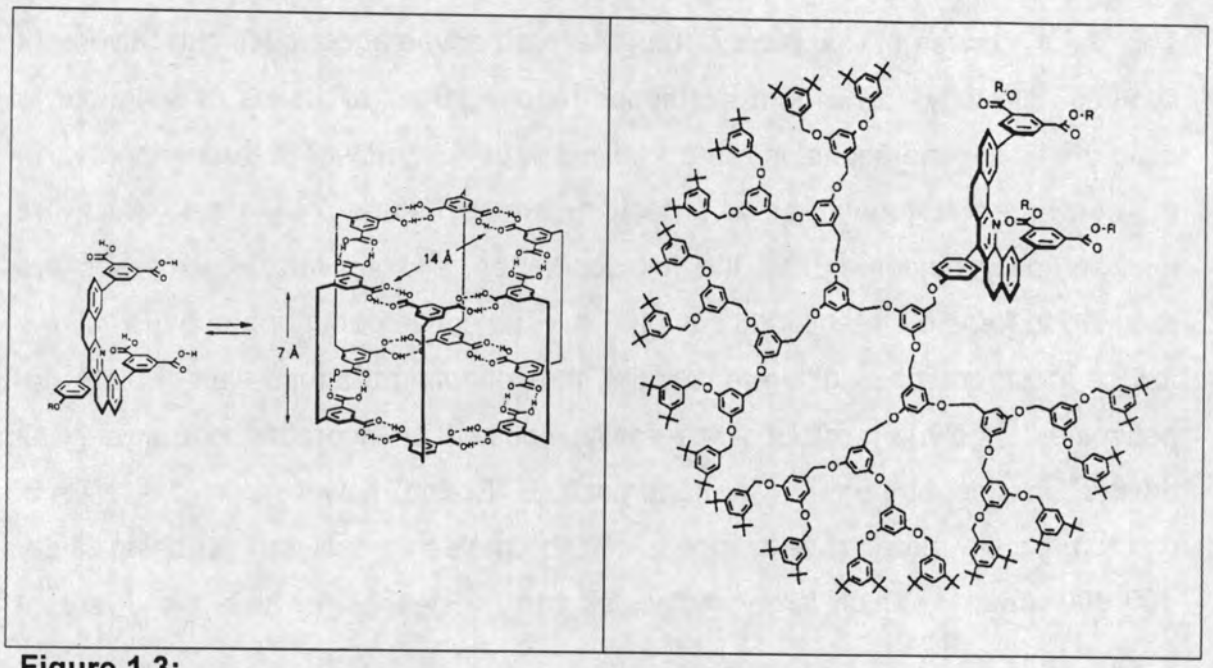


**Figure 1.3:**

a) The self-assembling organic moiety.

b) Dendritic wedge attached to self-assembling moiety.

**Organometallic dendrimers**

Up until 1993, very few of the reported dendrimers contained organometallic functionalities. Astruc and colleagues had synthesised dendrimers containing [$CpFe(C_6R_6)$] moieties [18] and, in 1993, Moss and Liao reported the first series of organotransition metal dendrimers containing metal-carbon σ-bonds on the periphery of the molecule. [19] With the recent wealth of research in the field of dendrimers, there has been a concomitant increase in the number of organometallic dendrimers reported. These dendrimers are synthesised by both the convergent and divergent approaches, and the metal functionalities are found to be incorporated in the monomeric repeat unit, as well as the core and the terminal groups. [20,21,22] Many different metals have now been incorporated into a dendrimer structure, including iron, platinum, tungsten, gold, rhodium, palladium, copper, ruthenium, nickel, chromium and osmium. [23,24] A few recent examples are indicated in Figure 1.4.

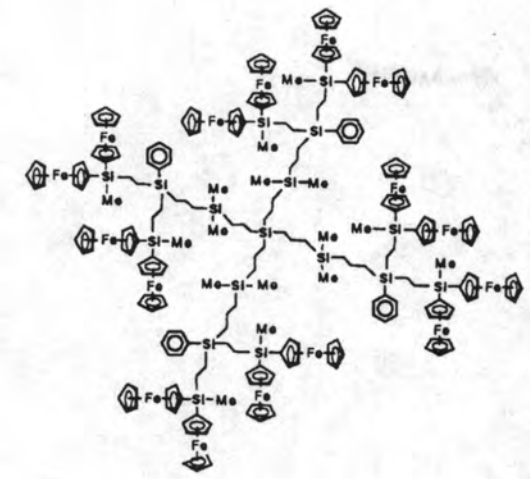

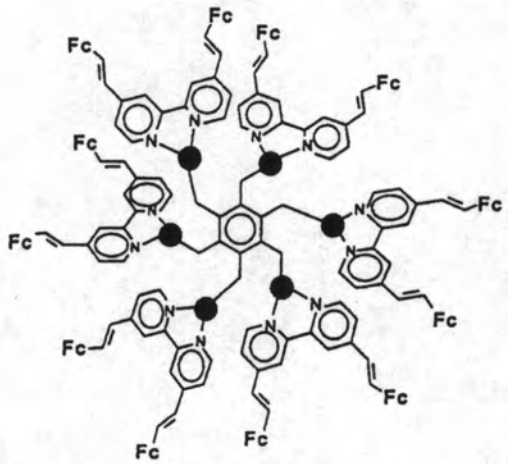

● = $PtMe_2Br$ Fc = Ferrocene

a) Top left - A silicon based ferrocenyl dendrimer [22]

b) Bottom left – a heterometallic dendrimer [21]

c) Below – a ruthenium polypyridine dendrimer [20]

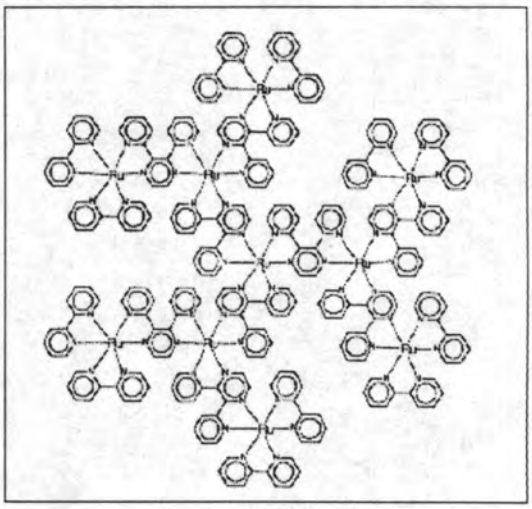

**Figure 1.4**: Examples of some recently reported organometallic dendrimers

**Applications**

The reason for such a general interest in dendrimer research, and particularly organometallic dendrimers, is that their novel structure is expected to produce unique properties. Their highly branched nature generates properties quite different to those of traditional linear polymers. [16] The relatively large size and hollow centre of these molecules, compared to the densely packed surface, makes them ideal drug carriers. Goddard *et al* have shown that dendrimers can be used to encapsulate Bengal Rose dye molecules (see Figure 1.5 for a diagram of this), [25] and several other researchers have successfully used PAMAM dendrimers as gene transport vectors. [2]

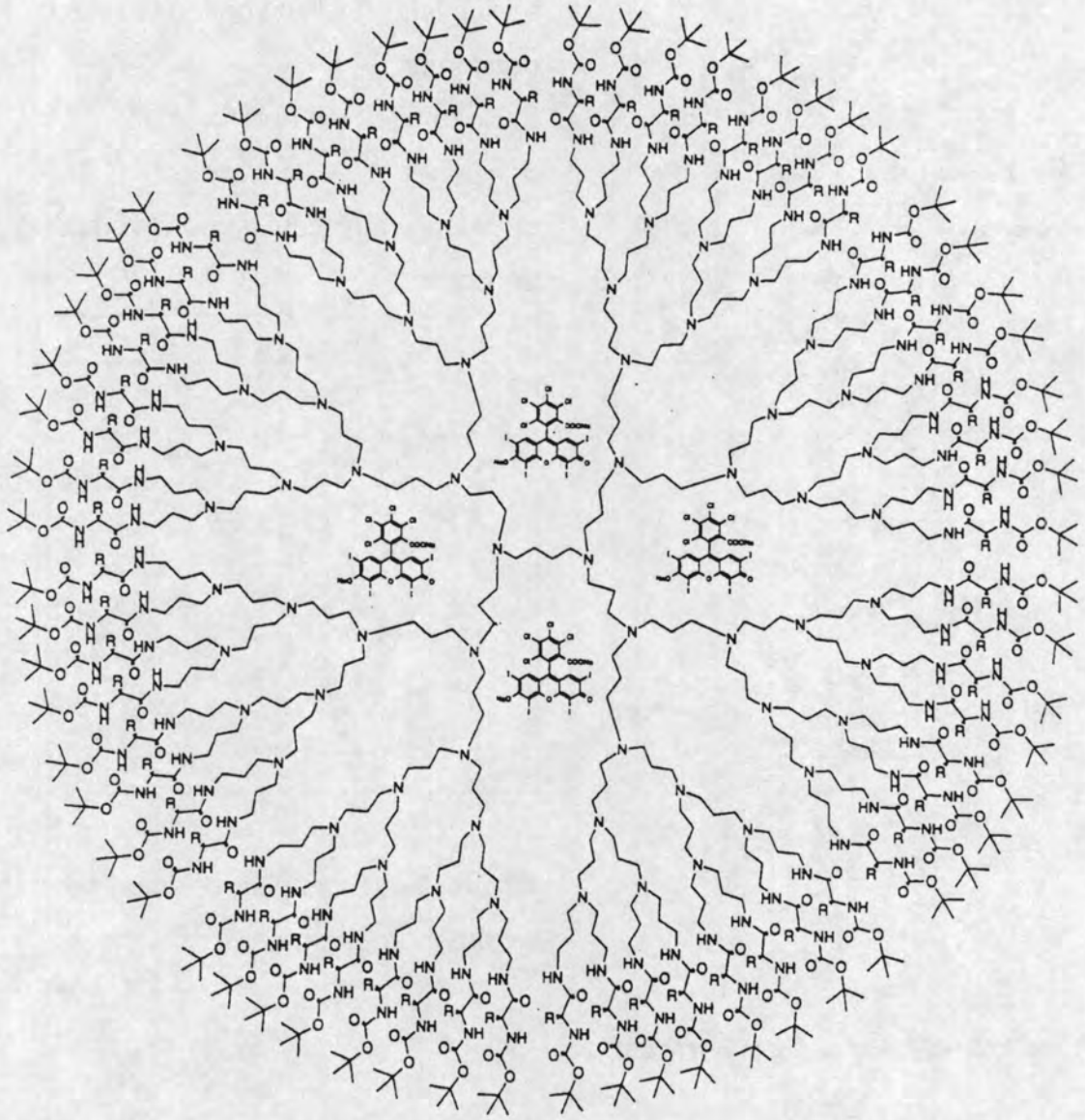

**Figure 1.5:** The Meijer dendrimer box, with four Bengal Rose molecules inside it.

A truly exciting aspect of dendrimers is that, just by changing the core molecule, the repeat unit, or the terminal groups, it is possible to tailor-make a dendrimer to display a particular property. Electrically conducting dendrimers have been synthesised, [26] and a photoswitchable dendrimer has even been produced. [27] Liquid crystalline dendrimers, made from shape-persistent dendrimers with a disc-like shape were reported by Moore *et al* very recently. [28] Moore, along with other co-workers, has also proposed the use of phenylacetylene dendrimers as photonic antenna systems. [29] Figure 1.6 shows an example of a phenylacetylene dendrimer.

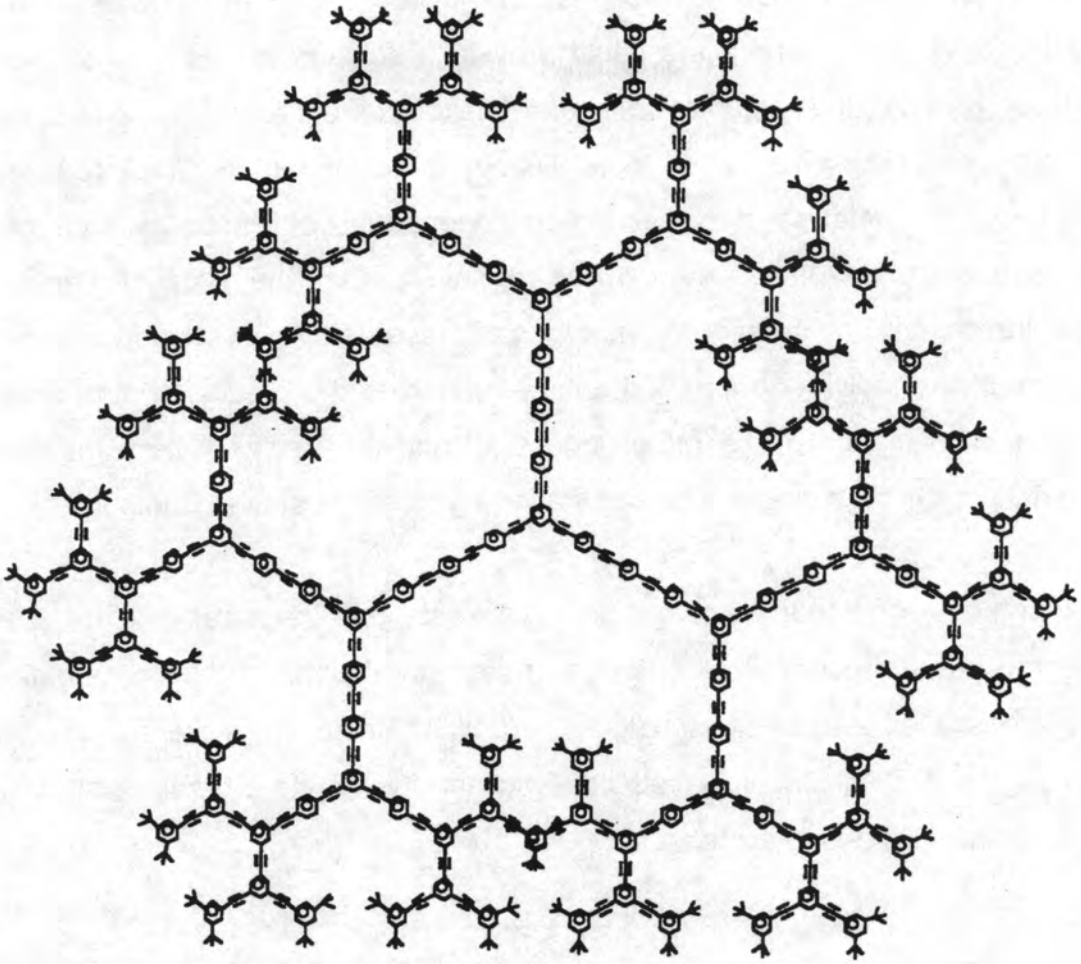

**Figure 1.6:** A phenylacetylene dendrimer – a potential antenna system.

Incorporation of metal groups into the dendrimer architecture, has resulted in the preparation of dendrimers with an even wider range of potentially useful properties. For example, four different ferrocene-containing dendrimers have been synthesised recently, each with a different organic "backbone". [22,30,31,32] The ferrocenyl groups are incorporated on the periphery of the molecule, and can be electronically communicated, [22] or act as independent redox sites, [30] depending on the method of synthesis chosen. In one case, the resulting dendrimer displays liquid crystalline properties. [31]

Perhaps the most useful application of organometallic dendrimers is as catalyst supports, where they could bridge the divide between homogeneous and heterogeneous catalysis. Homogeneously catalysed reactions are typically far quicker and more selective than their heterogeneous counterparts, however suffer

from the difficulty of separation of the catalyst (usually quite valuable) from the product mixture. [2] Dendrimers could provide a solution to this problem, as the terminal groups and organic backbone make the entire molecule soluble in common organic solvents, so catalytically active metals incorporated at the periphery can catalyse the reaction homogeneously. The large size of the dendrimers means that they can be removed from the product stream by ultrafiltration, [33] to be reused. Advantages of these dendrimer supported catalysts over traditional polymer supported catalysts, include the precise control over the number and location of the metal groups, [33] and the relatively large number of terminal groups on a single dendrimer, allowing for high catalyst loading.

This potential of dendrimers to act as catalysts has been realised by several research groups recently. In 1994 van Koten *et al* reported their preparation of polycarbosilane dendrimers functionalised with amino arylnickel(II) complexes (see Figure 1.7) which displayed catalytic activity for the Kharasch addition of polyhalogenoalkanes to alkenes. [3]

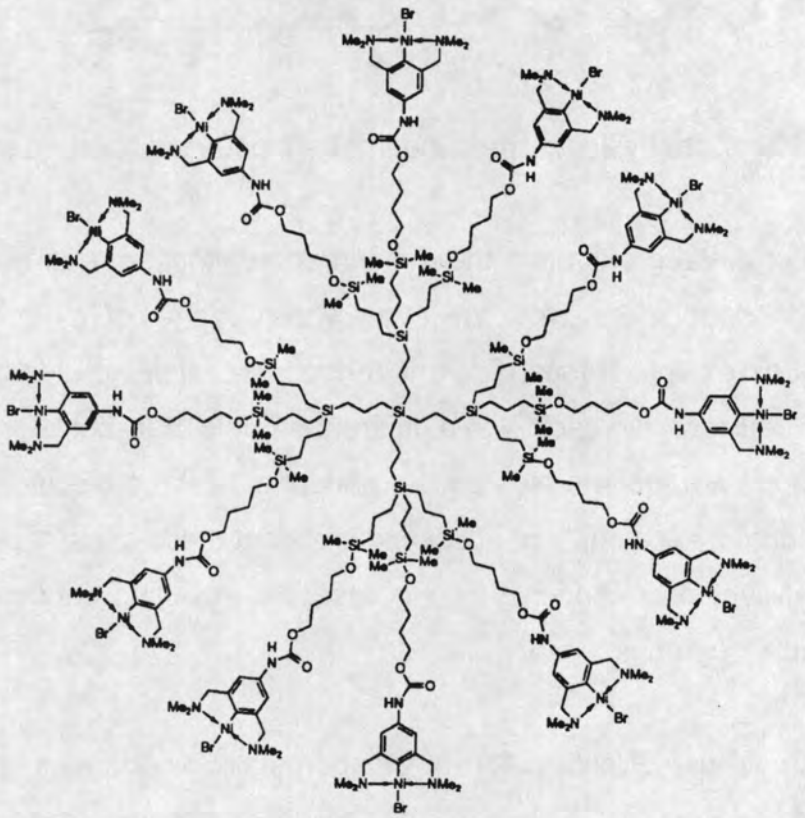

**Figure 1.7:** van Kotens' catalytically active dendrimer.

More recently, Reetz and co-workers have synthesised dendritic phosphane-metal complexes and proven their application in catalysis; in fact, their dendritic catalyst works considerably better than the corresponding monomeric catalyst, and is recyclable. [34]

**Characterisation**

The bulk of dendrimers reported in the literature have been well characterised by several techniques. Elemental analysis, $^{1}H$- and $^{13}C$ NMR, IR spectroscopy, mass spectroscopy (CI, FAB, and MALDI TOF) and titration are all standard techniques which have been applied to these new molecules. [4] Size exclusion chromatography (SEC), low-angle laser light scattering (LALLS) and intrinsic viscosity measurements have been employed to obtain dimensional and homogeneity information. [4] The structural integrity of dendrimers can be unequivocally determined by a combination of these techniques, however very little is known about the three-dimensional structure of dendrimeric compounds. Their fractal nature, and non-crystallinity makes obtaining structural information by x-ray techniques problematic, [4] and it may be that theoretical methods are the only way of obtaining this information. A number of papers dealing with computational studies of dendrimers have been published, and these will be discussed in the introduction to Chapter 4, along with some other recently utilised analytical techniques.

**Objectives**

The work presented in this thesis has several objectives. Firstly, to synthesise a novel organometallic dendrimer in which the metal is incorporated into the molecule exclusively as a surface functionality. This would give us access to a series of multimetallic compounds. The second objective is to examine the structure and properties of these new dendrimers by computational techniques.

The dendritic system chosen for investigation is the Fréchet type poly(benzyl phenyl ether) dendrimers (as shown in Figure 1.2). This selection was made on the basis that others in our laboratories have successfully synthesised novel organometallic dendrimers of this type. [10] Functionalisation of the peripheral aromatic rings as (arene)tricarbonylchromium(0) complexes through the use of the

convergent synthetic approach, could provide a conceptually simple route to new organometallic dendrimers. Furthermore, these new organochromium dendrimers might have application as catalysts. [35]

The second aspect of the work is an investigation of the structure of these dendrimers by molecular mechanics and dynamics techniques. As far as we are aware, no such studies have been performed on poly(benzyl phenyl ether) dendrimers, and no calculations have been performed on any organometallic dendrimers. This will enable us to investigate the structure of the dendrimers, and properties such as the density distribution within the macromolecule and the accessibility of the surface groups. This information is not currently available by any experimental technique.

**References**


1. D. O'Sullivan, *Chem. Eng. News*, August 16, 1993, 20-23
2. R.F. Service, *Science*, 1995, **267**, 458-459
3. J.W.J. Knapen, A.W. van der Made, J.C. de Wilde, P.W.N.M. van Leeuwen, P. Wijkens, D.M. Grove and G. van Koten, *Nature*, 1994, **372**, 659-663
4. D.A. Tomalia, A.M. Naylor and W.A. Goddard III, *Angew. Chem. Int. Ed. Engl.*, 1990, **29**, 138-175
5. E. Buhlein, W. Wehner and F. Vögtle, *Synthesis*, 1978, 155
6. F. Zeng and S.C. Zimmerman, *Chem. Rev.*, 1997, **97**, 1681-1712
7. D.A. Tomalia and H.D. Durst, *Top. Curr. Chem.,* 1993, **165**, 193-313
8. C.J. Hawker and J.M.J. Fréchet, *J. Am. Chem. Soc.*, 1990, **112**, 7638-7647
9. D.A. Tomalia, *Aldrichimica Acta*, 1993, **26**, 91-101
10. Y-H. Liao and J.R. Moss, *Organometallics*, 1996, **15**, 4307-4316
11. A. Buyle Padias, H.K. Hall, Jr., D.A. Tomalia and J.R. McConnell, *J. Org. Chem.*, 1987, **52**, 5305-5312
12. Z. Xu, M. Kahr, K.L. Walker, C.L. Wilkins and J.S. Moore, *J. Am. Chem. Soc.*, 1994, **116**, 4537-4550
13. T. Kawaguchi, K.L. Walker, C.L. Wilkins and J.S. Moore, *J. Am. Chem. Soc.*, 1995, **117**, 2159-2165

14. K.L. Wooley, C.J. Hawker and J.M.J. Fréchet, *Angew. Chem. Int. Ed. Engl.*, 1994, **33**, 82-85
15. R. Spindler and J.M.J. Fréchet, *J. Chem. Soc., Perkin Trans.* 1, 1993, 913-918
16. S.C. Stinson, *Chem. Eng. News*, September 22, 1997, 28-30
17. S. C. Zimmerman, F. Zeng, D.E.C. Reichert and S.V. Kolotuchin, *Science*, 1996, **271**, 1095-1098
18. F. Moulines, L. Djakovitch, R. Boese, B. Gloaguen, W. Thiel, J.-L. Fillaut, M.-H. Delville and D. Astruc, *Angew. Chem. Int. Ed. Engl.*, 1993, **32**, 1075
19. Y-H. Liao and J.R. Moss, *J. Chem. Soc., Chem. Commun.*, 1993, 1774
20. S. Campagna, G. Denti, S. Serroni, A. Juris, M Venturi, V. Ricevuto and V. Balzani, *Chem. Eur. J.*, 1995, **1**, 211-221
21. S. Achar, C.E. Immoos, M.G. Hill and V.J. Catalano, *Inorg. Chem.*, 1997, **36**, 2314-2320
22. I. Cuadrado, C.M. Casado, B. Alonso, M. Morán, J. Losada and V. Belski, *J. Am. Chem. Soc.*, 1997, **119**, 7613-7614
23. M. Bardaji, M. Kustos, A-M. Caminade, J-P. Majoral and B. Chaudret, *Organometallics*, 1997, **16**, 403-410 and refs. cited therein.
24. F. Lobete, I. Cuadrado, C. M. Casado, B. Alonso, M. Morán and J. Losada, *J. Organomet. Chem.*, 1996, **509**, 109-113
25. P. Miklis, T. Çağin and W.A. Goddard III, *J. Am. Chem. Soc.*, 1997, **119**, 7458-7462
26. L. L. Miller, R.G. Duan, D.C. Tully and D.A. Tomalia, *J. Am. Chem. Soc.*, 1997, **119**, 1005-1010
27. D.M. Junge and D.V. McGrath, *J. Chem. Soc., Chem. Commun.*, 1997, 857-858
28. D.J. Pesak and J.S. Moore, *Angew. Chem. Int. Ed. Engl.*, 1997, **36**, 1636-1639
29. R. Kopelman, M. Shortreen, Z-Y. Shi, W. Tan, Z. Xu, J.S. Moore, A. Bar-Haim and J. Klafter, *Phys. Rev. Lett.*, 1997, **78**, 1239-1242
30. C-F. Shu and H-M. Shen, *J. Mater. Chem.*, 1997, **7**, 47-52
31. R. Deschenaux, E. Serrano and A-M. Levelut, *J. Chem. Soc., Chem. Commun.*, 1997, 1577-1578

32. C. Valério, J-L. Fillaut, J. Ruiz, J. Guittard, J-C. Blais and D. Astruc, *J. Am. Chem. Soc.*, 1997, **119**, 2588-2589

33. D.A. Tomalia and P. R. Dvornic, *Nature*, 1994, **372**, 617-618

34. M.T. Reetz, G. Lohmer and R. Schwickardi, *Angew. Chem. Int. Ed. Engl.*, 1997, **36**, 1526-1529

35. *Comprehensive Organometallic Chemistry II*, E.W. Abel, F.G.A. Stone, G. Wilkinson, J.A. Labinger and M.J. Winter, Pergamon, New York, 1995, vol. 9, ch.8, p. 528 and refs. therein.

# Chapter 2 Synthetic studies toward organochromium dendrimers

## 2.1 Proposed synthetic strategies

The synthesis of poly(benzyl phenyl ether) dendrimers according to the convergent approach of Hawker and Fréchet, [1] is indicated in Scheme 2.1 below. This synthesis begins at what will be the surface groups of the molecule, and through the use of two iterative synthetic steps – coupling and activation – builds up to the desired size of dendrimer. Each time a coupling occurs, the molecule is said to go through another "generation" of growth. [1]

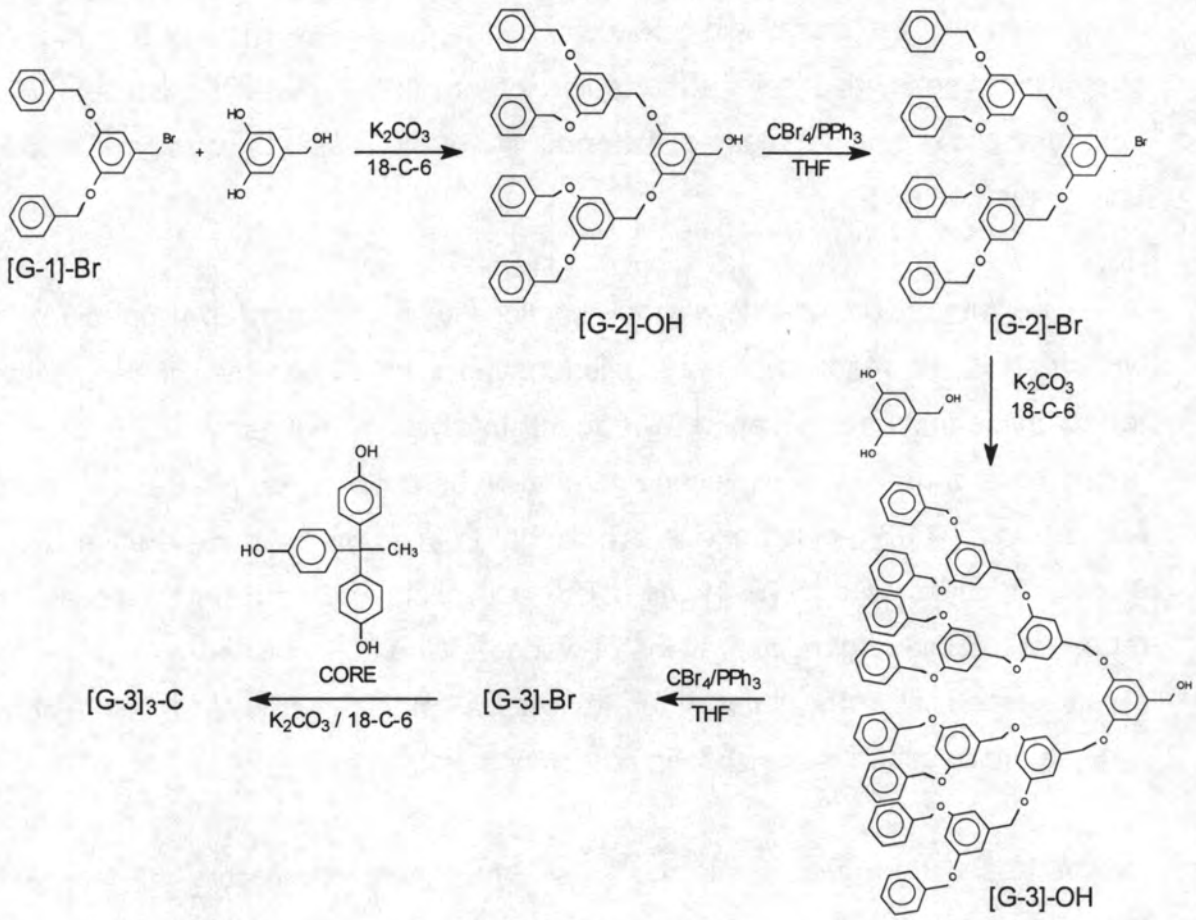


**Scheme 2.1:** The synthesis of poly(benzyl phenyl ether) dendrimers via the convergent synthetic strategy reported by Hawker and Fréchet. [1]

Note that in this particular synthesis, the starting material is not a simple benzylic halide or alcohol, but is in fact the first generation dendritic bromide wedge, 3,5-bis(benzyloxy)benzyl bromide (**[G-1]-Br**). This dendritic bromide was an available starting material, [2] and reduced the number of steps required for the synthesis of higher generation dendritic wedges. Conceptually however, the convergent approach could begin with a simple benzyl halide.

In the first iterative step, the first generation benzylic halide is coupled to the branching monomer, in this case 3,5-dihydroxybenzyl alcohol, to give the second generation alcohol **[G-2]-OH**. The choice of branching monomer, and methodology was based on the high yields that can be obtained for the formation of benzyl ethers from phenols and benzylic halides. [1] The optimum reaction conditions for the coupling were found to be potassium carbonate, with 18-crown-6 (18-C-6), in refluxing acetone. [1] As potassium carbonate is a relatively weak base, it only removes the more acidic phenolic hydrogens. This ensures that only the phenolic oxygens, and not the benzylic oxygen, will displace the halide. Once both phenolic sites have reacted, the dendritic wedge is said to have gone through one generation of growth.

In the next iterative step, the alcohol functionality is converted to a bromide. As with the coupling reaction, various halogenating agents were investigated: carbon tetrabromide/triphenylphosphine was found to give the highest yields through all generations of growth. This second generation benzyl bromide **[G-2]-Br**, is primed for coupling with 3,5-dihydroxybenzyl alcohol to yield the third generation benzyl alcohol dendritic wedge **[G-3]-OH**. The activation and coupling steps can be repeated to build larger generations of wedge. When the desired generation has been reached (after the third generation activation in Scheme 2.1), the dendritic wedges are attached to the chosen core molecule.

Hawker and Fréchet selected as the core molecule 1,1,1-tris(4′-hydroxyphenyl)ethane, so as to allow the use of the same coupling chemistry employed in the growth stages. [1] Three dendritic wedges are attached to one core molecule to give the final poly(benzyl phenyl ether) dendrimer **[G-3]$_3$-C** (Scheme

2.1). The convergent methodology is extremely flexible, and can be extended to include other branching monomers, and coupling chemistries.

**Chromium-containing dendrimers**

The first proposed synthetic route to chromium-containing dendrimers follows very closely the synthesis described above. A difference does occur however, in the choice of starting material. It was envisaged that the chromium species be incorporated into the dendrimer as ($\eta^6$-arene) complexes at the periphery of the molecule. To be consistent with the convergent ethos, the starting material deemed most suitable, was ($\eta^6$-benzyl alcohol)tricarbonylchromium(0). This complex is readily available from benzyl alcohol, [3] and conversion to the corresponding benzyl chloride has also been reported. [4] Scheme 2.2 outlines the proposed procedure for the synthesis of a first generation organometallic dendrimer, with chromium tricarbonyl groups exclusively at the periphery of the molecule.

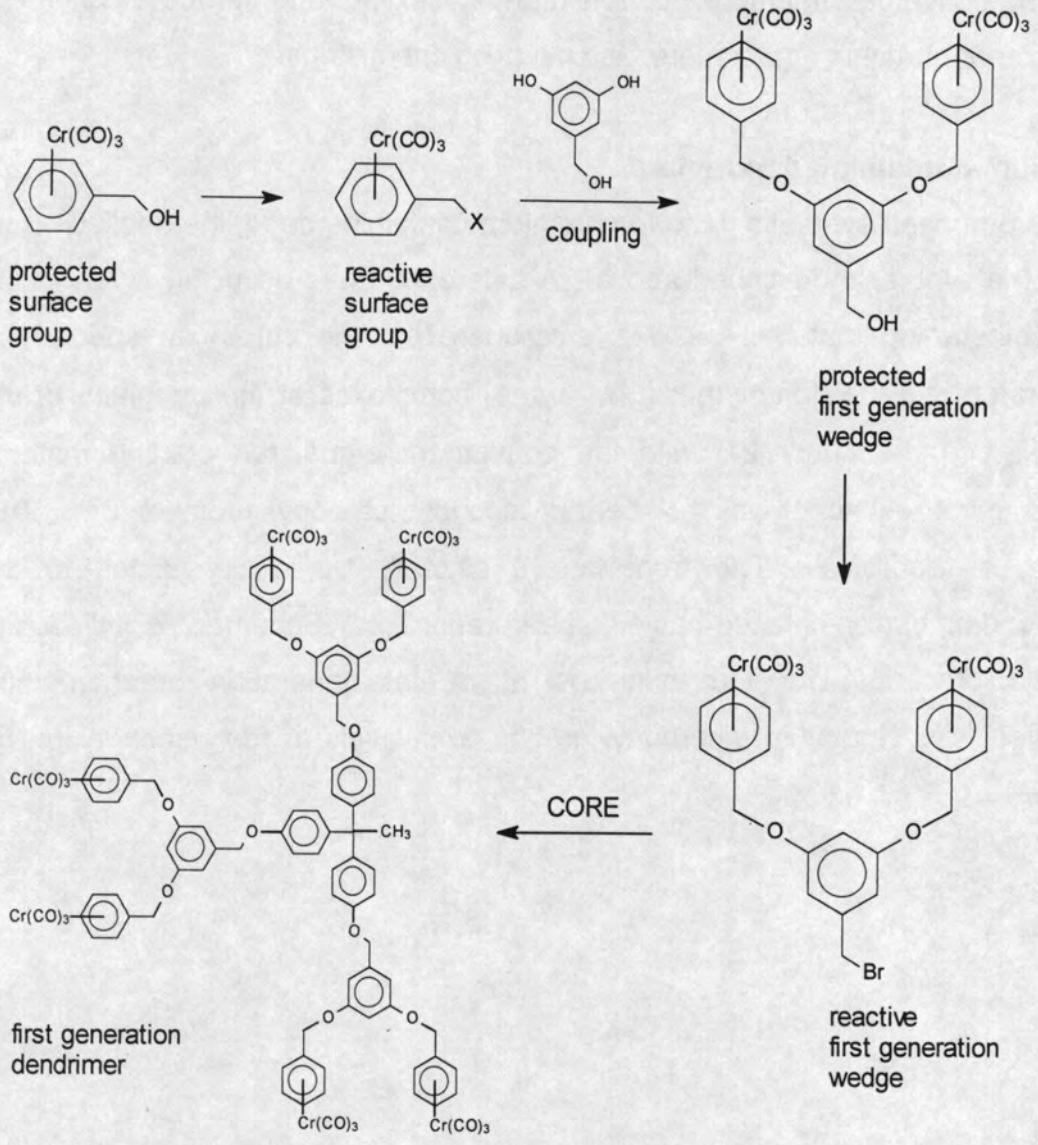


**Scheme 2.2:** The proposed synthetic route for the synthesis of a first generation chromium poly(benzyl phenyl ether) dendrimer.

An alternative synthetic approach that was investigated, is shown in Scheme 2.3. This also follows convergent methodology, and like the Hawker/Fréchet route, utilises a first generation dendritic wedge as starting material.

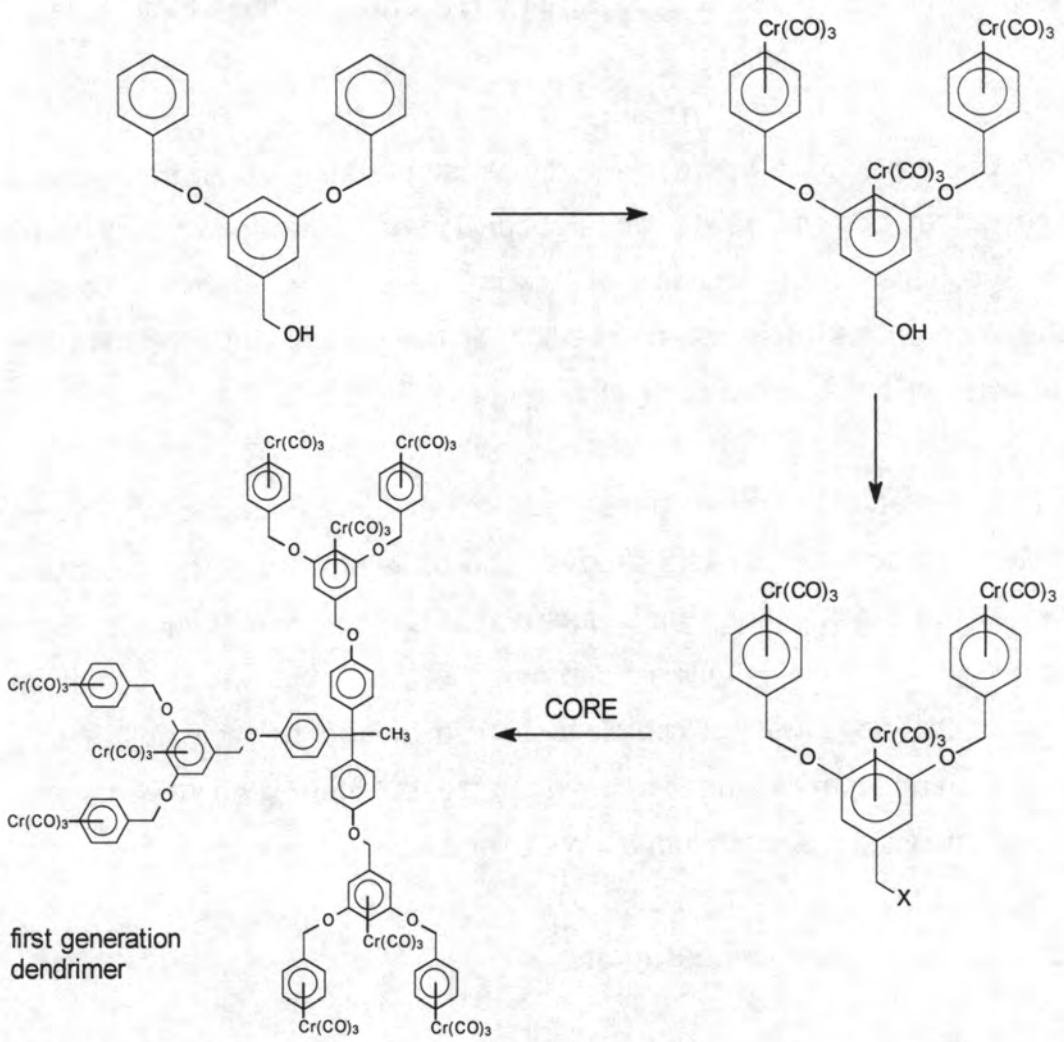


**Scheme 2.3:** A proposed alternative synthetic approach for the first generation chromium poly(benzyl phenyl ether) dendrimer.

This approach has an advantage over the previously discussed route, in the number of synthetic steps which would involve chromium tricarbonyl moieties. Chromium arene complexes are photo-oxidised, and so are air- and light-sensitive. These complexes are fairly stable in the solid state, under nitrogen, but much less so in solution. [5] If several steps of the synthesis can be carried out without incorporating tricarbonylchromium(0), the overall yield for the synthesis is likely to be higher, and the synthetic steps involved, simpler.

The anticipated product of this route is different from that of the first strategy. In the first proposal, the chromium groups are exclusively at the periphery of the

molecule, whereas in this approach, all three aromatic rings of the wedge are complexed.

In both of the proposed approaches, direct complexation to the benzyl halide, or first generation benzylic halide, was not considered. Reaction of benzylic halides under complexation conditions, with even a labile source of tricarbonylchromium(0) leads to insertion of the chromium(0) into the benzylic halide bond, with subsequent reductive coupling. [6]

Direct complexation to the pre-formed organic dendrimer was also considered as a possible approach. This has the advantage of incorporating the organometallic species at the last step only, but suffers from a lack of control over the location of these groups. It is highly unlikely that only the outer rings will be complexed, or that all of the rings will be complexed. It might be possible to determine *a posteriori* which aromatic rings are co-ordinated, but there is no way to control this without introducing the chromium at an earlier stage.

## 2.2 Synthesis of organic dendrimers

In order to prepare starting materials for the proposed synthetic strategies, the synthesis of a first generation organic dendrimer was conducted. The intermediates of this synthesis *viz.* the first generation wedges, as well as the actual dendrimer, also serve as a basis for comparison with their organometallic counterparts.

### Preparation of starting material and coupling reactions

3,5-Dihydroxybenzyl alcohol **1**, the branching monomer, was prepared from methyl 3,5-dihydroxybenzoate according to a literature procedure. [7] The first generation benzyl alcohol wedge **3** was then synthesised via two routes, as shown in Scheme 2.4.

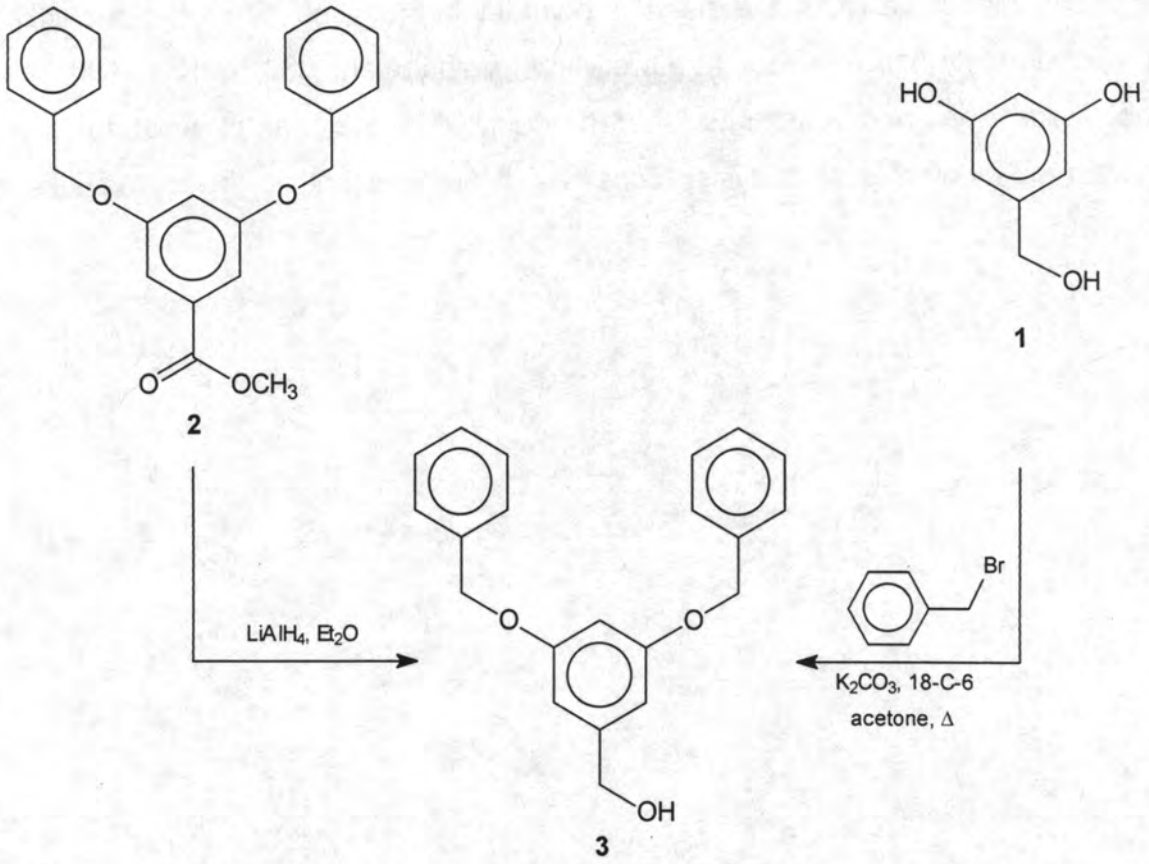


**Scheme 2.4**

The literature procedure, i.e. reduction of methyl 3,5-bis(benzyloxy)benzoate **2**, [2] gives access to the 3,5-bis(benzyloxy)benzyl alcohol **3** in high yield (94%). An alternative synthesis starting from benzyl bromide, was also investigated, to provide a comparison with the reactivity of the corresponding chromium complex at this stage of the synthesis. A much lower yield (42%) of **3** was obtained for this route, however the viability of the approach was confirmed. The products from both syntheses were characterised by several techniques, including $^{1}H$ and $^{13}C$ NMR spectroscopy.

**Activation methodologies**

Conversion of the benzylic alcohol **3** to a benzylic bromide **4** was also investigated by two routes. Phosphorus tribromide effects this conversion in good yield (76%) as reported. [2] The use of carbon tetrabromide/triphenylphosphine was explored, as this is the reagent combination of choice for bromination of later generation dendritic alcohols. [1] The yield obtained from the use of these reagents was much lower however (44%) and the product required separation from residual

triphenylphosphine. As the melting point in both cases differed substantially (approximately 5°) from the literature value, both $^{1}H$ and $^{13}C$ NMR spectra were obtained. The spectra indicated that the desired product was pure, and this was confirmed by elemental analysis. Scheme 2.5 indicates both of the routes utilised.

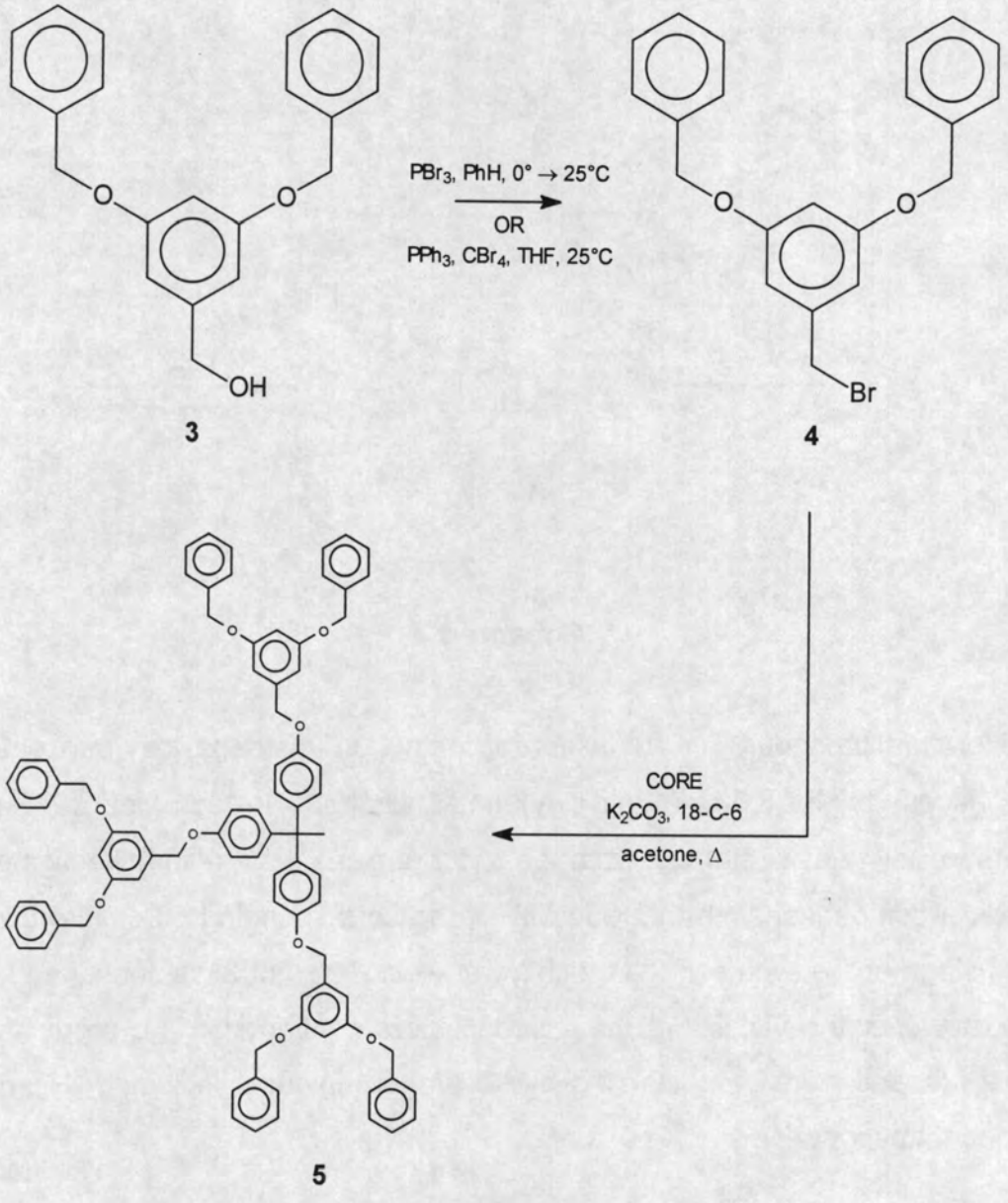


**Scheme 2.5**

**Preparation of the dendrimer**

With the dendritic bromide wedge in hand, a first generation poly(benzyl phenyl ether) dendrimer **5** was prepared by coupling with the core molecule: 1,1,1-tris(4´-hydroxyphenyl)ethane (i.e. CORE) (Scheme 2.5). A portion of the desired product

was purified, and displayed the expected spectroscopic data ($^{1}H$, $^{13}C$ NMR, FAB MS and IR).

## 2.3 Synthesis of chromium-containing dendrimers

The synthesis of dendrimers which incorporate chromium tricarbonyl, was investigated by several of the routes previously outlined. The initial synthetic strategy followed Scheme 2.2, where the starting material is (benzyl alcohol)tricarbonylchromium(0) **6**. This material is readily prepared (84%) by refluxing benzyl alcohol and chromium hexacarbonyl in a dibutyl ether/THF mixture (see Scheme 2.6). [3] These reaction conditions are typical of a direct complexation reaction, and are utilised in all direct complexation reactions reported in this thesis. The complex was identified by melting point and IR, where characteristic stretching frequencies are observed in the carbonyl region. For comparative purposes, both $^{1}H$ and $^{13}C$ NMR data were acquired.

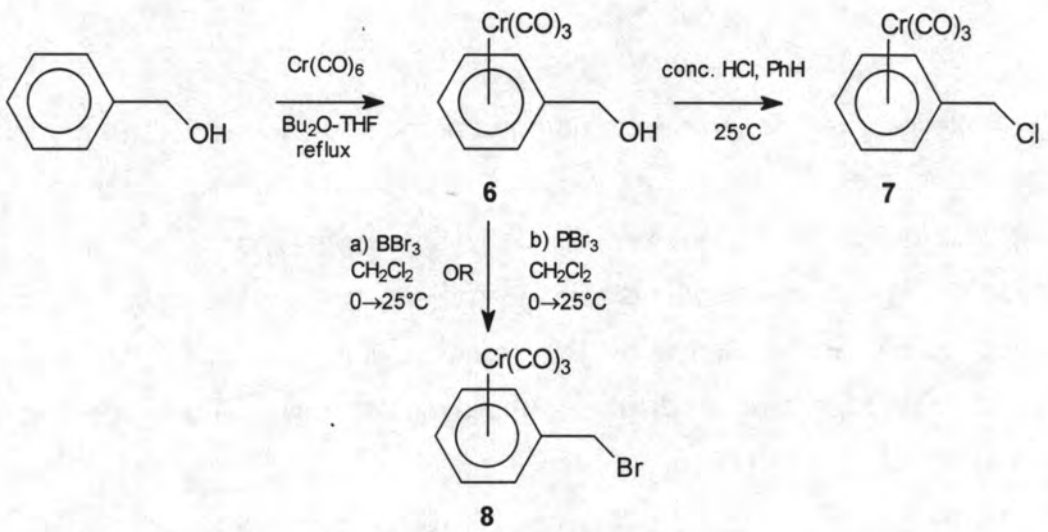


**Scheme 2.6**

### Activation methodologies

Conversion of the benzyl alcohol complex **6** to (benzyl chloride)tricarbonylchromium(0) **7**, has been reported in varying yields. [8] This conversion was effected in low yield (33%), by addition of concentrated hydrochloric acid to a solution of the alcohol **6** in benzene. The product **7** was

purified by recrystallisation, and the melting point and elemental analysis were as expected. However both the $^{1}H$ and $^{13}C$ NMR spectra indicate the presence of an impurity, possibly a small amount of uncomplexed benzyl chloride. This impurity might be an artefact resulting from the instability of the complex **7** in solution. Column chromatography (alumina) failed to improve the product purity, and a substantial amount of material was not recovered from the column.

The low yield and questionable purity for this conversion were disappointing. Dendrimer syntheses require many synthetic steps, thus a low yielding reaction early on in the sequence, decreases the viability of the route as a whole. Alternative activation methodologies obviously needed to be examined.

Conversion of the benzyl alcohol complex **6** to the (benzyl bromide)tricarbonylchromium(0) complex **8** was investigated by several routes. The use of carbon tetrabromide/triphenylphosphine, as in the organic dendrimer synthesis, did not provide any stable product. It is possible that the triphenylphosphine caused the decomplexation of the chromium tricarbonyl moiety due to its electron-donating nature.

A recent publication reported the preparation of tricarbonylchromium(0) complexes of benzylic bromides in excellent yield, by the addition of boron tribromide to the tricarbonylchromium(0) complexes of benzylic alcohols and ethers. [8] The activation of the benzyl alcohol complex **6** to the corresponding benzyl bromide **8** was successfully accomplished by this route in high yield (84%) as shown in Scheme 2.6; and the product displayed the expected physical and spectroscopic characteristics (m.p, IR, $^{1}H$ and $^{13}C$ NMR).

Although boron tribromide is an excellent reagent for effecting the conversion of a chromium-complexed benzylic alcohol to the corresponding bromide complex, its use might be limited later on in the synthetic sequence. It is such a reactive species that it also converts benzylic ethers to benzylic bromides, thus a first-generation dendritic wedge, which contains two benzyl ether linkages, would be fragmented by the use of this reagent.

With this in mind, phosphorus tribromide was investigated as a possible halogenating agent. It was shown to be successful in the organic dendrimer synthesis, in activating the first generation alcohol wedge **3** to the bromide wedge **4**. Unlike the carbon tetrabromide/triphenylphosphine reagent combination, phosphorus tribromide is unlikely to cause decomplexation of the chromium tricarbonyl moiety, due to its weaker electron donating character. Reaction of the benzyl alcohol complex **6**, with phosphorus tribromide gave access to (benzyl bromide)tricarbonylchromium(0) **8** in excellent yield (87%). This product was identical to that prepared by the use of boron tribromide.

Thus, it seems that phosphorus tribromide is an ideal activating reagent. It will not cleave the aryl ether linkages of dendritic wedges under these reaction conditions, and it does not cause decomplexation of the chromium tricarbonyl moiety. Thus, one reagent can be used for activation throughout the entire synthetic sequence. In addition, the conversion is high yielding both in the presence of chromium tricarbonyl and for purely organic dendritic wedges.

**Coupling reactions**

With the activation methodology well established, it was possible to research the coupling of the benzylic halides **7** and **8** with the branching monomer. Reaction of (benzyl chloride)tricarbonylchromium(0) **7** with 3,5-dihydroxybenzyl alcohol **1**, under the same conditions as for organic coupling reactions (see Scheme 2.7), did not give access to the desired first generation wedge. Instead, the yellow crystalline product obtained was shown to be the bis-complex (dibenzyl ether)bis[tricarbonylchromium(0)] **9** (47%). The structure of this unexpected compound was assigned from mass spectral and NMR data.

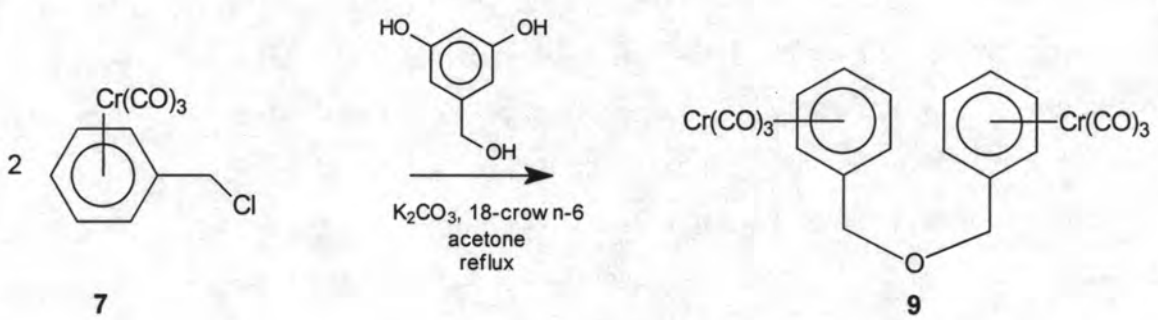


**7** **9**

**Scheme 2.7**

The mass spectrum displayed the parent ion, and the $^{1}H$ and $^{13}C$ NMR spectra indicated the presence of a symmetrical molecule with one type of complexed aromatic ring and no evidence of any uncomplexed arene. Comparison of both the carbon and proton signals of the benzyl group with other benzylic chromium complexes, allowed the compound to be unambiguously defined as a chromium complexed benzyl ether. In Table 2.1, the $^{13}C$ NMR data of several chromium complexes are displayed for comparison with (dibenzyl ether)bis[tricarbonylchromium(0)] **9**. Elemental analysis data agreed with the proposed structure, and the IR spectrum displayed the characteristic carbonyl stretching frequencies.

**Table 2.1:** $^{13}C$ NMR chemical shift data (ppm) for selected tricarbonyl chromium complexes

| Carbon | 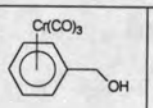 **6**[a] | 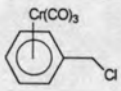 **7**[b] | 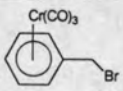 **8**[c] | 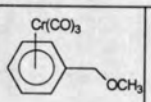 **14**[d] | 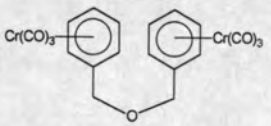 **9**[e] |
|---|---|---|---|---|---|
| $ArCH_2X$ | 63.3 | 45.1 | 31.8 | 72.9 | 70.4 |
| *o* | 90.8/93.0 | 92.3/92.8 | 92.3/93.3 | 91.9/92.8 | 93.8/94.8 |
| *m* | 90.8/93.0 | 92.3/92.8 | 92.3/93.3 | 91.9/92.8 | 93.8/94.8 |
| *p* | 91.7 | 91.6 | 91.6 | 91.4 | 93.7 |
| *ipso* | 111.8 | 102.8 | 105.5 | 107.7 | 111.0 |
| CO | 232.7 | 231.9 | 232.0 | 232.6 | 232.5 |

a) Reference 3 b) Reference 8 c) Reference 8

d) The preparation of this compound is described later in this chapter.

This previously unreported compound **9** is an example of a bis-complexed diaromatic system, of which there are relatively few examples in the literature. This is due to the electron-withdrawing effect of the tricarbonyl chromium moiety. Direct complexation is the usual method for synthesis of chromium arene complexes, however the formation of the complex is facilitated by electron donating substituents. [10] Once the initial ring of a diaromatic ligand is complexed,

the chromium tricarbonyl group withdraws electron density from this ring, [10] thus impeding a second such reaction at the adjacent aromatic ring.

The formation of the product **9** in this instance, is not by direct complexation to a diaromatic ligand. It is proposed that partial hydrolysis of the starting material, viz. (benzyl chloride)tricarbonylchromium(0) **7** by adventitious moisture, possibly present in the acetone, provides the corresponding benzyl alcohol complex **6**. This is available for reaction with remaining starting material, to give (dibenzyl ether)bis[tricarbonylchromium(0)] **9** as shown in Scheme 2.8.

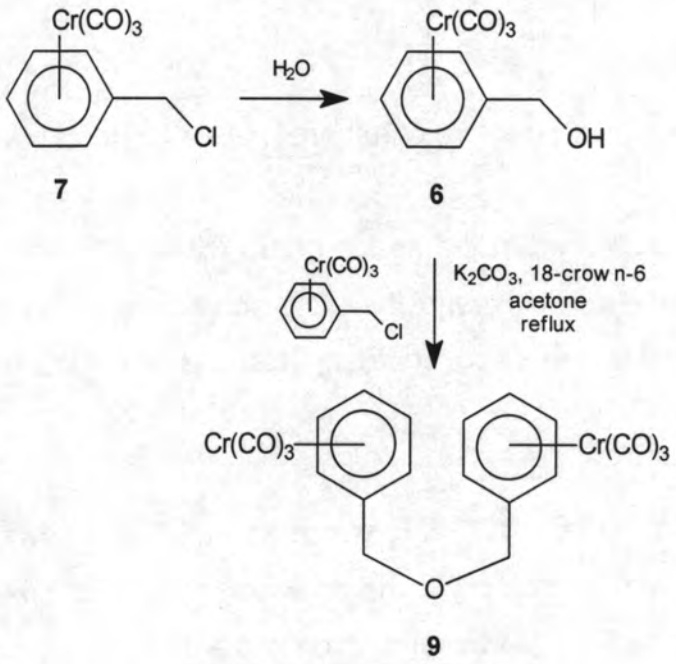


**Scheme 2.8**

This unusual compound is a bimetallic analogue of the polymetallic dendrimers investigated in this work. As such, it can provide us with useful information, such as any interaction between the chromium tricarbonyl groups. As will be described later in Chapter 3, it can also contribute to parameterisation of the forcefield employed in the molecular mechanics calculations. It was thus considered both interesting and advantageous to determine the crystal structure of this novel compound.

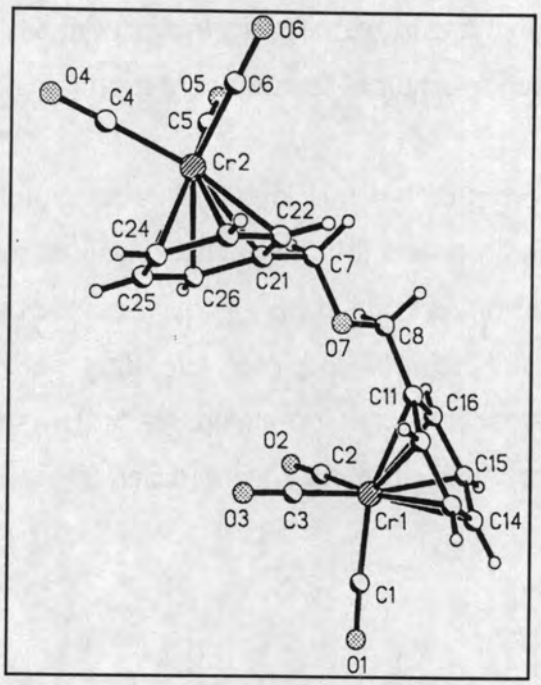


**Figure 2.1:** The crystal structure of (dibenzyl ether)bis[tricarbonylchromium(0)] **9**.

The compound crystallised in the space group $P2_1/n$ with $Z$=4. The molecule is located in a general position, and therefore the whole molecule constitutes the asymmetric unit. More details regarding this crystal structure can be found in Chapter 3.

A low temperature (-60°C) $^{13}C$ NMR spectrum in $CDCl_3$ shows some splitting of the carbonyl resonance frequency; this indicates, that at a low temperature, it is possible to "freeze out" the carbonyl rotation into a discrete rotamer as found in the crystal structure.

Although the coupling reaction employing (benzyl chloride)tricarbonylchromium(0) **7** did not allow access to the desired product, *viz.* the first generation dendritic wedge, with 2 peripheral tricarbonylchromium functionalities, the use of (benzyl bromide)tricarbonylchromium(0) **8**, might. A bromide is a superior leaving group to a chloride, thus the reactivity towards 3,5-dihydroxy benzyl alcohol is enhanced. The readily available benzyl bromide complex, is also of higher purity than the chloride complex, and this might preclude undesired side reactions. Scheme 2.9 describes however, what did happen in this reaction.

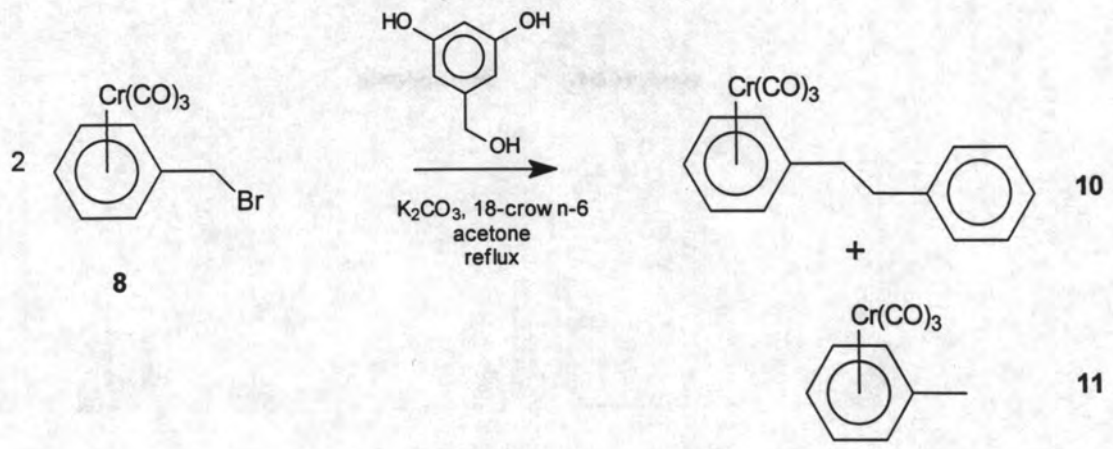


**Scheme 2.9**

As can be seen from Scheme 2.9, the desired first generation wedge was not obtained from the reaction. A mixture of (bibenzyl)tricarbonylchromium(0) **10** and (toluene)tricarbonylchromium(0) **11** (1:1) was obtained, with no evidence of either the desired product or, as in the case of the benzyl chloride complex, (dibenzyl ether)bis[tricarbonylchromium(0)] **9**.

(Bibenzyl)tricarbonylchromium(0) **10** is a known compound, reported to be formed along with the toluene complex **11**, under standard complexation conditions, in the presence of a labile source of chromium tricarbonyl such as $Cr(CO)_3(NH_3)_3$. [6] It is proposed that the product **10** is formed in this reaction by the insertion of chromium into the carbon-bromine bond, followed by reductive coupling with (benzyl bromide)tricarbonylchromium(0) **8**. [8]

The structural elucidation of the products was complicated by their inseparability, and similar structures, resulting in a great deal of overlap in the $^{1}H$ and $^{13}C$ NMR spectra (see Figure 2.2).

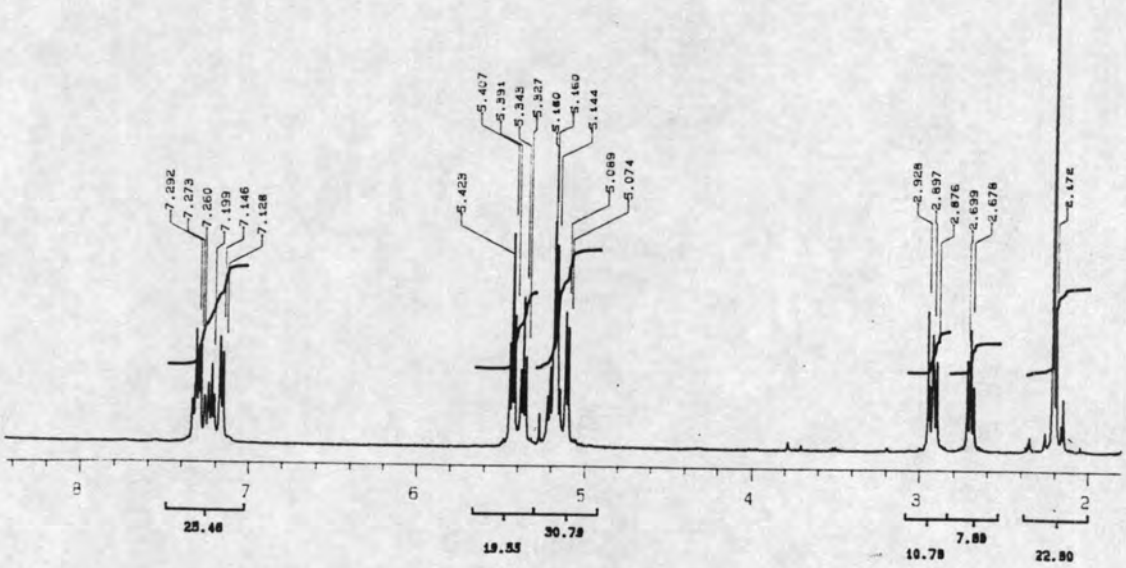


**Figure 2.2:** $^{1}$H NMR spectrum of product mixture **10** and **11**.

One set of uncomplexed aromatic ring signals can be seen in Figure 2.2, as well as two sets of complexed aromatic ring signals. It is clear that the uncomplexed region is due to a monosubstituted ring, as separate resonances are distinguishable for the ortho, meta and para protons. The $^{13}$C signals in the uncomplexed aromatic region clearly indicate all three types of carbons (*o*,*m*,*p*). The complexed region also appears to result from monosubstituted rings, however there is considerable overlap in this region.

The benzyl alcohol protons of the desired dendritic wedge, would be expected to appear at around $\delta$ 4.6 ppm. Additionally, the benzyl ether signals would be expected in the same region of the spectrum. Instead, three different signals are observed, namely two triplets at $\delta$ 2.7 and $\delta$ 2.9 ppm, and a singlet at $\delta$ 2.2 ppm. A combination of COSY and HMQC spectra allowed the triplets to be unequivocally assigned as an ethylene fragment, and the singlet as being due to a methyl group.

The $^{1}$H and $^{13}$C NMR spectra of the toluene complex **11**, have been previously reported. [11] These correlate very well with those assigned to the toluene complex component of this product mixture. In the case of the bibenzyl complex **10**, only the $^{1}$H NMR spectrum had been previously reported, [12] which also correlated well with the assignments for the product mixture. The $^{13}$C NMR spectrum has been

fully assigned, by a combination of HMQC and COSY spectra, and by analogy with the toluene complex.

Further support for the proposed structures, came from the observation of the parent ions of both components in the mass spectral data. The reported carbonyl stretching frequencies in the IR spectra of the two compounds are very similar, *viz.* 1968, 1895 $cm^{-1}$ ($CCl_4$) for the bibenzyl complex, and 1968, 1886 $cm^{-1}$ ($CH_2Cl_2$) for the toluene complex. [11,12] The observed carbonyl stretching frequencies for the product mixture, *viz.* 1968, 1890 $cm^{-1}$ ($CDCl_3$) appear to be due to a combination of both compounds, as the 1968 $cm^{-1}$ band is fairly sharp, whereas the lower frequency band (1890 $cm^{-1}$) is somewhat broader.

Neither of the coupling reactions involving (benzyl chloride)tricarbonylchromium(0) **7** or (benzyl bromide)tricarbonylchromium(0) **8** with 3,5-dihydroxybenzyl alcohol **1** afforded the desired product. In both cases, the benzylic halide was more reactive towards itself than towards 3,5-dihydroxybenzyl alcohol. In an attempt to increase the reactivity of the branching monomer, a different approach was employed. The base utilised in all coupling reactions to this point was potassium carbonate, which is sufficiently strong enough to remove the phenolic protons in the presence of the benzylic protons, without affecting the benzyl alcohol functionality. Potassium carbonate was replaced by sodium hydride, and the branching monomer was changed to methyl 3,5-dihydroxybenzoate, so as to protect the benzyl group. The reaction is outlined in Scheme 2.10, and as shown, an unidentifiable mixture of compounds resulted, with no evidence for the formation of the desired product.

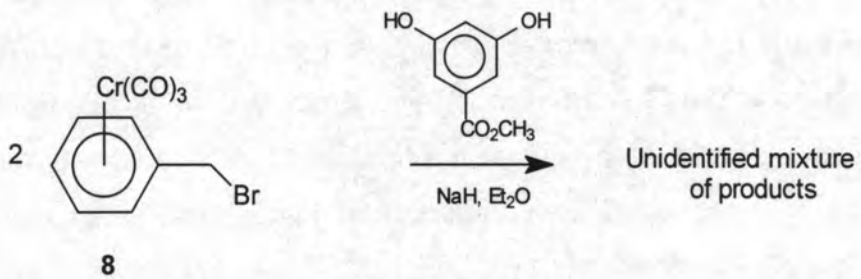


**Scheme 2.10**

**Alternative synthetic routes**

All avenues of synthesis via the first synthetic route, starting from benzyl alcohol, have been explored. The desired first generation wedge, containing two peripheral tricarbonyl chromium functionalities, was not synthesised by this approach, thus the second proposed synthetic route, outlined in Scheme 2.3, was investigated. The starting material in this synthesis was the pre-formed organic first generation alcoholic wedge **3**. Direct complexation of chromium hexacarbonyl to this wedge, was anticipated to produce a mixture of products. Scheme 2.3 indicates the desired product, a tris-complex, where all three aromatic rings are complexed with chromium tricarbonyl.

Typical complexation conditions were employed, with more than three equivalents of chromium hexacarbonyl in an attempt to complex all three rings. There is literature precedent of a benzyl alcohol group directing the complexation, through interaction of the oxygen with a chromium atom. [13] Thus, it seemed that the likely product of mono-complexation would be as shown in Figure 2.3 (a). This tricarbonyl chromium group should not be as available for reactions as peripheral groups would be, and so would be of less use catalytically. In order to have both of the peripheral aromatic rings complexed, the electron withdrawing effect of the tricarbonyl chromium group required consideration.

It is well documented that chromium-arene complexes form more easily with electron donating substituents on the aromatic ring. [10] Once the first chromium group has complexed, the electron-withdrawing nature of this moiety would diminish the likelihood of a proximal second ring being complexed. As the central ring is most likely to be complexed initially, this posed a problem. An excess of hexacarbonylchromium (3.7 equivalents) was employed, in an attempt to force the reaction to completion. In any event, the final reaction product was anticipated to be a mixture of the desired tris-complex, and the intermediates (a) and (b) as shown in Figure 2.3 below.

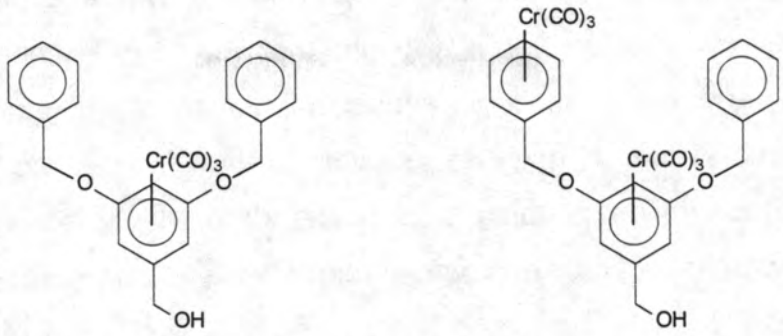


(a) (b)

**Figure 2.3:** Possible intermediates in the synthesis of the tris-complex

The complexation was carried out according to Scheme 2.11. Despite the careful thought that had gone into prediction of the reaction outcome, the final product was an unexpected single compound, the (toluene)tricarbonylchromium(0) complex **11** (44%). This known compound, has previously been formed as a side-product, in a reaction discussed earlier (see Scheme 2.9).

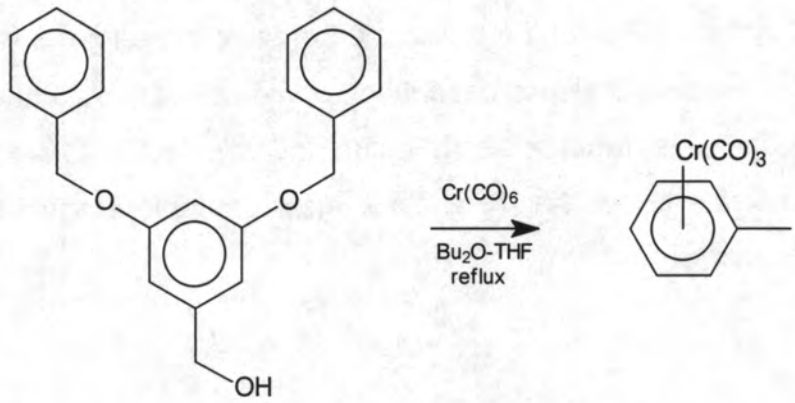


**3** **11**

**Scheme 2.11**

The complex **11** was identified by $^{1}H$ NMR, which displayed the distinctive methyl singlet at $\delta$ 2.18 ppm, and also by $^{13}C$ NMR, IR, and microanalysis. The melting point was substantially lower and took place over a broader range than the literature value. [11] This is possibly due to the presence of a small amount of higher molecular weight compounds, as evidenced by small high mass peaks in a mass spectrum of the product.

The formation of this product is unprecedented, and as yet no explanation can be found for this observation. It is thought that the high excess of chromium hexacarbonyl and harsh reaction conditions played a important role in the cleavage of the wedge. It might be possible to form the desired product in this manner, but under milder conditions, i.e. using a more labile source of chromium tricarbonyl - such as tricarbonylchromiumtriammine, and lower temperatures.

Phosphorus tribromide should be able to convert this tris-complexed alcoholic wedge to the bromide wedge, as this chemistry has already been established. However, the coupling of the resulting bromide wedge with the core molecule, might very well not lead to the desired first generation dendrimer. The same conditions are employed for coupling to 3,5-dihydroxybenzyl alcohol and to the core, and it has already been described that the benzyl bromide complex prefers to react with itself, rather than with the branching monomer, under these conditions.

The final conceptual approach toward synthesising organochromium dendrimers, was the direct complexation of the pre-formed organic dendrimer **5** with chromium hexacarbonyl. The results just described, of complexation to the pre-formed wedge, precluded this reaction from being investigated. The conditions for reaction would again be too harsh, and the most probable product would be the toluene complex **11**.

## 2.4 Related reactions

During the course of the work described in this chapter, several reactions were conducted, which were not directly part of the attempted dendrimer syntheses, but were in some way related. These reactions and their relation to the work done, are now described.

(Dibenzyl ether)bis[tricarbonylchromium(0)] **9** was synthesised, for the first time, during an attempted coupling reaction (see Scheme 2.7). As this compound should also be accessible by direct complexation, but had not yet been prepared

by this route, this reaction was attempted. Scheme 2.12 indicates the products formed.

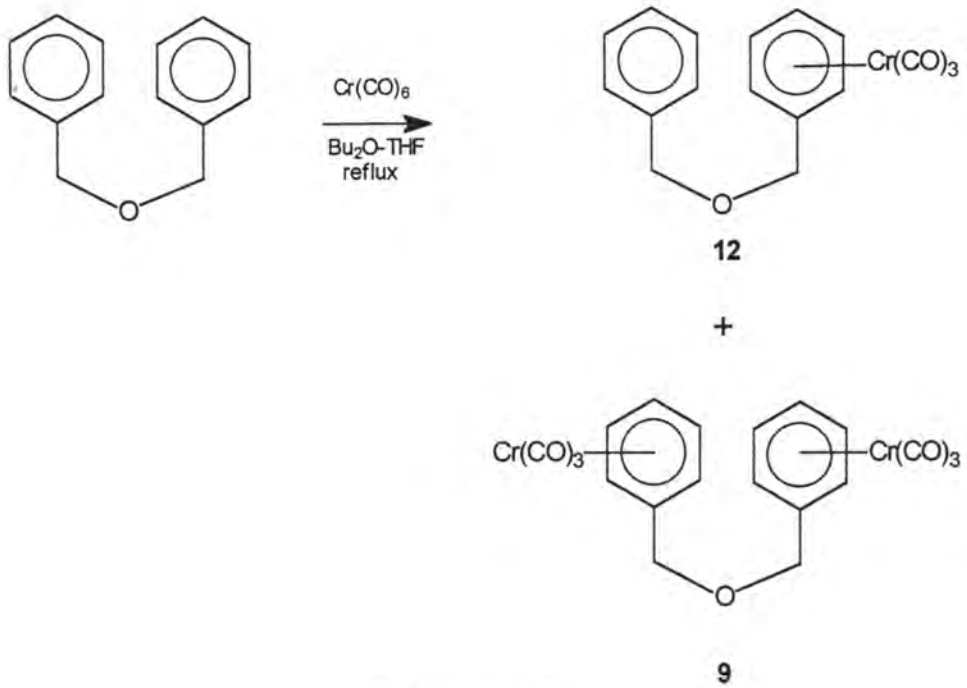


**Scheme 2.12**

The expected product **9**, was obtained in 49% yield, along with the intermediate monometallic species **12** in 34% yield. The relatively low yield of **9** can be attributed to the electron withdrawing character of the tricarbonylchromium group, which impedes complexation to the second ring. Excess hexacarbonylchromium was used in an attempt to force the reaction to completion, however the reaction was stopped when signs of decomposition were observed. The intermediate is a known compound, previously synthesised via a different route. [14] The overall yield for the reaction is 83%, a fairly typical yield for complexation reactions. (Dibenzyl ether)tricarbonylchromium(0) **12**, is a yellow oil, and was characterised by IR, $^{1}H$ and $^{13}C$ NMR and mass spectroscopy. The bimetallic species was characterised by melting point, IR and $^{1}H$ NMR, and was identical to that prepared previously.

As the bis-complex **9** is a bimetallic analogue of the chromium dendrimers, and an available material, the use of triphenylphosphine/carbon tetrabromide as a halogenating agent was investigated on this substrate. This reagent combination is used by Hawker and Fréchet for the conversion of alcoholic wedges to the corresponding bromide wedges. [1] Furthermore, it has already been established

that triphenylphosphine/carbon tetrabromide is not a suitable reagent for the conversion of benzylic alcohols to bromides if the aromatic ring is complexed to chromium tricarbonyl. The organometallic wedge envisaged to be synthesised by the first synthetic route, would effectively have a purely organic alcohol functionality, as the chromium would be complexed not to the central aromatic ring, but to a remote ring. (Dibenzyl ether)bis[tricarbonylchromium(0)] has no reactive functionality, and thus is an excellent substrate for examining whether the reagent combination triphenylphosphine/carbon tetrabromide will cause decomplexation of the peripheral chromium groups in a dendrimer.

From the reaction of (dibenzyl ether)bis[tricarbonylchromium(0)] with carbon tetrabromide/triphenylphosphine, under the same conditions as utilised for halogenation, [1] it was established that substantial decomplexation does occur. Scheme 2.13 shows the products of the reaction *viz.* the monometallic species first mentioned in the foregoing reaction scheme (Scheme 2.12), along with the completely decomplexed dibenzyl ether, in a 3:2 ratio.

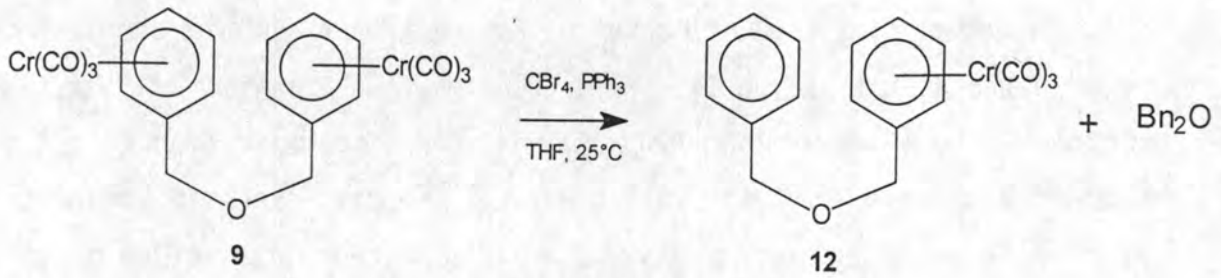


**Scheme 2.13**

The product mixture was identified by $^1$H-NMR. The mononuclear chromium complex **12** was also characterised by IR and mass spectra. These results demonstrate that carbon tetrabromide/triphenylphosphine should not be used as a halogenating agent in the presence of chromium arene complexes.

Finally, another chromium arene complex was synthesised, again for model study purposes. (Benzyl methyl ether)tricarbonylchromium(0) is a known compound. [14] It is also a simple model for the chromium groups at the surface of the dendrimer, which are benzyl phenyl ether complexes. The crystal structure of this compound,

has not previously been determined. This, along with the crystal structure detailed earlier, would provide useful information for the force-field calculations described in Chapter 3.

Benzyl methyl ether **13**, was prepared by methylation of benzyl alcohol with sodium hydride and methyl iodide (36 %). [14] Complexation of this compound with chromium hexacarbonyl, as shown in Scheme 2.14, afforded the desired product **14** (44%). The crystal structure of this compound was solved, and is displayed in Figure 2.4.

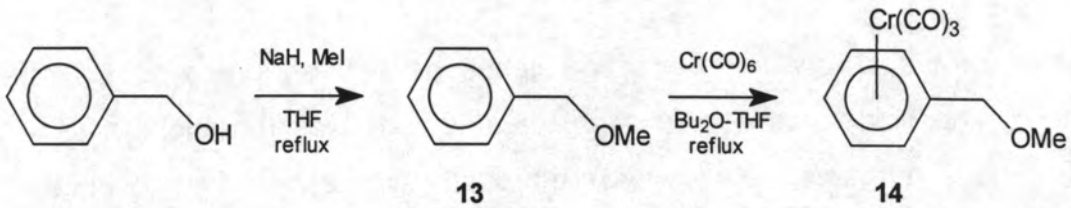


**13** **14**

**Scheme 2.14**

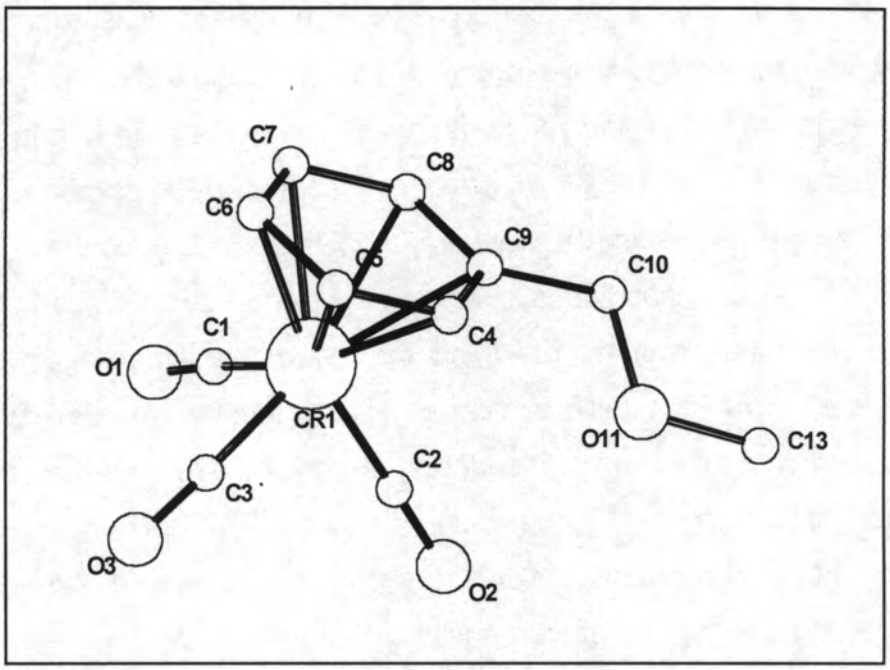


**Figure 2.4:** The crystal structure of the (benzyl methyl ether)tricarbonylchromium(0) complex **14**.

The compound crystallised in the space group $P\bar{1}$, with Z=2. The molecule is located in a general position, and thus a whole molecule constitutes the

asymmetric unit. More details regarding this crystal structure can be found in Chapter 3.

## 2.5 Conclusions

A first generation organic dendrimer, and the first generation benzylic alcohol and bromide wedges, have been synthesised. These compounds were prepared both as starting materials for the synthesis of chromium-containing dendrimers, and to establish the methodology for the corresponding chromium complexes at each stage of the synthesis.

Several of the chromium arene complexes have been prepared via different routes. The halogenation (activation) methodology was thoroughly investigated with various reagents. Phosphorus tribromide was established to be the best brominating reagent for all stages of the synthesis.

The coupling chemistry of the benzyl halide complexes was then examined. Although it was not possible to prepare a first generation chromium complexed dendritic wedge by any of the methods investigated, some new and interesting chemistry was discovered. A previously unreported complex, (dibenzyl ether)bis[tricarbonylchromium(0)] was prepared, both under coupling conditions and direct complexation conditions. This novel compound is an example of a bis-complexed diaromatic system, of which there are few other examples in the literature. It is also a bimetallic analogue of the dendrimers under investigation. This compound was fully characterised, and the crystal structure was determined. Further interesting chemistry was observed when (bibenzyl)tricarbonylchromium(0) was unexpectedly prepared under coupling conditions, along with (toluene)tricarbonylchromium(0).

Alternative routes to chromium arene dendrimers were also investigated, however the first generation chromium complexed wedge remained elusive. Lastly, a monometallic analogue of the peripheral chromium groups was synthesised *viz.* (benzyl methyl ether)tricarbonylchromium(0), and the crystal structure of this compound was determined.

## 2.6 Experimental details

Melting points were measured using a Reichert Thermovar hot-stage microscope and are uncorrected. Infrared spectra were recorded in solution unless specified, using a Perkin-Elmer Paragon 1000 FT-IR spectrometer, over the range 4000-800 $cm^{-1}$. Microanalyses were determined at the University of Cape Town, using a Fisons EA 1108 CHNS-O instrument. Mass spectra were recorded on a VG micromass 16F spectrometer operating at 70 eV with an accelerating voltage of 4 kV and a variable source temperature (depending on the nature of the compound). Accurate masses were determined on a VG-70E spectrometer at the Cape Technikon. Fast atom bombardment (FAB) mass spectra were also obtained from the Cape Technikon. All $^{1}$H-NMR spectra were recorded, unless otherwise specified, as deuteriochloroform solutions using tetramethylsilane as an internal standard on a Varian VXR-200 (200 MHz) or a Varian Unity Spectrometer (400 MHz). $^{13}$C-NMR spectra were recorded on the same instruments at 50 or 100 MHz, also using tetramethylsilane as an internal standard.

Thin layer chromatography was performed on aluminium backed silica gel or aluminium oxide 60 $F_{254}$ plates in a variety of solvent systems, using the ascending technique. The plates were visualised by UV light or by anisaldehyde spray [freshly prepared from a 2.5% solution of *p*-methoxybenzaldehyde in ethanol (20 $cm^3$) and 18M sulphuric acid (1$cm^3$)], followed by baking at 200°C. Column chromatography was conducted with Merck Kieselgel 60 (70-230 mesh for gravity and 230-400 mesh for flash chromatography).

All reactions were carried out under an atmosphere of high purity nitrogen using standard Schlenk tube techniques, unless stated otherwise. Reactions containing chromium reagents were protected from light with aluminium foil.

All solvents used were analytical grade and were purified by distillation under a nitrogen atmosphere as described in the following text. Tetrahydrofuran (THF), and diethyl ether were dried by distillation over sodium/benzophenone. Hexane, benzene and toluene were distilled over sodium wire. Dichloromethane was distilled over anhydrous $CaCl_2$ and acetone was distilled over Drierite®.

All reagents used were supplied commercially by Aldrich, STREM Chemicals or BDH. Potassium carbonate was dried at 200°C for several hours before use.

The following abbreviations are used to assign NMR data for the dendrimers and wedges: Ar refers to aromatic rings derived from the monomer **1**, Ph refers to aromatic rings at the periphery of the molecule, and Ar' refers to aromatic rings derived from the core molecule.

A list of other abbreviations used can be found at the beginning of this thesis.

**3,5-Dihydroxybenzyl alcohol 1**

Trimethylsilylchloride (400 μl, 2.95 mmol) was added to a stirred suspension of methyl-3,5-dihydroxy benzoate (5.00 g, 29.7 mmol) in hexamethyldisilazane (10 $cm^3$). The resulting mixture was refluxed for 5h. The suspension changed to a solution, which was stirred for 16h at 25°C, while a white deposition formed on the glass surface above the solution. Diethyl ether (20 $cm^3$) was added, and the mixture was filtered. The flask was rinsed out with a further portion of diethyl ether (10 $cm^3$), filtered, and the solvent was removed under reduced pressure from the combined filtrates to give a pale yellow oil with low viscosity. The oil was dissolved in THF and slowly added over 1.5h to a heavily stirred suspension of lithium aluminium hydride (1.50 g, 39.5 mmol) in THF (100 $cm^3$). The mixture was refluxed for 4h and left stirring at 25°C for 17h, then saturated aqueous ammonium chloride (25 $cm^3$) was added dropwise, followed by 1M hydrochloric acid (*ca* 3 $cm^3$) in a similar fashion until the pH reached 3. The suspension was filtered and the solvent removed under reduced pressure to give a solid residue, which was washed with diethyl ether (3x 50 $cm^3$) and then dried under reduced pressure to afford the product **1** (3.274 g, 79%), m.p. 180-182°C (lit.,[7] 181-184°C); $\delta_H$ (400 MHz, $d_6$-acetone) 4.46 (2H, s, ArC$H_2$O), 6.22 (1H, m, Ar*H*), 6.35 (2H, m, Ar*H*); $\delta_C$ (100 MHz) 63.7 ($CH_2$OH), 101.0 (*p-C*), 104.8 (*o-C*), 144.7 (*ipso-C*), 158.4 (*m-C*).

**3,5-Bis(benzyloxy)benzyl alcohol 3**

a) Methyl-3,5-bis(benzyloxy)benzoate **2** (467 mg, 1.34 mmol) was added to a stirred suspension of lithium aluminium hydride (78 mg, 2.06 mmol) in diethyl ether (5 $cm^3$) and the resulting mixture was refluxed for 2.5h. A further portion of lithium aluminium hydride (60 mg, 1.58 mmol) was added and the mixture was refluxed for 17h. The reaction was quenched by the dropwise addition of water (10 $cm^3$) to the cooled reaction mixture, followed by addition of sulphuric acid (1 M, *ca* 10 $cm^3$) to dissolve the resulting residue. The mixture was extracted with diethyl ether (3x 20 $cm^3$), the combined organic phase was washed with brine (2x 15 $cm^3$), dried ($Na_2SO_4$) and evaporated under reduced pressure to give the product **3** (403 mg, 94%), m.p. 81-82°C (from methanol) (lit.,[2] 85-86°C) (Found: C, 78.5; H, 6.6%; $M^+$ 320. Calc. for $C_{21}H_{20}O_3$: C, 78.7; H, 6.3%; *M* 320); $\delta_H$ (200 MHz) 2.91 (1H, s $D_2O$ exch., $CH_2OH$), 4.61 (2H, s, $CH_2OH$), 5.05 (4H, s, $PhCH_2OAr$), 6.68 (3H, m, Ar*H*), 7.45 (10H, m, Ph*H*); $\delta_C$ (50 MHz) 64.9 ($CH_2OH$), 70.0 ($PhCH_2OAr$), 101.2, 105.8 (Ar *C*), 127.4, 127.9, 128.5 ( Ph *C*), 136.8, 143.6, 160.0 (Ph or Ar *C*).

b) Benzyl bromide (4.32 g, 25.3 mmol) was added to a vigorously stirred mixture of 3,5-dihydroxybenzyl alcohol **1** (1.77 g, 12.6 mmol), potassium carbonate (4.37 g, 31.6 mmol) and 18-crown-6 (0.7 g, 2.5 mmol) in acetone (100 $cm^3$) and the resulting mixture was refluxed for 30h. A further portion of benzyl bromide (1.14 g, 6.7 mmol) was added and the mixture was refluxed for 18h, then allowed to cool and evaporated under reduced pressure. The residue was partitioned between water (20 $cm^3$) and dichloromethane (20 $cm^3$) and the aqueous phase extracted with dichloromethane (3x 20 $cm^3$). The combined organic phase was dried ($Na_2SO_4$) and evaporated under reduced pressure to give a residue (3.78 g) which was chromatographed on silica gel (76 g) using ethyl acetate-toluene (1:19) as eluent to give the product **3** (1.68 g, 42%) which was identical to that prepared in the previous experiment.

**3,5-Bis(benzyloxy)benzyl bromide 4**

a) A solution of phosphorous tribromide (33 μl, 0.35 mmol) in benzene (25 $cm^3$) was added to a cooled (0°C), stirred solution of 3,5-bis(benzyloxy)benzyl alcohol **3** (300mg, 0.94 mmol) in benzene (2 $cm^3$). The resulting mixture was stirred for 15 min. at 0°C and for 2.5h at 25°C and then poured into ice-water. The benzene was removed under reduced pressure, and the residual solution was extracted with diethyl ether (2x 15 $cm^3$) and chloroform (2x 15 $cm^3$). The combined organic phase was dried ($MgSO_4$) and evaporated under reduced pressure to give the product **4** (245 mg, 76%), m.p. 85-87°C (from hexane) (lit.,[2] 92-93°C) (Found: C, 65.7; H, 5.4%. Calc. for $C_{21}H_{19}O_2Br$: C, 65.8; H, 5.0%); $\delta_H$ (200 MHz) 4.42 (2H, s, $CH_2Br$), 5.03 (4H, s, $PhCH_2OAr$), 6.60 (3H, m, Ar*H*), 7.40 (10H, m, Ph*H*); $\delta_C$ (50 MHz) 33.5 ($CH_2Br$), 70.2 ($PhCH_2OAr$), 102.3, 108.2 (Ar *C*), 127.5, 128.1, 128.6 (Ph *C*), 136.7, 139.8, 160.1 (Ph or Ar *C*).

b) Triphenylphosphine (205 mg, 0.78 mmol) was added to a stirred solution of 3,5-bis(benzyloxy)benzyl alcohol **3** (200 mg, 0.62 mmol) and carbon tetrabromide (260 mg, 0.78 mmol) in THF (1 $cm^3$). The resulting mixture was stirred at 25°C for 20 min., then poured into water and extracted with dichloromethane (3x 25 $cm^3$). The combined organic phase was dried ($Na_2SO_4$) and evaporated under reduced pressure to give a crystalline mass (346 mg) which was chromatographed on silica gel (10 g) using ethyl acetate-toluene (1:19) to afford the product **4** (106 mg, 44%) which was identical to that prepared in the previous experiment.

**First generation organic dendrimer 5**

3,5-Bis(benzyloxy)benzyl bromide **4** (100 mg, 0.26 mmol) was added to a vigorously stirred mixture of 1,1,1-tris(4'-hydroxyphenyl)ethane (CORE) (26 mg, 0.08 mmol), potassium carbonate (47 mg, 0.4 mmol) and 18-crown-6 (7 mg, 0.03 mmol) in acetone (15 $cm^3$) and the resulting mixture was refluxed for 48h. A further portion of CORE (26 mg, 0.08 mmol) was added, and the mixture was refluxed for 21h. After cooling and removal of the solvent under reduced pressure,

the residue was partitioned between water (20 $cm^3$) and dichloromethane (20 $cm^3$). The aqueous phase was extracted with dichloromethane (3x 20 $cm^3$), the combined organic phase was dried ($MgSO_4$) and the solvent was removed under reduced pressure to give a gummy residue (119 mg). This residue was flash chromatographed on silica gel (10 g) using dichloromethane-hexane (3:1) to give the product **5** (45 mg, 44%) as a gum; *m/z* 1212,1213 (FAB); $\nu_{max}/cm^{-1}$ 1601, 1457, 1375, 1168 and 1068 ($CH_2Cl_2$); $\delta_H$ (200 MHz) 2.12 (3H, s, C*H*$_3$), 4.99 (6H, s, ArC*H*$_2$O), 5.04 (12H, s, PhC*H*$_2$O), 6.57 (3H, t, *J*= 2 Hz, Ar*H*), 6.65 (6H, d, *J*= 2 Hz, Ar*H*), 6.82, (6H, d, *J*= 9 Hz, core Ar'*H*), 6.97 (6H, d, *J*= 9 Hz, core Ar'*H*), 7.28-7.46 (30H, m, Ph*H*); $\delta_C$ (50 MHz) 30.8 (*C*H$_3$), 50.7 (*C*CH$_3$), 70.0 (ArCH$_2$O), 70.1 (PhCH$_2$O), 101.6, 106.4 (Ar *C*), 114.1 (core Ar' *C*), 127.6, 128.0, 128.6 ( Ph *C*H), 129.7 (core Ar' *C*), 136.8, 139.7, 142.1, 156.8, 160.2 (Ar, Ar' and Ph *C*), followed by impure product (70 mg).

**(Benzyl alcohol)tricarbonylchromium(0) 6**

Chromium hexacarbonyl (414 mg, 1.85 mmol) was added to a stirred solution of benzyl alcohol (0.2 $cm^3$, 1.85 mmol) in dibutyl ether (10 $cm^3$) and THF (1 $cm^3$), and the resulting mixture was refluxed for 24h. The reaction mixture was allowed to cool, filtered through deactivated alumina and washed with dichloromethane. The solvent was evaporated under reduced pressure to yield a yellow crystalline product **6** (378 mg, 84%), m.p. 94-95°C (dichloromethane-hexane) (lit.,[3] 95.5-96.5°C); $\nu_{max}/cm^{-1}$ 3606br (OH), 1969vs and 1891vs (CO) ($CH_2Cl_2$); $\delta_H$ (200 MHz) 1.95 (1H, t, *J*= 6 Hz, $D_2O$ exch., O*H*), 4.48 (2H, d, *J*= 6 Hz, ArC*H*$_2$O), 5.28-5.46 (5H, m, Ar*H*); $\delta_C$ (50 MHz) 63.3 (*C*H$_2$OH), 91.7 (*p-C*), 90.8, 93.0 (*o*- and *m*- *C*), 111.8 (*ipso-C*), 232.7 (*C*O).

**(Benzyl chloride)tricarbonylchromium(0) 7**

(Benzyl alcohol)tricarbonylchromium(0) **6** (84 mg, 0.34 mmol) in benzene (5 $cm^3$) was shaken with concentrated hydrochloric acid (10 M, 4 $cm^3$) for 10 min. The

benzene layer was separated and washed with distilled water (2x 10 $cm^3$) and dried ($Na_2SO_4$). The solvent was removed under reduced pressure to give a yellow solid (36 mg), which was dissolved with dichloromethane and filtered through a small pad of alumina. After removal of the solvent under reduced pressure, recrystallisation from hexane gave impure product **7** as a yellow crystalline solid (30 mg, 33%), m.p. 60-62°C (lit.,[4] 63-64°C) (Found: C, 45.3; H, 2.7%. Calc. for $C_{10}H_7ClCrO_4$: C, 45.7; H, 2.7%); $\nu_{max}/cm^{-1}$ (CO) 1974vs and 1899vs ($CH_2Cl_2$); $\delta_H$ (200 MHz) 4.27 (2H, s, ArC$H_2$Cl), 5.36 (5H, s, Ar*H*) (also observed were small signals at $\delta$ 4.70 (s) and 7.40 (s), probably due to decomplexed benzyl chloride); $\delta_C$ (50 MHz) 45.1 (*C*$H_2$Cl), 91.6 (*p-C*), 92.3, 92.8 (*o-* and *m-C*), 102.8 (*ipso-C*), 231.9 (*C*O) (also observed were small signals at $\delta$ 126.9, 127.7 and 128.6 due to decomplexed benzyl chloride).

**(Benzyl bromide)tricarbonylchromium(0) 8**

a) Boron tribromide (1 M in dichloromethane, 4 $cm^3$, 4 mmol) was added to a stirred suspension of (benzyl alcohol)tricarbonylchromium(0) **6** (0.5 g, 2.0 mmol) in dichloromethane (34 $cm^3$) at –78°C. The resulting yellow-brown solution was stirred at –78°C for 1h, after which a further portion of boron tribromide (1.2 $cm^3$, 1.2 mmol) was added, and the mixture was stirred at –78°C for a further 40 min. The reaction was quenched by the addition of sat. aq. sodium hydrogen carbonate (15 $cm^3$) and the product mixture was allowed to warm to room temperature before adding water (15 $cm^3$). The aqueous phase was extracted with diethyl ether (40 $cm^3$ and 20 $cm^3$), washed with brine (2x 15 $cm^3$) and dried ($MgSO_4$), then filtered through Celite and evaporated under reduced pressure to yield the complex **8** as a yellow solid (513.5 mg, 84%), m.p. 71-74°C (lit.,[8] 73-75°C); $\nu_{max}/cm^{-1}$ (CO) 1983vs, 1921vs and 1914vs (cyclohexane); $\delta_H$ (200 MHz) 4.14 (2H, s, C$H_2$Br), 5.35 (5H, s, Ar*H*); $\delta_C$ (50 MHz) 31.8 (*C*$H_2$Br), 91.6 (*p-C*), 92.3 93.3 (*o-* and *m-C*), 105.5 (*ipso-C*), 232.0 (*C*O).

b) A solution of phosphor us tribromide (43 µl, 0.45 mmol) in toluene (20 $cm^3$) was added to a cooled (0°C), stirred solution of (benzyl alcohol)tricarbonylchromium(0)

**6** (300 mg, 1.23 mmol) in toluene (2 $cm^3$). The resulting mixture was stirred for 3h at 0°C, after which a further portion of phosphorous tribromide (30 μl, 0.31 mmol) was added. This mixture was stirred at 0°C for 5h, then the reaction was quenched by the addition of sat. aq. sodium hydrogen carbonate (10 $cm^3$) followed by water (4 $cm^3$). The aqueous phase was extracted with diethyl ether (40 $cm^3$ and 20 $cm^3$) and the combined organic phase was dried ($MgSO_4$) and filtered through Celite. The solvent was removed under reduced pressure to give the product **8** (328 mg, 87%) which was identical to that prepared in the previous experiment.

c) Triphenylphosphine (65 mg, 0.25 mmol) was added to a stirred solution of (benzyl alcohol)tricarbonylchromium(0) **6** (50 mg, 0.20 mmol) and carbon tetrabromide (82 mg, 0.25 mmol) in THF (1 $cm^3$). The reaction mixture was stirred for 10 min., followed by the addition of further portions of triphenylphosphine (65 mg, 0.25 mmol) and carbon tetrabromide (0.8 mg, 0.25 mmol). The mixture was stirred for a further 10 min at which time TLC ($Ch_2Cl_2$) indicated the presence of a yellow product along with some starting material. The solution had started to go cloudy, so the reaction mixture was poured into water (10 $cm^3$) and extracted with dichloromethane (3x 15 $cm^3$). The product solution was concentrated under reduced pressure to give a bright yellow oil which decomposed while drying under high vacuum. TLC ($CH_2Cl_2$) of the residue showed that no yellow compounds were present.

**(Dibenzyl ether) bis[tricarbonylchromium(0)] 9**

(Benzyl chloride)tricarbonylchromium(0) **7** (440 mg, 1.67 mmol) was added to a vigorously stirred mixture of 3,5-dihydroxybenzyl alcohol **1** (116 mg, 0.80 mmol), potassium carbonate (330 mg, 2.38 mmol) and 18-crown-6 (42 mg, 0.15 mmol) in acetone (18 $cm^3$). The resulting yellow solution was refluxed for 41h, after which further portions of potassium carbonate (150 mg, 1.08 mmol) and 18-crown-6 (42 mg, 0.15 mmol) were added and the mixture was refluxed for a further 51h. The reaction mixture was cooled and the solvent was removed under reduced

pressure. The resulting dark green oil was redissolved in dichloromethane and filtered through deactivated alumina, to give a clear yellow solution. The solvent was removed under reduced pressure, to give a yellow residue (571 mg) which was adsorbed onto deactivated alumina (50 g) and eluted with dichloromethane-hexane (3:7) to afford unchanged material **7** (100 mg, 23%). Further elution with dichloromethane afforded the *product* **9** (184 mg, 47%), m.p. 128-130°C (Found: C, 51.1; H, 2.95%; $M^+$ 470. $C_{20}H_{14}Cr_2O_7$ requires C, 51.1; H, 3.0%; *M* 470); $\nu_{max}/cm^{-1}$ (CO) 1970vs and 1892vs ($CH_2Cl_2$); $\delta_H$ (400 MHz) 4.36 (4H, s, ArC$H_2$O), 5.26-5.44 (10H, m, Ar*H*); $\delta_C$ (100 MHz) 70.4 (*C*$H_2$O), 93.7 (*p-C*), 93.8, 94.8 (*o*- and *m-C*), 111.0 (*ipso-C*), 191.1 (*C*O).

**Reaction of (benzyl bromide)tricarbonylchromium(0) 8 with 3,5-dihydroxybenzyl alcohol 1**

(Benzyl bromide)tricarbonylchromium(0) **8** (478 mg, 1.63 mmol) was added to a vigorously stirred mixture of 3,5-dihydroxybenzyl alcohol **1** (104 mg, 0.74 mmol), potassium carbonate (256 mg, 1.85 mmol) and 18-crown-6 (39 mg, 0.15 mmol) in acetone (10 $cm^3$). The mixture was refluxed for 117 h, and it was observed that the heterogeneous mixture changed from an initial yellow colour to an orange colour within an hour of refluxing. The reaction mixture was allowed to cool, and the residue partitioned between water (15 $cm^3$) and dichloromethane (30 $cm^3$). The aqueous phase was extracted with dichloromethane (2x 25 $cm^3$), the combined organic phase was filtered through Celite and the solvent was removed under reduced pressure. The resulting residue (224 mg) was chromatographed on silica gel (23 g). Elution with dichloromethane-hexane (3:7) afforded an inseparable mixture of (bibenzyl)tricarbonylchromium(0) **10** and (toluene)tricarbonylchromium(0) **11** (40 mg); *m/z* 318, 228; $\nu_{max}/cm^{-1}$ (CO) 1968vs and 1890vs ($CHCl_3$); $\delta_H$ (400 MHz) (for **10** *ca* 50%) 2.70 (1H, t, *J*= 6.8 Hz, ArC$H_2$), 2.90 (1H, t, *J*= 6.8 Hz, ArC$H_2$), 5.12-5.20 (3H, m, *o*- and *p-H*), 5.41 (1H, t, *J*= 6.4 Hz, *m-H*), 7.14 (2H, d, *J*= 7.2 Hz, *o-H*), 7.17-7.25 (1H, m, *p-H*), 7.29 (2H, t, *J*= 7.2 Hz, *m-H*); (for **11**, *ca* 50%) 2.19 (3H, s, C$H_3$), 5.08 (2H, d, *J*= 6.8 Hz, *o-H*), 5.12-5.20 (1H, m, *p-H*), 5.35 (1H, t, *J*= 6.8 Hz, *m-H*); $\delta_C$ (100 MHz) (for **10**) 37.1, 37.3

($ArCH_2$), 90.4 (*p-C*), 92.7( *o-C*), 94.3 (*m- C*), 112.5 (*ipso-C*), 126.4 (*p-C*), 128.4, 128.5 (*o-* and *m-C*), 140.0 (*ipso-C*), 233.1 (*CO*); (for **11**) 20.8 ($CH_3$), 89.6 (*p-C*), 92.6 (*o-C*), 93.7 (*m-C*), 109.6 (*ipso-C*), 233.2 (*CO*). Further elution with dichloromethane and methanol failed to provide any characterisable products.

**Reaction of (benzyl bromide)tricarbonylchromium(0) 8 with methyl 3,5-dihydroxybenzoate**

Sodium hydride (57 mg, 2.38 mmol) was added to a stirred solution of methyl 3,5-dihydroxybenzoate (76 mg, 0.46 mmol) in diethyl ether (5 $cm^3$). The resulting suspension was stirred at 30°C for 3h. A solution of (benzyl bromide)tricarbonylchromium(0) **8** in diethyl ether (3 $cm^3$) was added to the cooled (0°C) mixture, and the resulting suspension was stirred at 25°C for 18h. No reaction was observed (TLC). The solvent was removed by evaporation to give and orange solid residue, which was redissolved in THF (2 $cm^3$), and the mixture was refluxed for 1h. The reaction mixture was cooled, and quenched by the addition of water (15 $cm^3$). The aqueous phase was extracted with diethyl ether (3x 15 $cm^3$) and the combined organic phase washed with brine (15 $cm^3$), dried ($MgSO_4$), and filtered through Celite. The solvent was removed under reduced pressure to give an orange residue (330 mg). Chromatography on silica gel (33 g) eluting with dichloromethane-hexane (gradient elution 30→100%) failed to isolate any characterisable products.

**Complexation of chromium hexacarbonyl to 3,5-bis(benzyloxy)benzyl alcohol 3**

Chromium hexacarbonyl (330 mg, 1.50 mmol) was added to a stirred solution of 3,5-bis(benzyloxy)benzyl alcohol **3** (150 mg, 0.47 mmol) in dibutyl ether (9 $cm^3$) and THF (1 $cm^3$), and the resulting yellow solution was refluxed for 21h. A further portion of chromium hexacarbonyl (50 mg, 0.23 mmol) was then added, and the mixture was refluxed for 3h. The solution was allowed to cool and was concentrated under reduced pressure. This concentrate was filtered through

deactivated alumina and washed with dichloromethane to give a clear yellow solution. The solvent was evaporated under reduced pressure to yield a dark yellow solid (100 mg), which was chromatographed on silica gel (10 g), eluting with dichloromethane-hexane (3:7) to give (toluene)tricarbonylchromium(0) **11** (47 mg, 44%), m.p. 63-67°C (hexane) (lit.,[11a] 81-82.5°C) (Found: C, 52.8; H, 3.8%; $M^+$ 228. Calc. for $C_{10}H_8CrO_3$: C, 52.6; H, 3.5%; *M* 228); $\nu_{max}/cm^{-1}$ (CO) 1979s and 1910vs (hexane); $\delta_H$ (200 MHz) 2.18 (3H, s, ArC$H_3$), 4.9-5.5 (5H, m, Ar*H*); $\delta_C$ (50 MHz) 20.8 (*C*$H_3$), 89.6 (*p-C*), 92.7 (*o-C*), 94.3 (*m-C*), 109.5 (*ipso-C*), 233.2 (*C*O).

**Complexation of chromium hexacarbonyl to dibenzyl ether**

Chromium hexacarbonyl (2.43 g, 11.0 mmol) was added to a stirred solution of dibenzyl ether (1 $cm^3$, 5.26 mmol) in dibutyl ether (45 $cm^3$) and THF (4 $cm^3$), and the resulting yellow solution was refluxed for 29h. A further portion of chromium hexacarbonyl (0.50 g, 2.3 mmol) was then added, and the mixture was refluxed for 3h. The solution was allowed to cool and the solvent removed under reduced pressure to give a yellow solid with some dark decomposition product present. The resulting residue was redissolved in dichloromethane and filtered through Celite to give a clear yellow solution. The solvent was evaporated under reduced pressure to once again give a yellow solid along with some decomposition product (2.251 g). This mixture was flash chromatographed on silica gel (80 g) eluting with toluene-hexane (9:1) to give (dibenzyl ether)tricarbonylchromium(0) **12** as a yellow oil (216 mg), followed by mixed fractions. The mixed fractions were flash chromatographed on silica gel (150 g), eluting with toluene-hexane (9:1) to afford a further portion of **12** (374 mg, 34% combined); *m/z* 334; $\nu_{max}/cm^{-1}$ (CO) 1981vs and 1913vs (hexane); $\delta_H$ (400 MHz) 4.17 (2H, s, ArC$H_2$O), 4.55 (2H, s, ArC$H_2$O), 5.15-5.30 (5H, m, Ar*H*), 7.15-7.30 (5H, m, Ar*H*); $\delta_C$ (100 MHz) 70.2 (Ar*C*$H_2$O), 73.0 (Ar*C*$H_2$O), 91.5 (*p-C*), 92.0, 92.8 (*o-* and *m-C*), 107.9 (*ipso-C*), 127.9 (*p-C*), 127.7, 128.5 (*o-* and *m-C*), 137.4 (*ipso-C*), 232.6 (*C*O) (some small peaks due to uncomplexed dibenzyl ether are also present), followed by **9** (1.199 g, 48.5%), m.p. 126-127°C (dichloromethane-hexane); *m/z* 470, $\nu_{max}/cm^{-1}$ (CO) 1970vs and 1890vs ($CH_2Cl_2$); $\delta_H$ (200 MHz) 4.35 (4H, s, ArC$H_2$O), 5.25-5.43 (10H, m, Ar*H*).

**Carbon tetrabromide/Triphenylphosphine treatment of (dibenzyl ether) bis[tricarbonylchromium(0)] 9**

a) Triphenylphosphine (22 mg, 0.082 mmol) was added to a stirred solution of (dibenzyl ether)bis[tricarbonylchromium(0)] **9** (50 mg, 0.11 mmol) and carbon tetrabromide (27mg, 0.082 mmol) in a minimum volume of THF (*ca* 1 $cm^3$). The reaction mixture was stirred for 10 min, followed by the addition of further portions of triphenylphosphine (22 mg, 0.082 mmol) and carbon tetrabromide (27 mg, 0.082 mmol). The resulting mixture was stirred for a further 10 min. Removal of solvent and chromatography of the residue over silica gel (10 g) afforded an inseparable mixture of dibenzyl ether and (dibenzyl ether)tricarbonylchromium(0) **12** (15 mg); *m/z* 334; $\nu_{max}/cm^{-1}$ (CO) 1981vs and 1913vs (hexane); $\delta_H$ (400 MHz) (for dibenzyl ether *ca* 60%) 4.50 (4H, s, ArC$H_2$O), 7.2-7.4 (10H, m, Ar*H*); (for **12** *ca* 40%) 4.18 (2H, s, ArC$H_2$O), 4.57 (2H, s, ArC$H_2$O), 5.20-5.40 (5H, m, Ar*H*), 7.20-7.40 (5H, m, Ar*H*).

**Benzyl methyl ether 13**

Sodium hydride (60% w/w in mineral oil) (2.2 g, 55 mmol) was washed with hexane (2x 25 $cm^3$). A solution of benzyl alcohol (4.9 $cm^3$, 47 mmol) in THF (25 $cm^3$) was added and the mixture was stirred for 3.5h. Methyl iodide (3.4 $cm^3$, 55 mmol) was added to the cooled solution (0°C) and the mixture was stirred at 25°C for 16h. Diethyl ether (100 $cm^3$) was added and the mixture was filtered through Celite. Evaporation under reduced pressure, followed by distillation afforded the product **13** as a colourless liquid (2.07 g, 36%), b.p. 29-30°C (0.1 mmHg) [lit.,[14] 29-30°C (0.1mmHg )]; $\nu_{max}/cm^{-1}$ 1104, 740 and 694 (film); $\delta_H$ (200 MHz) 3.41 (3H, s, C$H_3$), 4.49 (2H, s, PhC$H_2$O), 7.36 (5H, m, Ph*H*); $\delta_C$ (50 MHz) 58.0 (O$CH_3$), 74.7 (Ph$CH_2$O), 127.6 (*p-C*), 127.7 (*m-C*), 128.3 (*o-C*), 138.2 (*ipso-C*).

**(Benzyl methyl ether)tricarbonylchromium(0) 14**

Chromium hexacarbonyl (2.87 g, 13.0 mmol) was added to a stirred solution of benzyl methyl ether **13** (1.06g , 8.68 mmol) in dibutyl ether (48 $cm^3$) and THF (5 $cm^3$), and the resulting mixture was refluxed for 24h. The reaction mixture was allowed to cool, and was filtered through a small pad of silica. The solvent was evaporated under reduced pressure to yield a yellow solid (2.27 g), a portion of which was recrystallised from dichloromethane-hexane to give the product **14** (0.97g, 44%), m.p. 38-40°C (lit.,[14] 40°C); *m/z* 258; $\nu_{max}/cm^{-1}$ (CO) 1970vs and 1887vs ($CH_2Cl_2$); $\delta_H$ (200 MHz) 3.44 (3H, s, $OCH_3$), 4.16 (2H, s, $ArCH_2O$), 5.21-5.42 (5H, m, Ar*H*); $\delta_C$ (50 MHz) 58.9 ($OCH_3$), 72.9 ($ArCH_2O$), 91.4 (*p-C*), 91.9, 92.8 (*o-* and *m-C*), 107.7 (*ipso-C*), 232.6 (*C*O).

**Preparation of crystals of (dibenzyl ether)bis[tricarbonylchromium(0)] 9**

Single crystals of (dibenzyl ether)bis[tricarbonylchromium(0)] were recrystallised from dichloromethane-hexane at 3° C.

**Preparation of crystals of (methyl ethyl ether)tricarbonylchromium(0) 14**

Single crystals of (methyl ethyl ether)tricarbonylchromium(0) were recrystallised from dichloromethane-hexane at 3° C.

## 2.7 References


1. C.J. Hawker and J.M.J. Fréchet, *J. Am. Chem. Soc.*, 1990, **112**, 7638-7647
2. E. Reimann, *Chem. Ber.*, 1969, **102**, 2881
3. B. Nicholls and M.C. Whiting, *J. Chem. Soc.*, 1959, 551
4. J.D. Holmes, D.A.K. Jones and R. Pettit, *J. Organomet. Chem.*, 1965, **4**, 324
5. C.A.L. Mahaffy and P.L. Pauson, *Inorg. Synth.*, 1971, **19**, 154
6. H.G. Wey and H. Butenschön, *Chem. Ber.*, 1990, **123**, 93
7. .C.G. Pitt, Y. Sayed, H.H. Seltzmann, C.W. Twine Jr. and D.L. Williams, *J. Org. Chem.*, 1979, **44**, incl. p 679
8. S.E. Gibson and G.A. Schmid, *J. Chem., Soc. Chem. Commun.*, 1997, 865

9. *Dictionary of Organometallic Compounds*, J. Buckingham and J. Macintyre, Chapman and Hall, London, 1984, vol.1, pp. 539-566
10. A.Solladié-Cavallo, *Polyhedron*, 1985, **4**, 901
11. F. van Meurs, J.M. van der Toorn and H. van Bekkum, *J. Organomet. Chem.*, 1976, **113**, 341. W.R. Jackson, C.F. Pincombe, I.D. Rae and S. Thapebinkarn, *Aust. J. Chem.*, 1975, **28**, 1535
12. G.R. Knox, D.G. Leppard, P.L. Pauson and W.E. Watts, *J. Organomet. Chem.*, 1972, **34**, 347
13. *Comprehensive Organometallic Chemistry II*, E.W. Abel, F.G.A. Stone, G. Wilkinson, J.A. Labinger and M.J. Winter, Pergamon, New York, 1995, vol. 9, ch.8, p. 504
14. J. Blagg, S.G. Davies, N.J. Holman, C.A. Laughton and B.E. Mobbs, *J. Chem. Soc., Perkin Trans.1*, 1986, 1581

# Chapter 3 Parameterisation of a dendrimer force field

## 3.1 Introduction

As was stated in Chapter One, the second aspect of the work presented in this thesis was an investigation into the structure of both organic and organochromium poly(benzyl phenyl ether) dendrimers by molecular mechanics and molecular dynamics techniques. As far as we are aware, no such studies have been carried out on these dendrimers, and no calculations have been performed at all on organometallic dendrimers. At the beginning of the study, several issues needed to be addressed:

- The choice of methodology – which methods are best suited to the purpose of the study.
- The theoretical basis of the chosen methods.
- What modifications are necessary to study the novel systems.

All of these issues are addressed in this chapter. Chapter Four deals with the simulation and analysis of generations one through five of both the organic and organometallic dendrimers.

## 3. 2 Methodology.

Computational chemistry can be broadly divided into two approaches, one empirical and the other mechanical. The empirical approach relies solely on experimental data and is very limited in terms of the properties which can be investigated. The mechanics approach uses the laws of physics as its basis, and thus allows a far wider range of physical properties to be examined. This approach can be further subdivided into the fields of statics and dynamics calculations. Statics calculations investigate the molecule in a stationary state, whereas dynamics calculations explore the phase space of the molecule.

In mechanics calculations, whether static or dynamic, the system can be treated either classically or quantum mechanically. The choice between the approaches is made on the basis of the property under investigation. If the problem is dominated by electronic effects, such as in a chemical reaction, then electronic structure methods are used. These calculations are based on the laws of quantum mechanics, and solve the Schrödinger equation. The technique of **quantum mechanics** is used for static calculations, and **quantum molecular dynamics** for dynamics calculations. These calculations are extremely CPU intensive and are usually only carried out on relatively small molecules.

If the problem is one of conformation then classical mechanics, which is based on the laws of classical physics, is used. In this approach only nuclear motions are examined, and a force field is employed to describe the interactions between the nuclei. The Born-Oppenheimer approximation states that electronic and nuclear motions can be uncoupled from one another and considered separately. Thus electrons are assumed to find their optimum distribution within the time scale of nuclear motion. Although electrons are not explicitly treated, they are implicitly included in the force field through parameterisation. The classical mechanical methods for statics and dynamics calculations respectively are **molecular mechanics** and **molecular dynamics**. These calculations are far less CPU intensive than the corresponding quantum calculations and thus are well suited to the study of large systems such as dendrimers, in which electronic effects are not predominant.

The work described in this thesis utilised quantum mechanics and molecular mechanics techniques for the statics calculations, and molecular dynamics for the dynamics calculations. These methods will now be described.

**Quantum Mechanics – *Ab initio* Molecular Orbital theory**

*Ab initio* Molecular Orbital theory is based on the laws of quantum mechanics and uses mathematical transformations and approximation techniques to solve the fundamental equations. [1] According to quantum mechanics, the Schrödinger equation describes the wavefunction of a particle. A technique called "separation of variables" allows us to write a time-independent Schrödinger equation. The *ab*

*initio* quantum mechanics program utilised in this work - Gaussian 94 – solves this equation. [1] Solutions to the time independent Schrödinger equation correspond to different stationary states of the particle (or molecule).

Hartree-Fock theory utilises Molecular Orbital theory, which decomposes the wavefunction into a combination of molecular orbitals. [1] These molecular orbitals are in turn expressed as a set of one-electron functions called "basis functions". [1] Basis functions in Gaussian 94 are comprised of primitive gaussian-type functions,[1] thus the basis set determines how the electrons are to be modelled. A larger basis set will result in a more accurate model.

The Hartree-Fock Self-Consistent Fields procedure is a computational technique which gives detailed numerical solutions for the wavefunctions and energies. [2] In brief, the Self-Consistent Fields (SCF) procedure starts with an initial guess as to the orbital configuration. Then a Schrödinger equation is written for one of the electrons in the system. This will take into account the average field of all the other electrons in their approximate orbitals. [2] This equation is solved by numerical integration, and will provide an updated orbital configuration. This procedure is then repeated for another orbital, and will now include the effect of the improved orbital. The solution of this next equation will give a second improved orbital. This procedure is repeated for all the electrons in the system. [2] Then the whole cycle is restarted until the orbitals and energies are no longer significantly different from those used at the start of the cycle. The solutions are then "self-consistent". [2] Accurate structures and energies can be obtained from these *ab initio* calculations, so quantum calculations can be used to parameterise molecular mechanics force fields. [3]

**The Molecular Mechanics Approach and Energy Minimisation**

In the molecular mechanics approach, molecules are treated as if they are a collection of masses (balls) bound by harmonic forces (springs). [3] The total energy of this "ball and spring" system, is described by a set of classical mechanical potential functions, which includes terms for bond stretching, angle deformation, torsional rotation, and nonbonded interactions. Any deformation (such as a bond stretch) from an idealised geometry will cause the potential energy of the molecule

to increase. The computer program employed to perform both the molecular mechanics and dynamics calculations was CHARMm, which was specifically designed for molecular mechanics and dynamics calculations on macromolecules. [4] The CHARMm empirical energy function utilised in this work has the following form: [4]

$$E_{tot} = E_b + E_\theta + E_\phi + E_\omega + E_{vdw} + E_{el} + E_{hb} + E_{cr} + E_{c\phi} \quad (1)$$

Each of the contributing terms will be discussed in turn.

$E_b$ This is the bond potential term. Bond stretching is described using Hookes law (a harmonic approximation), $r_0$ is the equilibrium value of the bond length. At room temperatures and in the absence of chemical reactions, these deformations are small enough for harmonic conditions to apply. [4]

$$E_b = \Sigma\, k_b\, (r - r_0)^2 \quad (2)$$

$E_\theta$ This is the bond angle potential, and is also described using a harmonic approximation, $\theta_0$ is the value of the angle at equilibrium.

$$E_\theta = \Sigma\, k_\theta\, (\theta - \theta_0)^2 \quad (3)$$

$E_\phi$ The dihedral angle potential is a four atom term, based on the dihedral angle $\phi$, about an axis defined by the middle pair of atoms. This potential is described by a Fourier term:

$$E_\phi = \Sigma\, |k_\phi| - k_\phi \cos(n\phi) \quad (4)$$

Where $n$ = (1,2,3,4,6)

$E_\omega$ This improper torsion term was designed to maintain chirality about a tetrahedral heavy extended atom (e.g. a carbon atom with no explicit hydrogen), as well as maintaining planarity about planar atoms, such as carbonyl carbons. [4]

$$E_{\omega} = \Sigma\, k_{\omega}\,(\omega - \omega_0)^2 \qquad \textbf{(5)}$$

The improper torsion angle $\omega$ is defined as the torsion angle $\phi_{ABCD}$ in the diagram below. [4]

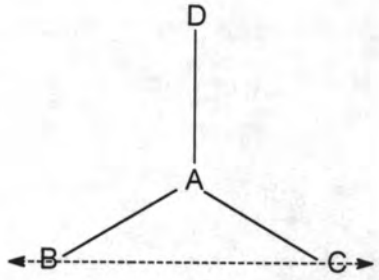


**Figure 3.1:** The definition of an improper torsion angle $\phi_{ABCD}$

***$E_{vdw}$*** Calculation of non-bonded Van der Waals and electrostatic interactions can be very computationally intensive, as all atom pairs of the molecule are involved. Better efficiency can be achieved by employing various truncation schemes. In this work, Van der Waals interactions are calculated using a 6-12 potential is utilised, with a switch smoothing function. The effect of this switching function is to reduce the pair contributions after a specified distance, and to switch the potential off completely after a cut-off distance. [4]

$$E_{vdw} = \sum_{\text{excl}(i,j)=1} (A_{i,j}/r^{12}{}_{i,j} - B_{i,j}/r^{6}{}_{i,j})\ \text{sw}(r^2{}_{i,j},\, r^2{}_{on},\, r^2{}_{off}) \qquad \textbf{(6)}$$

sw is the switching function defined by: [4]

$\text{sw}(x, x_{on}, x_{off}) = 1$ when $x \le x_{on}$

$\text{sw}(x, x_{on}, x_{off}) = (x_{off} - x^2)\,(x_{off} + 2x - 3x_{on}) / (x_{off} - x_{on})^3$ when $x_{on} < x \le x_{off}$

$\text{sw}(x, x_{on}, x_{off}) = 0$ when $x > x_{off}$

excl$(i,j)$ = 0 if atoms are connected by angles or bonds, or $i \ge j$

= 1 otherwise

***$E_{el}$*** The electrostatic interactions are calculated with a constant dielectric term. In this case, a shifting potential modifies the radial function so that the energy and forces go to zero at some cut-off distance. [4]

$$E_{el} = \sum_{\text{excl}(i,j)=1} (q_i q_j / 4\pi\varepsilon_0 r_{ij}) [1 - (2r^2_{i,j} / r^2_{cut}) - (r^4_{i,j} / r^4_{cut})] \qquad \textbf{(7)}$$

$\boldsymbol{E_{hb}}$ The hydrogen bonding contribution term involves 4 atoms: hydrogen (H), the donor atom (D) , the acceptor (A) and the acceptor antecedent (AA). The selection of hydrogen bonds is based on the A-D distance and the A-H-D angle. The total term is zero if $\theta_{A\text{-}H\text{-}D}$ is less than 90°, or if $n$ is greater than 0 and $\theta_{AA\text{-}A\text{-}H}$ is less than 90°.

$$E_{hb} = \Sigma \; (A'/r^j_{AD} - B'/r^j_{AD}) \cos^m (\theta_{A\text{-}H\text{-}D}) \times \cos^n (\theta_{AA\text{-}A\text{-}H}) \times \text{sw}(r^2_{AD}, r^2_{hon}, r^2_{hoff}) \times \text{sw}[\cos^2(\theta_{A\text{-}H\text{-}D}), \cos^2(\theta_{hon}), \cos^2(\theta_{hoff})] \qquad \textbf{(8)}$$

where $m$ = (0,2,4)
$n$ = (0,2)

$\boldsymbol{E_{cr}}$ Atom constraints can be useful for various purposes. $E_{cr}$ is the atom harmonic constraint term, used to avoid large displacements of atoms. [4]

$$E_{cr} = \Sigma \, K_i (r_i - r_{i0})^2 \qquad \textbf{(9)}$$

$\boldsymbol{E_{c\phi}}$ Dihedral constraints are used to maintain local conformations, or when a series of different conformations needs to be examined, as for a potential energy surface. [4]

$$E_{c\phi} = \Sigma \, K_i (\phi_i - \phi_{i0})^2 \qquad \textbf{(10)}$$

This set of potential functions forming the empirical energy equation, the idealised geometries (e.g. $r_0$, $\theta_0$, $\omega_0$ ) and any constants required ($k_b$, $A_{i,j}$ ,etc.), are collectively known as the **force field**. Molecular mechanics and molecular dynamics are both force field methods. The idealised geometries and constants are together referred to as parameters, and the validity of the force field hinges on these values. [3]

Parameters can be obtained from a variety of sources. It is very common for force field parameters to be fitted to experimental data, such as crystal structures (from which geometric constants can be obtained), infra-red data (from which force constants can be derived), x-ray data, NMR data, and energy and lattice dynamics. [5] This reliance on experiment explains why the CHARMm potential function is termed an "empirical energy equation".

Parameters can also be obtained from *ab initio* quantum mechanics calculations on small compounds. [5] The quality of the parameters depends heavily on the quality of this source data, and on the level of accuracy required. [3] Generally, parameters are specific to a particular force field, and are not transferable. This is because of parameter "correlation", whereby error in the force field is minimised in different ways in different force fields. [3]

The empirical energy equation, such as that for CHARMm discussed above, allows the energy of a molecule to be determined with respect to the forces that are present. Thus it is possible, by a technique known as energy minimisation, to find a minimum value of this potential, which would correspond to a local or global minimum on the potential energy surface of the molecule. Energy minimisation can be very useful for finding preferred conformers by measuring relative energies, for relieving strain in a structure derived by model building or from experimental data, and also for energy mapping of the potential energy surface. [4] The latter is only feasible for small molecules, as macromolecular systems are far too large for exhaustive searches. [4] An energy minimised structure is often used as the starting structure for a molecular dynamics (MD) simulation.

Several different energy minimisation schemes are available, with varying degrees of complexity. The simplest approach is the **steepest descents** minimisation technique. This is a gradient technique, which means that only the first derivative (gradient) of the potential energy is utilised, and not the second derivative. In each step, a displacement opposite to the gradient is added to the coordinates. If a lower energy results, the step size is increased, if not, the step size is decreased. [4] This is a very good method when far from the minimum, where the forces are

large, but when the forces are small much closer to the minimum, then it is slow and does not converge well. For these reasons, steepest descents is referred to as a nonconvergent method, and is often used for adjusting a geometry before refinement by another method, such as **conjugate gradients**. This is also a gradient method, however, it makes use of the previous minimisation step as well as the current gradient to make the following step, thus it has much better convergence characteristics. [4] The conjugate gradients algorithm is fairly economical, and so is used after steepest descents minimisation in this work to obtain energy minima. Figure 3.2 displays minimisation paths of both steepest descents and conjugate gradients for a simple energy surface.

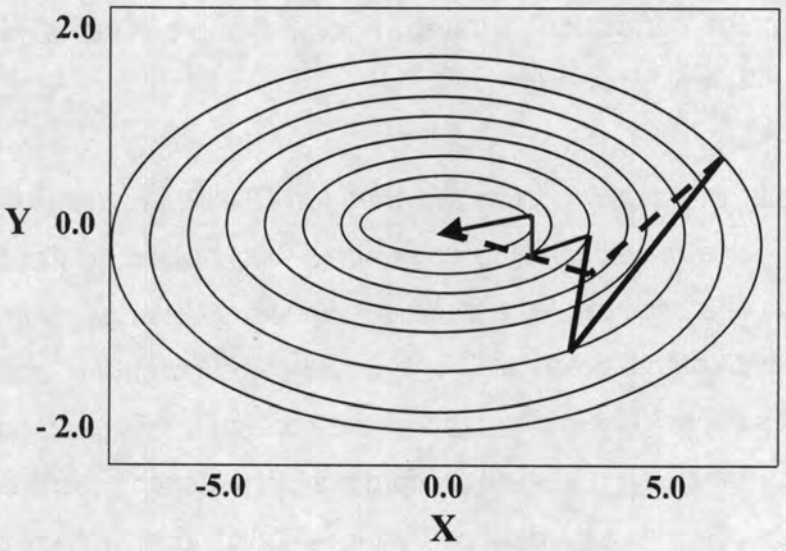


**Figure 3.2**: Minimisation paths for a simple energy surface:
Steepest descents ——→ Conjugate gradients - - - - - -

Molecular mechanics can also be used to map the potential energy surface of single molecules as a function of the component dihedral angles. Dihedral constraints are applied to the molecule, followed by energy minimisation of the constrained system. The energy of the conformer can be measured, the next set of dihedral constraints imposed, and the process iteratively repeated stepping through the full set of dihedral angle combinations. A potential energy surface as a function of the dihedral angles is obtained, from which energy barriers and low energy regions can be found.

Another way to search conformational space is to generate an ensemble of conformations. Molecular dynamics simulation methods provide one manner in which to do this, with the advantage of obtaining dynamical information about the system as well. [5] Both the canonical ensemble (NVT) and the microcanonical ensemble (NVE) can be generated by modifying the conditions under which the simulation is performed.

**Molecular Dynamics**

In the molecular dynamics technique, the time-dependent behaviour of a system is monitored by solving Newton's second law at regular time intervals. [6] In this way, the motions of the system are simulated with respect to the forces (described in the force field) that are present. In contrast to minimisation algorithms, which drive the conformation to the nearest local minimum, MD can overcome conformational barriers. [7]

Newton's second law, F = ma, can be written in a terms of displacement (s).

$$\delta^2 s_i / \delta t^2 = F_i \, m_i \qquad \textbf{(11)}$$

Double integration of this with respect to time, gives: [6]

$$s_i = u_i t + \tfrac{1}{2} a_i t^2 + c \qquad \textbf{(12)}$$

Thus, it is possible to calculate displacement from an initial velocity $u_i$ and the acceleration, which can be derived from $a_i = F_i / m_i$. [6] CHARMm can numerically integrate these equations for all the atoms in the molecule with the Leapfrog Verlet algorithm. [4] A key approximation in this method is that acceleration varies slowly over the time period. Therefore, the smaller the time step involved, the better this approximation. [4] For this reason, the time step should be significantly smaller than the fastest motion in the system, which is usually due to stretching frequencies involving hydrogen. These can be removed providing that they do not interact with any motions of interest, thus allowing the time step to be increased to around 1fs. The constraint algorithm SHAKE is used to do this across time steps of the Verlet algorithm. [4]

There are several stages to a MD simulation. Firstly the system needs to be minimised in order to remove large sources of strain. As the temperature of the minimised structure is 0 K, it must be heated to the temperature at which the simulation will take place. Temperature is calculated from the kinetic energy of all the atoms in the system, however at time t=0, no velocities are known. [6] The initial velocities are randomly assigned according to a Gaussian distribution for the initial temperature. Usually the system is gradually heated in steps, with a number of intermediate temperatures before the desired temperature is reached. Once the first velocities are assigned and the initial geometry is given, the system is self-perpetuating. [6] The acceleration of an atom *i* can be calculated from the forces present on the atom (according to the potential energy function), and the new position can be determined. This is an iterative procedure, as indicated in Figure 3.3, and is done for every atom in the molecular system.

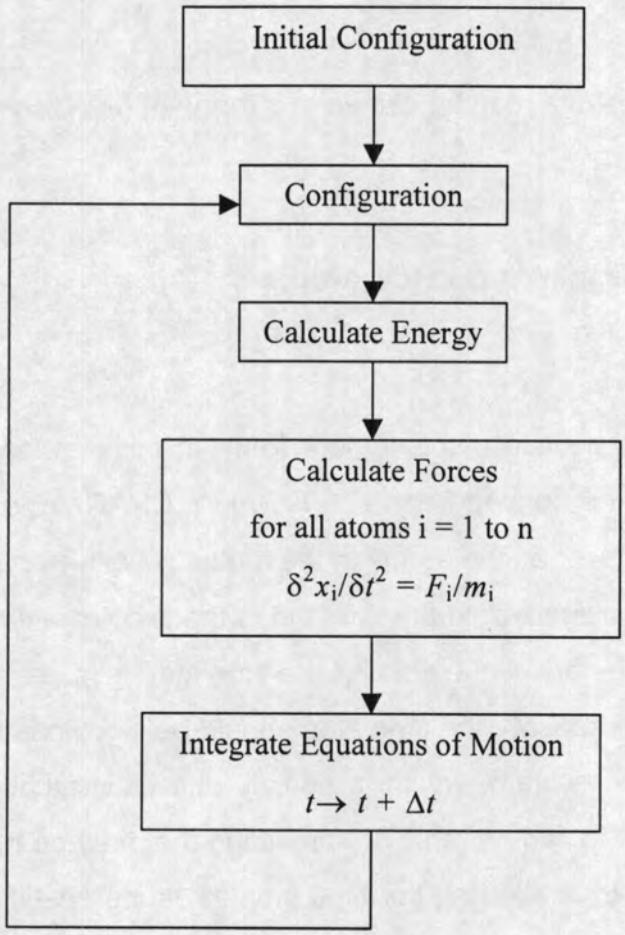


**Figure 3.3:** The iterative procedure of molecular dynamics for an n atom molecular system.

The next stage after heating is an equilibration period. In this time interval the system's energy should redistribute to ensure stability, [6] and the velocities are periodically rescaled to maintain the desired temperature. The length of the equilibration period depends on the properties under observation. An indication of whether the system is equilibrated in an NVE ensemble (constant no. of particles, volume and total energy) can be obtained by monitoring total energy to see if it has converged and is fluctuating about a stable average. [6]

The final stage of the simulation is the production dynamics. The product of this stage is a collection of positions and velocities (the trajectory) saved at regular time intervals throughout the dynamics period. [4]

After the simulation is complete, the trajectory can be analysed, to obtain both static and dynamic information about the system. [4] Numerous properties can be extracted from the stored co-ordinates of the trajectory, including structural data, such as average structures or root-mean-square differences. The conformation of a specific dihedral angle can be monitored with respect to time, and detailed energetic data can be used to find the barriers to conformational changes. Time dependent properties can be calculated with time correlation functions. There is a wealth of information contained in the dynamics trajectory, which can be calculated with statistical mechanics theory; this is the power of the molecular dynamics method.

### 3.3 Modification of the existing force field

It has already been established that the validity of a force field is dependent on the values of the parameters employed within it. In general, parameters for the organic monomers were obtained from a CHARMm polymer force field currently under development. [8a] Furthermore, the CHARMm protein force field [8b] was utilised to extend the existing parameter set in order to study the dendrimer system. Parameters for the organometallic moiety were obtained by analogy to the iron carbonyl values already present in the force field and were adapted to be consistent with literature data and the two crystal structures discussed in Chapter

2, namely (dibenzyl ether)bis[tricarbonylchromium(0)] **9** and (benzyl methyl ether)tricarbonylchromium(0) **14**. [9]

Two main areas of importance were focused upon in this parameterisation study. Firstly, there is an ether linkage torsion angle, which occurs throughout the dendrimer, which plays a significant role in the topology of the macromolecule. Figure 3.4 displays a full first generation organic dendrimer, and the important ether linkage torsion angle Ψ.

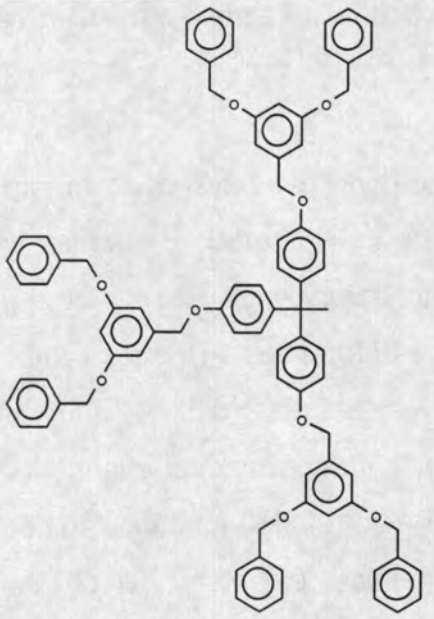

a) A first generation organic dendrimer

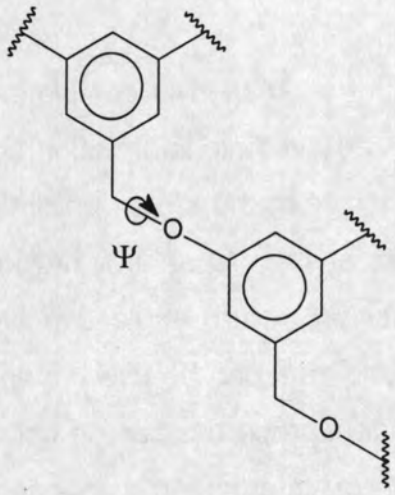


b) The ether linkage torsion angle Ψ

**Figure 3.4**

This torsion angle is present where surface groups are connected to the interior monomers, as well as in the links between monomers in a wedge, and monomers to the CORE. As such, it will have a significant effect on the temporal behaviour of the dendrimer. Thus it is crucial that this torsion angle be parameterised properly in order for the simulation results to have any validity.

The parameters for this torsion angle were adapted from the CHARMm polymer force field. [8a] To ensure that this torsion is treated correctly, molecular mechanics calculations were carried out on a model compound, and the results were compared to *ab initio* quantum mechanical calculations on the same model.

The second area of importance was the tricarbonylchromium arene functionality. To ensure that this group is properly parameterised, one of the crystal structures determined in Chapter Two *viz.* (dibenzyl ether)bis[tricarbonylchromium(0)] was simulated and compared to the experimental structure.

### 3.3.1 Parameterisation of the ether linkage torsion angle

The model system investigated in the parameterisation of the ether link was benzyl phenyl ether, (See Figure 3.5). This contains the all-important torsion angle Ψ as found in the dendrimer, *viz.* C2-C3-O4-C5, and is the simplest model for the repeat unit.

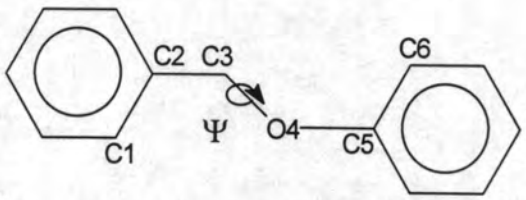


**Figure 3.5:** Benzyl phenyl ether

Parameters can be optimised by least-squares fitting, or on a trial-and-error basis. [3] In this work, the approach adopted is a trial-and-error fitting of torsional rotation data to *ab initio* quantum mechanical data.

**Energy Scans and Parameterisation**

Using CHARMm, [4] benzyl phenyl ether was constructed and energy minimised. An energy scan as a function of Ψ (Ψ= C2-C3-O4-C5) was obtained by varying Ψ through 360° and constraining Ψ at 10° intervals. In addition to this, two adjacent torsion angles were systematically varied. (C1-C2-C3-O4) and (C6-C5-O4-C3) determine the orientation of the aromatic rings. These rings were rigidly rotated from –180° to 180° at 30° intervals followed by minimisation. Every permutation of the two ring orientations was explored for each value of Ψ, and the lowest energy structure was recorded.

The minimised co-ordinates at each step were then imported into Gaussian 94, [1] and a single point energy calculation was carried out on the co-ordinate set. The intended level of these calculations was Møller-Plesset theory, with the 6-31+G(d) basis set, however these calculations were extremely CPU intensive, as was the same calculation at the Hartree-Fock level with the same basis set. For this reason, the single point energy calculations were carried out on the Hartree-Fock level with the 6-31G(d) basis set. An *ab initio* energy scan of the benzyl phenyl ether conformation as a function of Ψ was obtained.

Figure 3.6 shows a comparison of the two energy scans before any parameterisation has been attempted. Figure 3.6a displays the two scans on the same energy scale, Figure 3.6b shows the two scans on different energy scales (y-axes).

**a)**

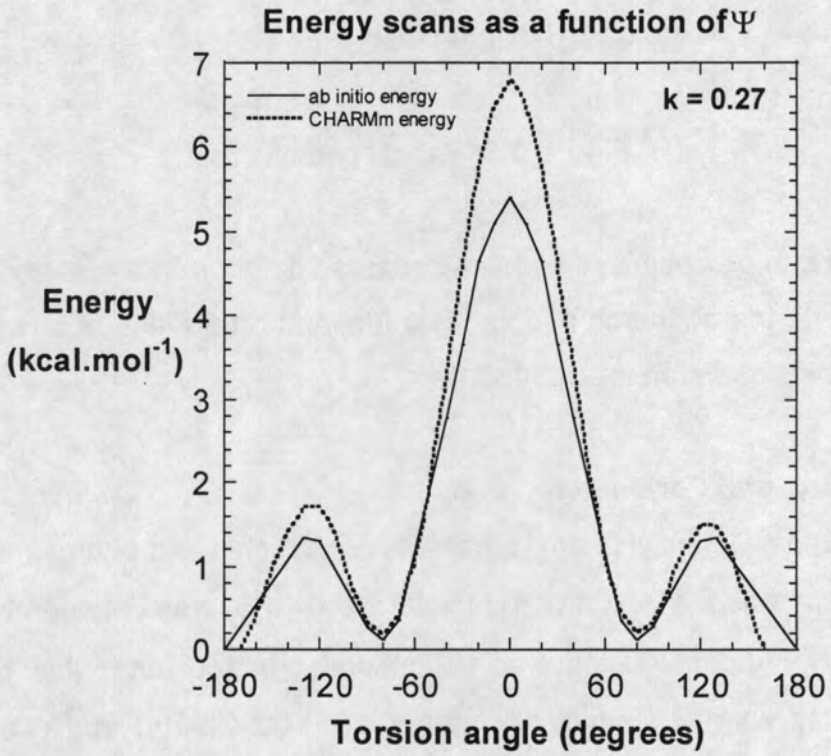

b)

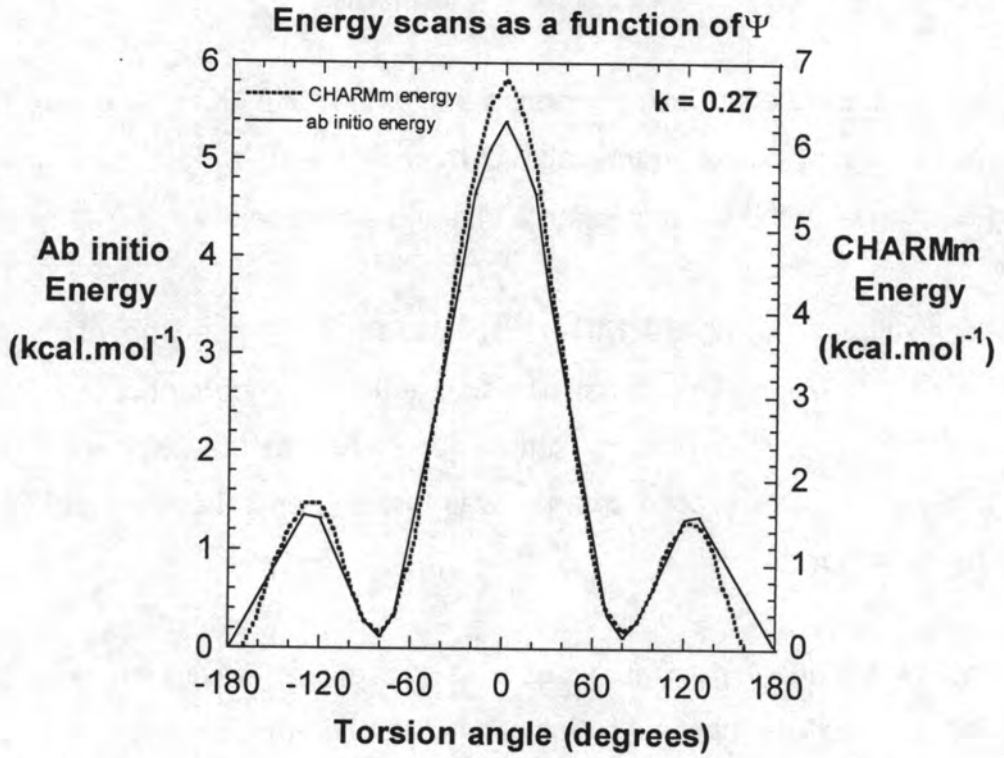


**Figure 3.6:** The CHARMm and *ab initio* energy scans for benzyl phenyl ether, as a function of Ψ

The shape of the two energy scans are as expected for the benzyl phenyl ether molecule, with 3 barriers to rotation. The global maximum occurs at 0°, where the molecule is in the *syn* periplanar conformation. As the torsion angle is increased the energy drops, until a local minimum, corresponding to the first gauche conformation, is reached. With further rotation of the torsion angle, a second eclipsed conformation is reached. The eclipsing interaction is between a hydrogen atom and the phenyl ring, hence the fairly low energy barrier for this local maximum. Further rotation brings the molecule into the energetically favourable *anti* periplanar conformation which is at the global minimum of the energy surface. The symmetry of the molecule is responsible for the observed symmetry of the energy scans.

The CHARMm scan is not perfectly symmetrical however. Close inspection of Figure 3.6 reveals that the local maximum at –120° is slightly higher in energy than the local maximum at +120°. This is due to the presence of two local minima

corresponding to different ring conformations, both minima are equally valid, and differ by only 0.2 kcal.mol$^{-1}$.

To parameterise the ether linkage torsion angle, the CHARMm data were fitted to the *ab initio* data, by changing the value of the coefficient $k_\phi$ in the torsional energy term (Equation 4) of the force field, on a trial-and-error basis.

The initial value of $k_\phi$ was 0.27 kcal.mol$^{-1}$radian$^{-2}$. Comparison of the energy scans was made using two criteria. The first and most important criterion was the ratio of the value of the local maximum (at +120°) to the value of the global maximum (at 0°). The second criterion was the difference between the values of the global maxima.

The ratio of the local maximum value to the global maximum value is very important, as this is the best indication of whether the ether linkage torsion angle is parameterised correctly in the CHARMm force field. The aim of this parameterisation is to best represent the torsional angle contribution to the total energy of the molecule. If the torsional contribution is overemphasised, then it might swamp the contribution from the other energy terms, and remove the essential chemistry of the molecule. The *ab initio* calculations provide the total energy of the system as a function of the dihedral angle and includes the contribution from all of the energy terms. Thus, the relative values of the local and global maxima obtained by this method, will be correct. Matching the CHARMm values as closely as possible to the *ab initio* values will allow the best representation of the torsion angle contribution.

The second criterion on which the comparison was based, was the value of the global maximum. The CHARMm and *ab initio* scans should have similar values for the total energy of this conformation. A list of trial $k_\phi$ values is given in Table 3.1, the value which best fits the *ab initio* data is highlighted.

**Table 3.1:** Trial $k_\phi$ values and comparison criteria

| $k_\phi$ | Difference in relative values of local and global max. | Difference in value of global maximum |
|---|---|---|
| 0.27 | 0.41 | 1.40 |
| 0.25 | 0.40 | 1.80 |
| 0.23 | 0.16 | 1.78 |
| 0.20 | 0.25 | 1.75 |
| 0.17 | 0.16 | 1.69 |
| **0.15** | **0.11** | **1.60** |

Overall, the best agreement with the *ab initio* data was found with $k_\phi$ = 0.15. The relative values of the local and global maxima closely match the *ab initio* data. Furthermore, the value of the global maximum is fairly close to that found in the *ab initio* scan.

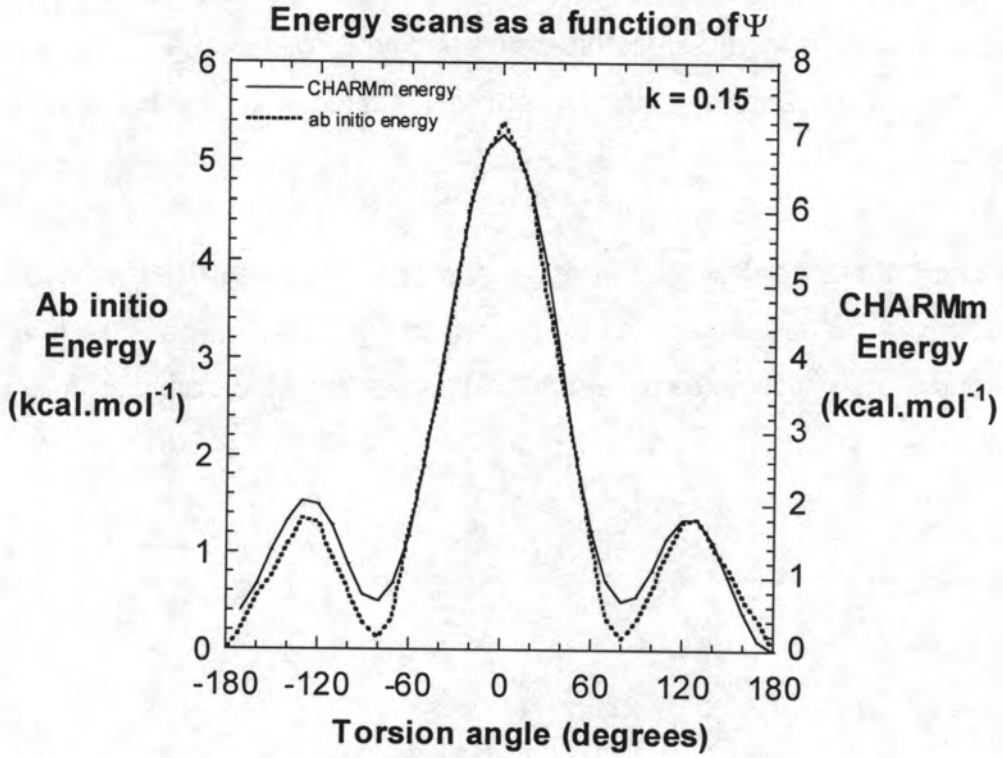


**Figure 3.7:** The modified CHARMm and ab-initio energy scans as a function of Ψ

The original $k_\phi$ = 0.27 resulted in a better match of global maxima values, but a worse match for the relative values of the global and local maxima. As has been explained, the latter is the most important as it is a measure of the accuracy of the

torsion angle contribution. The difference in values between the global maxima is an indication of the accuracy of the entire parameter set. This difference in global maxima values is not so high as to be unacceptable, and might simply be a result of the relatively low level of theory used in the *ab initio* calculations. A repeat of this study with Møller-Plesset calculations might show better agreement with the CHARMm data. This was not feasible in this work due to time constraints, as calculations at this level, on a system of this size, are extremely expensive.

Alternatively, the difference in global maxima might be ascribed to nonbonded contributions to the total energy. Full parameterisation of the force field is not the purpose of this work, thus no investigations were carried out into the nonbonded interaction contributions. If the (higher) CHARMm global maximum value is indeed due to too large a contribution from nonbonded interactions, then the effect this would have on the dynamics trajectories would be to slow them down. The nonbonded term would hinder torsional rotation slightly more than it should, thus causing the system to undergo torsional changes more slowly. This should be kept in mind when analysing the dynamics trajectories of the full dendrimer, in Chapter 4.

At this point, the ether link torsion angle has been parameterised, without having to make any major adjustments to the force field, and it is now possible to examine the second area that requires parameterisation, *viz*. the tricarbonylchromium arene functionality.

### 3.3.2 Parameterisation of the tricarbonylchromium(0) arene moiety

In order to obtain parameters for the tricarbonylchromium moiety, the Cambridge Structural Database (CSD) was searched for crystal structures of simple benzylic aryl or alkyl ether complexes of chromium tricarbonyl. [10] Such complexes would serve as model compounds for the chromium groups at the periphery of the dendrimers, as these are benzyl aryl ether complexes. However, no examples could be found in the CSD. For this reason, it was necessary to solve the structures of two complexes, (dibenzyl ether)bis[tricarbonylchromium(0)] **9** and (benzyl methyl ether)tricarbonylchromium(0) **14**, both of which were prepared as part of the synthetic work.

**Crystal Structures**

In Chapter 2, the synthesis of (dibenzyl ether)bis[tricarbonylchromium(0)] **9** was discussed, and the crystal structure was reported. This new compound can serve as a model for the chromium groups at the surface of the dendrimer, and can provide an indication of whether the surface groups interact with one another. In the same chapter, the crystal structure of (benzyl methyl ether)tricarbonylchromium(0) **14** was also reported. This compound had previously been synthesised, however the crystal structure of the complex had not been reported.

The structures of both complexes were shown in Chapter 2 and will now be discussed in greater detail. Table 3.2 indicates the crystal data and data collection parameters for both structures.

**Table 3.2:** Crystal data and data collection parameters

| **Compound** | 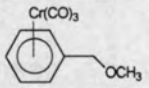 **14** | 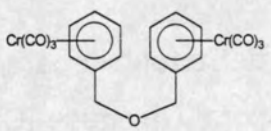 **9** |
|---|---|---|
| Empirical formula | $C_{11}H_{10}CrO_4$ | $C_{20}H_{14}Cr_2O_7$ |
| Formula weight | 258.19 | 470.31 |
| Temperature | 293(2)K | 150(2)K |
| Wavelength | 0.71069Å | 0.71073Å |
| Crystal system | Triclinic | Monoclinic |
| Space group | $P\bar{1}$ | $P2_1/n$ |
| Unit cell dimensions | a = 7.125(2) Å | a = 7.6251(1) Å |
| | b = 8.007(2) Å | b = 10.5323(2) Å |
| | c = 9.807(2) Å | c = 23.5630(2) Å |
| | α = 92.61(1)° | α = 90° |
| | β = 92.05(1)° | β = 90.613(1)° |
| | γ = 103.43(1)° | γ = 90° |
| Volume | 543.0(2) $Å^3$ | 1892.23(3) $Å^3$ |
| Z | 2 | 4 |
| Density (calculated) | 1.389 $Mg.m^{-3}$ | 1.651 $Mg.m^{-3}$ |
| Absorption coefficient | 1.037 $mm^{-1}$ | 1.189 $mm^{-1}$ |
| F(000) | 226 | 952 |
| Crystal size | 0.1 x 0.2 x 0.2 mm | 0.4 x 0.3 x 0.02 mm |
| Theta range for data collection | 2.08° to 29.96° | 1.73° to 25.00° |
| Limiting indices | $-10 \le h \le 9$ | $-9 \le h \le 9$ |
| | $0 \le k \le 11$ | $-13 \le k \le 13$ |
| | $-13 \le l \le 13$ | $-30 \le l \le 27$ |
| Reflections collected | 3160 | 14016 |
| Independent reflections | 3160 [R(int)=0.0000] | 3328 [R(int) = 0.0600] |
| Refinement method | Full-matrix | Full-matrix |
| | least-squares on $F^2$ | least-squares on $F^2$ |
| Data/restraints/parameters | 3160 / 0 / 151 | 3312 / 0 / 262 |
| Goodness-of-fit on $F^2$ | 0.997 | 1.247 |
| Final R indices [$I > 2\sigma(I)$] | R1 = 0.0658 | R1 = 0.0751 |
| | WR2 = 0.1606 | wR2 = 0.1929 |
| R indices (all data) | R1 = 0.1003 | R1 = 0.0893 |
| | WR2 = 0.1726 | wR2 = 0.1999 |
| Largest diff. Peak and hole | 1.596, –1.447e$Å^{-3}$ | 1.031, -0.917e$Å^{-3}$ |

Figures 3.8 and 3.9 show the crystal structures of compounds **9** and **14** respectively.

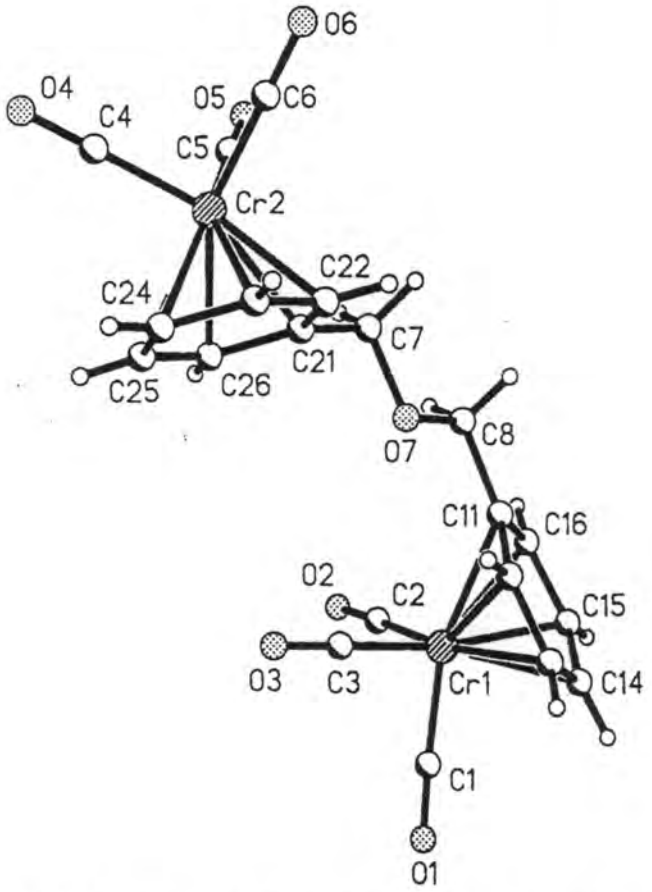


**Figure 3.8:** The crystal structure of (dibenzyl ether)bis[tricarbonylchromium(0)] **9**

Both complexes display the classic piano-stool structure, where the planar arene ring forms the "seat" of the stool, and the three carbonyl groups are the "legs". [11] The aromatic rings are essentially planar in both cases, with the aromatic ring of the benzyl methyl ether complex deviating less than 0.05Å from the mean plane. The metal lies directly beneath the ring centroid, at fairly typical distances of 1.72Å and 1.71Å for compound **9**, and 1.73Å for compound **14.**

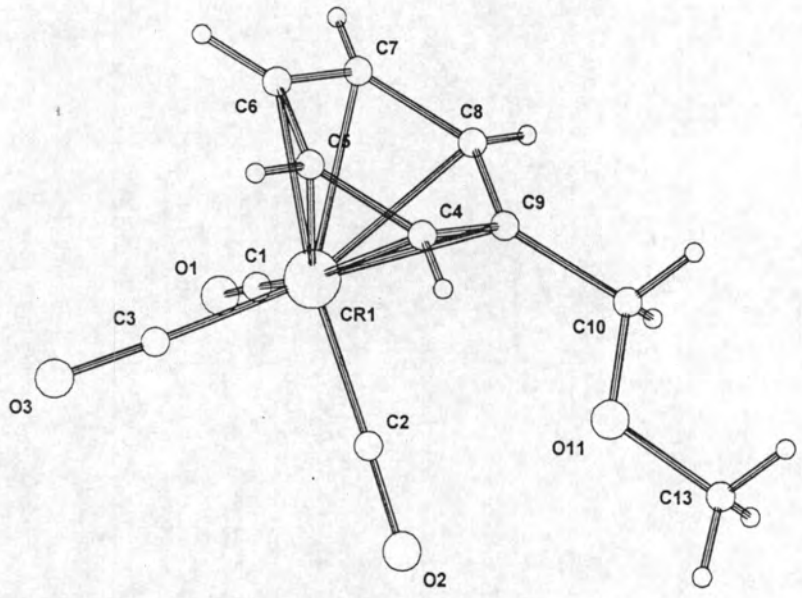


**Figure 3.9:** The crystal structure of the benzyl methyl ether complex **14**

Other interesting features of these structures include the conformation of the chromium tricarbonyl tripod in relation to the ring, and bond length alternation. The conformation of tricarbonyl chromium complexes in the solid state is controlled electronically and is dependent on the arene substituents. [11] Typically, unsubstituted arenes adopt the staggered conformation as shown in Figure 3.10 (a). Monosubstituted arenes are almost invariably eclipsed, in one of two conformations. If the substituent is electron donating, then the *syn* eclipsed form (b) is favoured. If the substituent is electron withdrawing, then the *anti* eclipsed form (c) is preferred. [11]

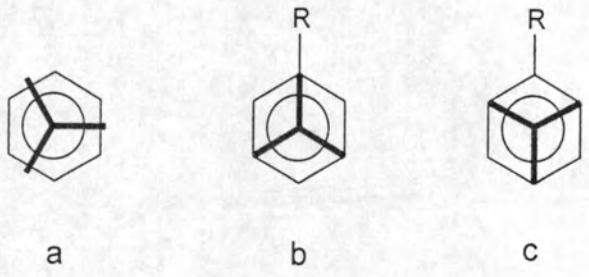


**Figure 3.10:** Conformations of chromium tricarbonyl in relation to the ring [11]

The benzyl methyl ether complex **14** behaves as expected. The electron donating methyl ether substituent causes the tripod to adopt an almost *syn* eclipsed conformation (b). In fact, the conformation is not perfectly eclipsed, but is slightly staggered. Figure 3.11 is a view down the centroid-chromium axis, and clearly displays the conformation. The dibenzyl ether complex **9** however, is very interesting. There are two complexed aromatic rings in this structure, both of which were expected to adopt the *anti* eclipsed conformation, as the substituents in each case would be electron withdrawing due to the chromium tricarbonyl groups. Instead, what is observed is that only one of the rings (C11-C16) has the *anti* eclipsed conformation, while the other ring (C21-C26) is completely staggered, which is highly unusual for a monosubstituted arene complex. There is precedent for monosubstituted arene complexes adopting the staggered conformation due to strong steric effects, [12] however it is not clear whether steric reasons are the cause in this instance. Figure 3.12 shows the conformation of the 2 aromatic rings in the dibenzyl ether bis-complex

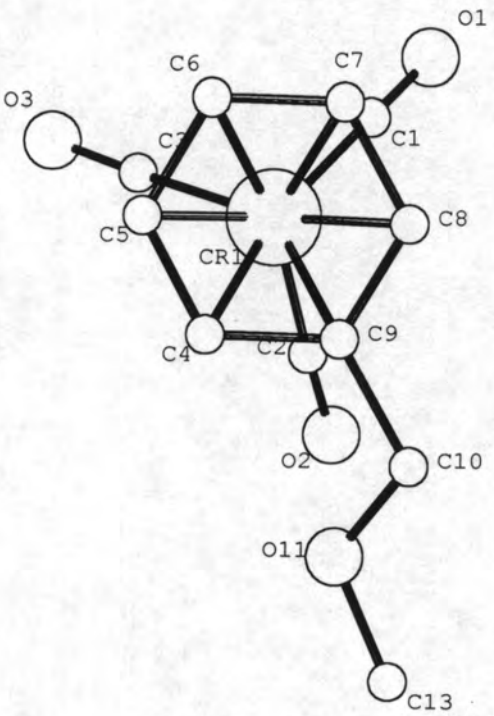


**Figure 3.11:** The conformation of the tripod in the benzyl methyl ether complex **14**

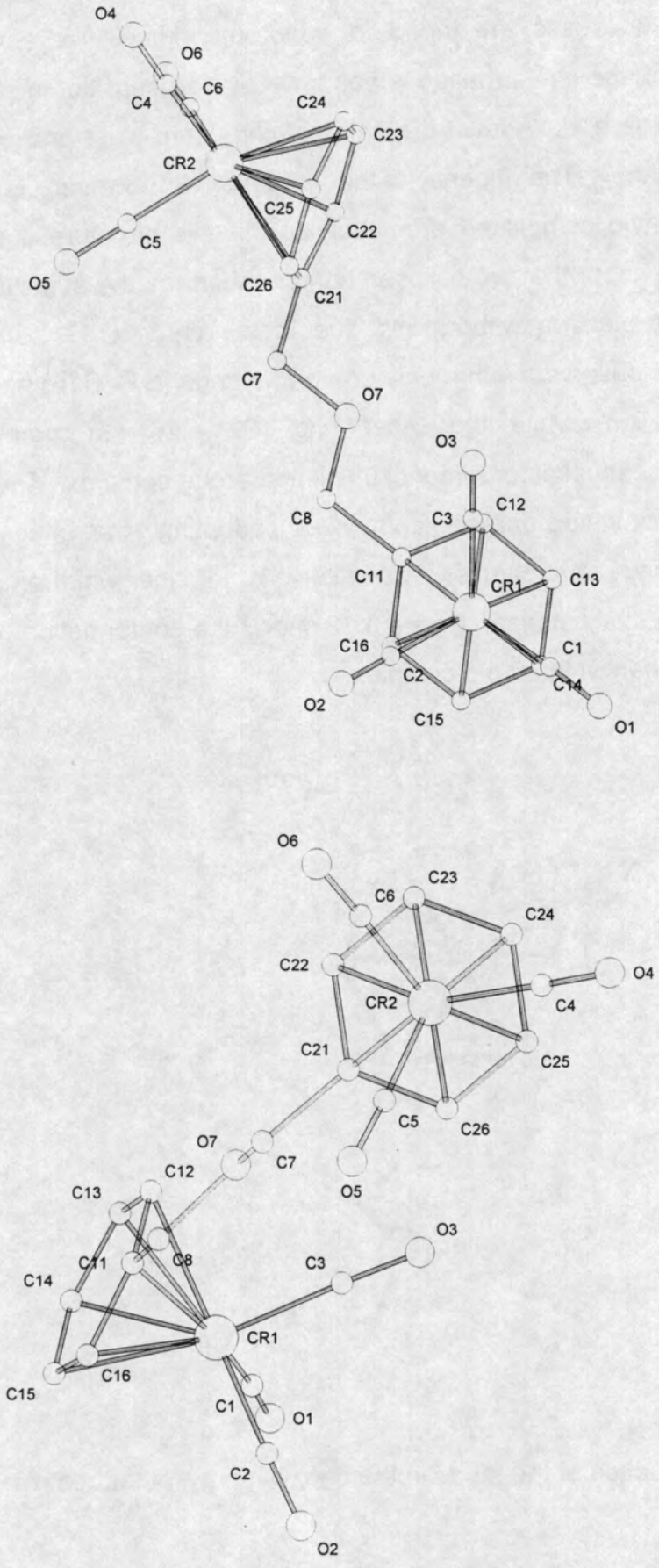


**Figure 3.12:** The aromatic ring conformations in the dibenzyl ether bis-complex **9**

In general, tricarbonylchromium complexes in solution readily interconvert between conformations, as the activation energy for rotation is low, but the preferred conformer is the same as in the solid state. [11] In Chapter 2, a low temperature (-60°C) $^{13}C$ NMR spectrum of **9** in $CDCl_3$ showed some splitting of the carbonyl resonance frequency which indicated that, at a low temperature, it may be possible to "freeze out" the carbonyl rotation into discrete rotamers as found in the crystal structure.

The other interesting feature is bond length alternation, which is related to the conformation. A low-temperature crystal structure study showed a staggered conformation for (hexamethylbenzene)tricarbonylchromium(0) with an average bond alternation of 0.021Å. [11] The carbon-carbon bonds situated above the carbonyl ligands were the ones that were lengthened. A similar result was observed for the staggered ring (C21 – C26) in the dibenzyl ether complex of this work, with an average bond alternation of 0.023Å. The *anti* eclipsed complexed ring (C11-C16) shows no significant bond length variation. Interestingly, the *syn* eclipsed ring of the benzyl methyl ether complex, does show bond alternation. This is probably due to the conformation being slightly staggered. The average bond length alternation in this case is 0.021Å.

Selected and/or average bond lengths, angles and dihedral angles for both complexes are listed in Tables 3.3 and 3.4 and 3.5. In some instances, two values are indicated on one line, this is because there are two average values for that parameter, due to bond length alternation in the aromatic ring.

**Table 3.3:** Selected bond distances from the crystal structures of compounds **9** and **14**

| Bond | Distance in Å | | |
|---|---|---|---|
| | (Benzyl methyl ether) complex | (Dibenzyl ether) bis-complex | |
| | Ring (C4-C9) | Ring 1 (C11-C16) | Ring 2 (C21-C26) |
| $C_{ring} - C_{ring}$ (ave.) | 1.39, 1.41* | 1.40* | 1.42, 1.40* |
| *$C_{ring}$ – Cr* | | | |
| C4/C11/C21 – Cr | 2.231(3) | 2.245(8) | 2.208(8) |
| C5/C12/C22 – Cr | 2.211(4) | 2.213(9) | 2.200(8) |
| C/6/C13/C23 – Cr | 2.221(4) | 2.199(9) | 2.205(8) |
| C7/C14/C24 – Cr | 2.209(4) | 2.226(8) | 2.233(8) |
| C8/C15/C25 – Cr | 2.218(4) | 2.229(8) | 2.246(8) |
| C9/C16/C26 – Cr | 2.230(3) | 2.201(8) | 2.237(8) |
| *Cr- $C_{CO}$* | | | |
| Cr – C3/C6 | 1.836(4) | 1.860(9) | 1.857(9) |
| Cr – C1/C4 | 1.838(4) | 1.836(9) | 1.866(9) |
| Cr – C2/C5 | 1.841(4) | 1.847(9) | 1.841(10) |
| Centroid – Cr | 1.73(2) | 1.72* | 1.71* |
| Centroid - $C_{ring}$ | 1.411,1.413 | | |
| $C_{ipso} - CH_2$ | 1.508(5) | 1.52(1) | 1.50(1) |
| $CH_2 - O$ | 1.400(5) | 1.43(1) | 1.43(1) |
| O – R | 1.412(5) | 1.43(1) | 1.43(1) |

* Where no errors are indicated, these values are averages or the errors were not available for these measurements

**Table 3.4:** Selected angles from both structures **9** and **14**

| Angle | Angle in degrees | | |
|---|---|---|---|
| | (Benzyl methyl ether) complex | (Dibenzyl ether) bis-complex | |
| | Cr1 | Cr1 | Cr2 |
| $C_{ring}$ – Cent – Cr | 89.4 ,89.9* | 90.2, 89.8* | 90.0, 90.0* |
| *Cent – Cr – $C_{CO}$* | | | |
| C1 | 128.4* | 123.6* | 125.1* |
| C2 | 126.5* | 125.5* | 128.8* |
| C3 | 126.0* | 128.2* | 126.8* |
| *Cr- $C_{CO}$ –$O_{CO}$* | | | |
| Cr – C1/C4-O1/O4 | 177.8(3) | 176.5(8) | 178.7(8) |
| Cr – C2/C5-O2/O5 | 177.3(4) | 177.9(8) | 177.4(8) |
| Cr – C3/C6-O3/O6 | 177.9(4) | 178.0(7) | 177.9(7) |
| $C_{CO}$ - *Cr* – $C_{CO}$ | | | |
| C1/C4 – Cr – C2/C5 | 86.9(2) | 88.8(4) | 89.9(4) |
| C2/C5 – Cr – C3/C6 | 89.4(2) | 86.0(4) | 83.7(4) |
| C1/C4 – Cr – C3/C6 | 86.4(2) | 91.2(4) | 89.3(4) |
| $C_{ipso}$ – $CH_2$ – O | 109.1(3) | 109.5(7) | 107.8(7) |
| $CH_2$ – O – R | 113.7(4) | 110.7(6) | 110.7(6) |

* Where no errors are indicated, these values are averages or the errors were not available for these measurements

**Table 3.5:** Selected torsion angles from both structures **9** and **14**

| Torsion Angle | Angle in degrees | | |
|---|---|---|---|
| | (Benzyl methyl ether) complex | (Dibenzyl ether) bis-complex | |
| | Ring (C4-C9) | Ring 1 (C11-C16) | Ring 2 (C21-C26) |
| $C_{ipso}$ – $CH_2$ – O – R | -177.3(4) | -179.4* | 175.7* |
| *$C_{ortho}$-$C_{ipso}$- $CH_2$–O* | | | |
| C8/C12/C22 –CCO | -148.4(4) | -24.6* | 91.4* |
| C4/C16/C26 –CCO | 33.1(5) | 156.9* | -88.6* |

* Where no errors are indicated, the errors were not available for these measurements

**(Arene)tricarbonylchromium parameters**

With the information from the crystal structures, it was possible to construct (arene)tricarbonylchromium complexes with CHARMm. The chromium tricarbonyl group was made in such a way that it could be attached to any aromatic ring. To do this, it was necessary to bond the metal directly to a "dummy" atom. The dummy atom is the centroid of the aromatic ring to which the tricarbonyl chromium group would be bound. In effect, the metal is only bound to the ring by one bond, and each ring carbon is bound to the dummy atom instead of the metal. Two types of aromatic ring carbons (CA and CA1) are present in each ring, to account for the variation in bond lengths and angles (such as bond length alternation).

To maintain the correct geometry, bonds and angles involving the dummy atom and surrounding ring carbons atoms were calculated, and were reported in the preceding Tables 3.3 and 3.4. These values, along with others from the same tables, were used to construct the CHARMm parameter set for the tricarbonylchromium moiety, reported in Tables 3.7 to 3.9. A listing of CHARMm atom classifications is shown in Table 3.6.

**Table 3.6:** CHARMm atom classification

| Name | Description |
|---|---|
| CA | Aromatic carbon |
| CA1 | Aromatic carbon in arene complex |
| MCR | Chromium metal atom |
| CM | Carbonyl carbon |
| OM | Carbonyl oxygen |
| DUM | Dummy atom for centroid |

**Table 3.7**

| **Bond Parameters:** $E_b = k_b (r - r_0)^2$ | | |
|---|---|---|
| **Bond** | $k_b$ **(kcal.mol$^{-1}$Å$^{-2}$)** | $r_0$ **(Å)** |
| MCR-CM | 300.0 | 1.84 |
| MCR-DUM | 210.0 | 1.73 |
| OM-CM | 1115.0 | 1.14 |
| CA1-DUM | 305.0 | 1.41 |
| CA-DUM | 305.0 | 1.41 |

**Table 3.8**

| Angle Parameters: $E_\theta = k_\theta (\theta - \theta_0)^2$ | | |
|---|---|---|
| **Angle** | **$k_\theta$ (kcal.mol$^{-1}$radian$^{-2}$)** | **$\theta_0$ (degrees)** |
| CM–MCR-CM | 5.00 | 90.0 |
| MCR-CM-OM | 25.00 | 179.0 |
| CM-MCR-DUM | 5.00 | 126.2 |
| CA-DUM-MCR | 50.00 | 90.0 |
| CA1-DUM-MCR | 50.00 | 89.4 |
| CA1-DUM-CA1 | 40.00 | 120.0 |
| CA1-DUM-CA | 40.00 | 60.0 |
| CA-DUM-CA | 40.00 | 120.0 |

**Table 3.9**

| Dihedral Parameters: $E_\phi = \lvert k_\phi \rvert - k_\phi \cos(n\phi)$ | | | |
|---|---|---|---|
| **Dihedral** | **$k_\phi$ (kcal.mol$^{-1}$radian$^{-2}$)** | **Periodicity** | **Phase(degrees)** |
| CA-DUM-MCR-CM | 0.0 | 6 | 180.0 |
| CA1-DUM-MCR-CM | 0.0 | 6 | 180.0 |
| X-MCR-CM-X | 0.0500 | 4 | 0.00 |

Only parameters for the chromium tricarbonyl group have been reported in the preceding tables. A full CHARMm dendrimer parameter set can be found in Appendix 1. Other chromium parameters not displayed here, such as the improper dihedral, and nonbonded parameters can also be found in the appendix.

The bulk of the $r_0$ and $\theta_0$ values were obtained from the crystal structure information, with the exception of some of the carbonyl parameters. These were already present in the CHARMm force field, and were checked to ensure that they did not deviate too much from the crystal structure values. Force constants, and dihedral angle values were obtained by analogy to similar parameters already present in the CHARMm protein force field, or from the literature. [9] The dummy atom was treated as a carbon atom, so carbon-like force constants were applied to it.

**Testing the Chromium parameters**

In the previous section, an initial estimate of chromium parameters was discussed. These parameters were developed for a CHARMm-like force field. They were further tested using a molecular dynamics simulation and crystal structure calculations.

The bis-complex i.e.(dibenzyl ether)tricarbonylchromium(0) **9** was constructed and energy minimised. The complex was then subjected to a 100ps dynamics simulation after heating to 300K, as a qualitative test of the parameters. If any of the force constants were severely erroneous, then the molecule would be unstable throughout the simulation period, and could even break apart. Particular attention was paid to the behaviour of the dummy atom.

During the simulation period, all motions of the molecule were observed and no odd behaviour was found. The ring carbon–dummy atom stretching frequency induced minor distortions, and the chromium tricarbonyl group was able to rotate. Some distortion of the carbonyl ligands away from 180° was observed, in keeping with the crystal structure values. Such distortion has previously been observed in a crystal structure of an osmium cluster complex. [13] That this behaviour is reproduced by the current force field without being explicitly included, is a demonstration of its reliability.

This simulation confirmed the viability of the parameter set, however further tests were required to determine the accuracy of the force field. The approach adopted was to simulate the crystal structure of the dibenzyl ether bis-complex **9** in two ways, using the CHARMm crystal simulation facility. [4] Firstly the energy surface of the complex was mapped, and the global minimum structure was identified. The crystal structure of this conformer was then simulated in the space group $P2_1/n$ with the lattice parameters derived from the experimental crystal structure determination. The results were compared to those obtained from a crystal structure simulation of the experimentally determined asymmetric unit with the same lattice parameters and space group.

**Mapping the energy surface of (dibenzyl ether)bis[tricarbonylchromium(0)]**

To find the global minimum conformation of the dibenzyl ether bis-complex **9**, the energy surface of the molecule was mapped as a function of two torsion angles Φ (C11-C18-O7-C7) and Ψ (C21-C7-O7-C8) as indicated on Figure 3.13. Two additional torsion angles were also taken into account when generating the energy surface, viz. T1 (C22-C21-C7-O7) and T2 (C12-C11-C8-O7). The latter torsion angles determine the orientation of the aromatic rings. This is of importance as there could be several minimum energy conformations for the rings to adopt at each Φ/Ψ combination.

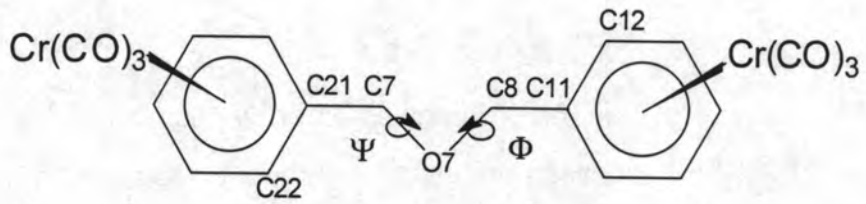


**Figure 3.13:** The torsion angles Φ and Ψ for the energy map

Using CHARMm, [4] (dibenzyl ether)bis[tricarbonylchromium(0)] **9** was constructed and minimised. The energy surface was mapped as a function of Φ and Ψ by rigidly rotating through all the Φ/Ψ combinations in 360° at 30° intervals. At each interval, the lowest energy local minimum was found by stepping through all of the T1 and T2 permutations at 30° intervals, followed by minimisation.

The resulting energy surface is displayed in Figure 3.14. Inspection of this surface reveals the presence of high energy barriers to rotation at Φ =0° and Ψ =0°. The global minimum was found to be at Φ = -180°, Ψ =180°, indicating that the molecule adopts the fully extended conformation in the global minimum structure. The two ring torsion angles (T1 and T2) were found to adopt gauche conformations. The values of these dihedral angles were compared to those found in the crystal structure and are listed in Table 3.10.

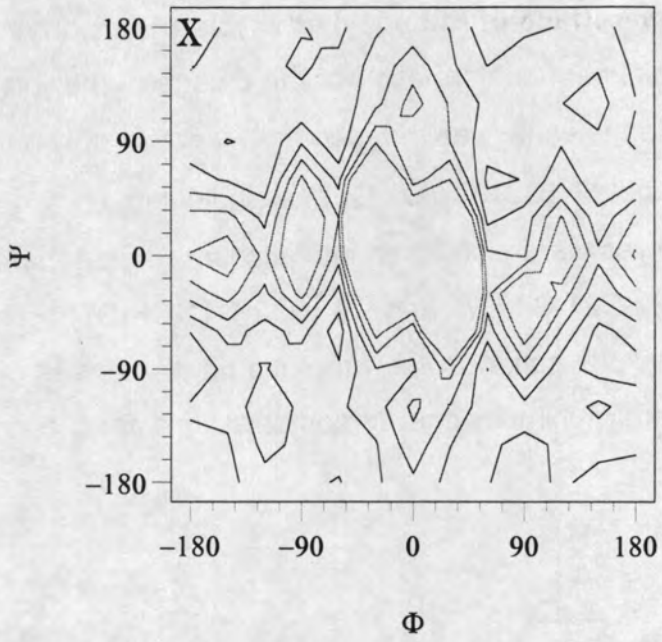


**Figure 3.14:** The energy surface of (dibenzyl ether)bis[tricarbonylchromium(0)] **9** as a function of Φ and Ψ, showing the global minimum near (-180,180). Contours are at 2 kcal.mol$^{-1}$ intervals above the minimum.

**Table 3.10:** Selected torsion angles from the two conformations

| Torsion Angle | Crystal structure | Global minimum structure |
|---|---|---|
| Φ | -179.4° | -180° |
| Ψ | 175.7° | 180° |
| T1 | -24.6° | 11.6° |
| T2 | 91.4° | -85.9° |

It is evident that although the crystal structure approximates the global minimum conformer in terms of the primary dihedral angles Φ and Ψ, the two structures differ to quite a large extent in the ring torsion angle orientations (T1 and T2), with the result that the molecules adopt very different conformations. The two structures are displayed in Figure 3.15 and the difference in conformation between the two is very clear. The orientation of the aromatic ring on the right-hand side in both (a) and (b) is determined by the ring torsion angle T1, whereas the aromatic ring on the left-hand side is controlled by T2.

a) The crystal structure conformer

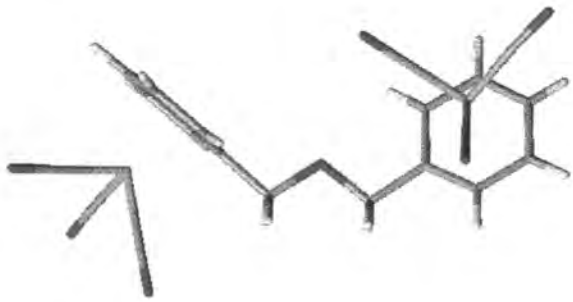

b) The global minimum conformer

**Figure 3.15:** The crystal structure conformation (a) and the global minimum structure (b).

The changed sign for T1 in the global minimum (+11.6° as compared to –24.6° in the crystal structure) results in an effective rotation of the aromatic ring through 36°. Thus the chromium tricarbonyl group remains on the same face of this ring. The changed sign of T2 (-85.9 as compared to +91.4 in the crystal structure) means in effect that the chromium atom is on the opposite face to that observed in the crystal structure, as it is rotated by more than 180° in relation to the latter. In Figure 3.15(a) the tricarbonylchromium group is on the underside of the ring, whereas in the global minimum structure (b) it is on the upper face.

The total energies of the global minimum structure and the experimental crystal structure conformation were compared. Prior to this, the crystal structure conformer was minimised in the CHARMm force field, to relax the structure. Small

adjustments were observed, but the molecule retained the same conformation, and therefore approximately the same values of Φ, Ψ, T1 and T2 (see Table 3.11 for these values). The global minimum was found to be lower in energy than the minimised crystallographic structure by 1.4 kcal.mol$^{-1}$. This difference in energy could be ascribed either to the molecule not adopting the lowest energy vacuum conformation in the crystal structure, or alternatively, it could be due to an error in the parameter set, which introduced a "false minimum".

To ensure that no false minimum was being observed, the individual contributions to the total energy of each conformer were analysed. No single contributing factor could be identified as the primary source of the energy difference, thus it was concluded that the molecule simply adopts a higher energy conformation in the crystal structure compared to the vacuum case, possibly due to packing effects. This was confirmed by the following crystal structure calculations.

**Simulation of the crystal structures**

Two crystal structures of the dibenzyl ether bis-complex **9** were simulated using the crystal build facility in CHARMm, with a cut-off of 24Å. The space group and lattice parameters from the crystal structure determination were used in both cases. The space group is $P2_1/n$, the crystal system and lattice parameters were listed in Table 3.2.

After minimisation, the crystal structure conformation was simulated in the lattice. This was achieved by generating images of the asymmetric unit with the relevant symmetry transformations, followed by minimisation of the asymmetric unit in this crystal environment, with no change to the lattice parameters allowed. It was found that the molecule was stabilised in the crystal by 11 kcal.mol$^{-1}$, with no significant change in conformation. The torsion angles of interest are listed in Table 3.11 for comparison with those of the alternative crystal structure simulation results. The molecule packs easily into this space group with no close contacts between the symmetry-induced images. This is a good indication that the force field is reliable, even though the crystallographic asymmetric unit was used, as it was minimised with the CHARMm force field both in vacuum and the crystal environment. The large decrease in energy from the vacuum conformer to the

molecule in the crystal environment, indicates that the crystal packing is energetically favourable.

The global minimum energy conformation was simulated in the crystal structure environment in an identical manner. This molecule does not pack well into the $P2_1/n$ space group due to close contacts between the asymmetric unit and the symmetry related images. To eliminate the close contacts but still pack into the same space group, severe distortion of the molecular conformation is necessary, this is reflected in the values of the torsion angles listed in Table 3.11. The conformer obtained after minimisation in the lattice is thus very different from the global minimum conformer, and has an energy much higher (30 kcal.mol$^{-1}$) than the previously simulated crystal structure.

**Table 3.11:** Selected torsion angles from both crystal structure calculations

| Torsion Angle | Crystal structure conformer minimised in vacuum | Minimisation of crystal structure conformer in lattice | Global minimum conformer | Minimisation of global minimum in lattice |
|---|---|---|---|---|
| Φ | -179.2° | 179.9° | -180° | -78.7° |
| Ψ | 173.3° | 173.3° | 180° | -152.4° |
| T1 | -29.7° | -29.7° | 11.6° | -93.4° |
| T2 | 96.0° | 96.0° | -85.9° | -115.4° |

Several conclusions can be drawn from these findings. Firstly, the crystal structure of the molecule was successfully simulated using the crystallographic asymmetric unit, with no significant change in the structure. This indicates that the initial CHARMm parameter set that was employed for these calculations is reliable. Secondly, the crystal structure of the molecule was successfully simulated using the global minimum energy structure. This conformer did not pack well into the experimentally derived space group and therefore is energetically disfavoured in the crystal environment. The conclusion that can be drawn from this is that packing effects cause the molecule to adopt a higher energy conformation in the crystal structure. Thus the force field employed is capable of calculating the energy surface and crystal structures accurately for the dibenzyl ether bis-

complex. As this molecule is a model for the peripheral groups of the organochromium dendrimers under investigation, this parameter set can be used with confidence for the dendrimer calculations.

### 3.4 Conclusions

In this chapter, the computational methods to be used in the dendrimer simulation studies were chosen and their underlying theory discussed. Molecular mechanics and molecular dynamics using classical force field methods, are the methods of choice for the simulation of the dendrimers. Molecular mechanics and *ab initio* calculations were selected to be used in the parameterisation of the CHARMm force field used for molecular mechanics and dynamics simulations. The existing CHARMm polymer parameter set was extended to include parameters for the tricarbonylchromium moiety. [8a] It was not the intention of this work to perform a full parameterisation of the force field however the accuracy of the new parameters required assessment.

The important ether linkage torsion angle parameter, which plays a large role in the topology of the dendrimer, was singled out for refinement. This torsion angle was parameterised using the model compound benzyl phenyl ether. The force constant $k_\phi$ for rotation about this dihedral was optimised by fitting the CHARMm results to *ab initio* rotational data.

The second area of parameterisation was the tricarbonylchromium group functionality. These parameters were obtained from the two crystal structures discussed in this chapter, as well as from the literature and modification of existing parameters within the CHARMm polymer force field. [8a] The accuracy and reliability of the resulting parameter set was assessed by simulation of the crystal structure of (dibenzyl ether)bis[tricarbonylchromium(0)] **9**. The energy surface of the molecule was mapped as a function of the ether linkage torsion angles $\Phi$ and $\Psi$, and a crystal structure was calculated for the global minimum energy conformer. This calculated crystal structure had a higher energy than the

simulated experimental crystal structure, indicating that the molecule adopts a higher energy conformation in the crystal structure due to packing effects.

The force field was shown to be reliable, and suitable for use in the simulation of the organic and organochromium dendrimers.

### 3.5 References


1. (a) J.B. Foresman and A.Frisch, *Exploring Chemistry with Electronic Structure Methods*, Gaussian Inc., Pittsburgh, 2nd edition, 1996, pp 253-271; (b) *Gaussian 94* (Revision D.3), M.J. Frisch, G.W. Trucks, H.B. Schlegel, P.M.W. Gill, B.G. Johnson, M.A. Robb, J.R. Cheeseman, T.A. Keith, G.A. Petersson, J.A. Montgomery, K. Raghavachari, M.A. Al-Laham, V.G. Zakrzewski, J.V. Ortiz, J.B. Foresman, J. Cioslowski, B.B. Stefanov, A. Nanayakkara, M. Challacombe, C.Y. Peng, P.Y. Ayala, W. Chen, M.W. Wong, J.L. Andres, E.S. Replogle, R. Gomperts, R.L. Martin, D.J. Fox, J.S. Binkley, D.J. Defrees, J. Baker, J.P. Stewart, M. Head-Gordon, C. Gonzalez, and J.A. Pople, Gaussian Inc. Pittsburgh PA, 1995
2. P.W. Atkins, *Physical Chemistry*, Oxford University Press, Oxford, 5th edition, 1994, ch. 13, pp. 446-447
3. J.P. Bowen and N.L. Allinger, *Reviews in Computational Chemistry*, K.B. Lipkowitz and D.B. Boyd, VCH, New York, 1991, vol.2, ch.3, pp. 81-97
4. B.R. Brooks, R.E. Bruccoleri, B.D. Olafson, D.J. States, S. Swaminathan and M. Karplus, *J. Comput. Chem.*, 1983, **4**, 187-217
5. W.F. can Gunsteren and H.J.C. Berendsen, *Angew. Chem. Int. Ed. Engl.*, 1990, **29**, 992-1023
6. G.H. Grant and W.G. Richards, *Computational Chemistry*, Oxford University Press, Oxford, 1995, ch.4, pp. 51-57
7. A.R. Leach, *Reviews in Computational Chemistry*, K.B. Lipkowitz and D.B. Boyd, VCH, New York, 1991, vol.2, ch.1, pp. 42-43
8. (a) K.J. Naidoo and K. Ueda, unpublished work; (b) A. D. MacKerell Jr., unpublished work.

9. (a) T.N. Doman, C.R. Landis and B. Bosnich, *J. Am. Chem. Soc.*, 1992, **114**, 7264-7272; (b) J.W. Lauher, *J. Am. Chem. Soc.*, 1986, **108**, 1521-1531
10. F.H. Allen and O. Kennard, *Chemical Design Automation News*, 1993, **8**(1), 1 & 31-37.
11. *Comprehensive Organometallic Chemistry II*, E.W. Abel, F.G.A. Stone, G. Wilkinson, J.A. Labinger and M.J. Winter, Pergamon, New York, 1995, vol.5, ch. 8, pp. 479-499.
12. A. Solladié-Cavallo, *Polyhedron*, 1985, **4**(6), 916
13. D.B. Firfiray, A. Irving and J.R. Moss, unpublished work.

# Chapter 4 Simulations of dendritic macromolecules

## 4.1 A review of dendrimer simulation studies

In comparison with the wealth of literature on the synthesis and properties of dendrimers, the number of papers reporting calculations of this particular class of macromolecules is rather meagre. The first attempt to analyse dendrimer structure was a theoretical paper involving no simulations. [1] The authors, de Gennes and Hervet, employed a self-consistent field approach on model dendrimers consisting of branch points connected by flexible linear portions called "spacers". On the assumptions that the spacers are strongly elongated and that the spacers of each generation lie in a concentric shell of their own, oriented away from the core, they investigated the "limiting generation number" beyond which perfect starburst growth is impossible.

The main conclusions drawn from this theoretical analysis, were that a limiting generation number does exist, and that it is an increasing function of spacer length. In addition, the density of the dendrimers is at a minimum near the core, and increases to a maximum at the surface, [1] with the result that the dendrimers should be flexible in the inner shell and rigid at the periphery. As a result of this, the branch ends lie exclusively on the surface of the molecule. [1]

This theoretical analysis provided a basis for comparison for all subsequent dendrimer simulation studies. These studies can be divided into two groups; monomer level calculations, which do not take into account atomic detail, and atomistic simulations which also factor in the molecular composition.

### 4.1.1 Monomer level simulations of dendrimers

Several groups have simulated model dendrimers using Monte Carlo methods or molecular dynamics simulations [2-6] and compared the results with the predictions of de Gennes and Hervet. In most of the studies, the dendrimers were modelled

as strings of beads, with trifunctional branch points, and flexible spacers. In some cases, the functionality of the branch points and the spacer lengths were chosen specifically to closely match PAMAM dendrimers. [2,4,5] This might provide a point of departure from the theoretical results, as PAMAM spacers are fairly short, whereas the de Gennes - Hervet model was based on long spacer lengths.

There are a few points of discord between the different coarse-grained models, however the general agreement between these separate studies is good over a number of properties, which are described below.

**Limiting generations**

In all of the studies a limiting generation number was observed, beyond which it is not possible to construct dendrimers with perfect starburst growth. [2-5] Lescanec and Muthukumar found this property to be an increasing function of spacer length,[2] in accordance with de Gennes and Hervet, however the average generation number reached in their simulations was found to be substantially lower than that predicted by the theoretical analysis, therefore indicating that the "starburst limit" is reached much earlier. [1,2]

**Density distribution**

Radial distribution functions calculated in most of the studies show that the density is highest at the centre, and decreases outwards toward the surface of the molecule. [2-5] This is in complete disagreement with the theoretical model, where a maximum at the periphery is predicted. [1] For some dendrimers, notably the higher generations, an interesting phenomenon is observed. In moving away from the centre, the density decreases rapidly to a local minimum, then increases again before continuing the general decline. [3-5] The study by Carl found internal voids close to the centre, which would seem to correspond to this local minimum in density. [3] Another study found that this local minimum is followed by a region of almost constant density, before the general decline is resumed. [6]

**Location and behaviour of terminal groups and internal monomers**

Hand-in-hand with the density distribution studies, were the efforts to locate the terminal groups of the dendrimers. Spatial location of these monomers is

necessary for structural analysis, but is of particular importance if the dendrimer is intended as a catalyst. The catalytically active metals could be bound on the outer generation of the dendrimer, but not necessarily physically present at the periphery of the molecule. If chain folding occurs to a large or even moderate extent, then the active sites might be buried deep within the dendrimer and thus not accessible for catalysis.

The de Gennes-Hervet model proposed that the terminal groups are rigid and inflexible, and are located exclusively at the periphery of the molecule. [1] This finding was refuted by all of the monomer-level studies. [2-6] Significant chain folding was observed with the result that the branch ends are found in all regions of the dendrimer, as evidenced by density profiles of these groups. [2-6]. The end spacers in particular are relaxed, while the inner spacers are more extended, especially in the higher generation dendrimers. [5] This effect is attributed to molecular crowding.

Murat and Grest have taken this density calculation further, and located the monomers from all generations of dendrimer growth. [6] It was found that the monomers belonging to the early generations are fairly localised, with little overlap of the density profiles of these generations. [6] As the generation number of the dendrimer increases, these peaks in the density profiles shift further away from the core, as a result of the early generations spacers becoming more extended, and more overlap between the peaks is observed. In the larger generation dendrimers, significant backfolding occurs, to such an extent that the terminal monomers are found in all regions of the dendrimer, including the core. [6]

This last finding obviously has tremendous significance if the intent were to utilise the surface groups of the dendrimer for any purpose, such as for catalyst support. It should be noted that the calculation of monomer density profiles as described above, effectively allows for the structural analysis of the macromolecule – something that is not currently available by any other technique. This calculation is therefore of significant interest.

**Intrinsic viscosity**

Intrinsic viscosities calculated from the simulation data were in good agreement with experimentally determined viscosities, particularly when short spacer lengths were used. [4] Typically, experimental intrinsic viscosity values pass through a maximum as a function of generation, this is reflected in the simulation results. [6]

**Relaxation times**

A rough estimation of the relaxation times of PAMAM dendrimers has been reported. [5] It was predicted that for later (seventh to ninth) generation PAMAM dendrimers, the relaxation times are in the microsecond regime. This property is a strong function of generation, thus for dendrimers smaller than the sixth generation the relaxation times are expected to be in the range of 100ps. [5] This is a more manageable time frame for dynamics calculations.

**Dendron segregation**

An intriguing phenomenon first noted by Mansfield is that, at equilibrium, chemically identical dendrons are segregated. [6,9] Segregation is also observed at subdendron level. [9] To prove that this behaviour was not a result of any inherent bias in the initial configurations, runs were performed from completely intermixed conditions, and the dendrons were found to spontaneously segregate. [9]

**Solvent effects**

Murat and Grest have reported the first example of a dendrimer study to include the effects of solvent quality. [6] In this work, the athermal solvent (infinitely good) was studied along with a good solvent, a $\Theta$ solvent, and a poor solvent. The effect of the solvent quality on several properties of the dendrimers was investigated.

Solvent quality had only a small effect on the density distribution, as the radial distribution functions remained essentially the same. The only difference that was observed, is that as the quality of the solvent worsens, the height of the constant density region increases, while the width decreases. [9] This indicates that the internal monomers become more condensed in a poor solvent. Radial density profiles of the monomers of each generation are also affected by the solvent quality to a certain degree. The peaks due to each generation are shifted to a

smaller distance from the core in worse solvents. These results are consistent with another finding by the same authors, that the dimensions of the dendrimers shrink as the solvent quality decreases. [6]

Dendron segregation behaviour was also affected by the solvent. It was found that segregation decreased as the solvent worsened, so that in a poor solvent the dendrons were completely intermixed. [6] Relaxation times were studied as well, and found to increase with solvent quality. [6]

A common feature of the all the coarse-grained calculations described above, is their lack of atomic detail. These simulations were designed to provide general properties for many starburst molecules, so-called "universal" properties, and may well do this quite successfully however no account is taken of atomic interactions, such as hydrogen bonding, [4,5] or of preferred conformations, such as *trans* vs. *cis*. [5] In addition, all bonds are treated as being the same length, while individual spacers may be more or less flexible than those in dendrimers. [5] This lack of attention to atomic detail could invalidate the applicability of the results. [2,3,5] The advantage of these coarse-grained models is that they allow a range of universal properties to be calculated on well equilibrated structures, even in the presence of solvent, [6] while being much less time intensive than atomistic studies. [5]

Bearing in mind the lack of any atomistic information, it is significant that the intrinsic viscosity calculations agree well with the experimental data for both PAMAM and poly(benzyl phenyl ether) dendrimers. [7,8] This would seem to be evidence that the simulations do indeed allow the determination of "universal" properties. It should be noted however, that the PAMAM and poly(benzyl phenyl ether) dendrimers have the same branch point multiplicity (number of branches at each branching point). This would make these dendrimers far more similar to each other, topologically speaking, than to other dendrimers with different branch point multiplicities. Several of the monomer-level studies were based on PAMAM branching functionality and spacer lengths, [2,4,5] thus the apparent capability to predict the behaviour of poly(benzyl phenyl ether) dendrimers might be due to the similarity of the two systems. Comparison of the simulated properties with experimental data from dendrimers with a higher branch point multiplicity such as

polysilane dendrimers, would provide a better indication of whether the results are truly "universal" or not.

### 4.1.2 Atomistic simulations of dendrimers

Very few examples of atomistic calculations on dendrimers exist in the literature, and most of these focus on the polyamidoamine (PAMAM) dendrimer system. [8,10,14] As with the monomer-level studies, several important properties were investigated by atomistic methods.

**Dendrimer morphology**

Naylor and Goddard reported a molecular dynamics study on PAMAM dendrimers constructed from β-alanine monomer units. [10] From molecular dynamics simulations of 5ps length, the maximal dimension and moments of inertia were measured for seven generations of growth. It was found that the early generations are asymmetric, with open and extended features. At generation four, a transition occurs, and the dendrimers become much more dense spheroidal structures with internal hollows connected by channels. [10]

Some evidence for this transition comes from experimental studies of poly(benzyl phenyl ether) dendrimers, containing a solvatochromic probe at the core of the molecule. [11] Small changes in the polarity of the environment of this probe cause changes in the UV-vis. spectra. This allows the microenvironment of the core to be studied as a function of generation. In low-polarity solvents, a significant change in the absorption maximum was observed between generations three and four. [11] The authors correlated this change to a crossover from an extended to a dense, globular structure. [11]

More supporting evidence for this transition to a globular structure was provided by other sources. The characteristic maximum observed in experimental intrinsic viscosity data occurs at generation three for poly(benzyl phenyl ether) dendrimers, and at the fourth generation for PAMAM dendrimers, [7,8] while experimental density measurements show that PAMAM dendrimer density reaches a minimum

between generations four and five. [8] These properties are quite conceivably due to this crossover to a more globular structure.

Electron paramagnetic resonance spectra on the same system also indicated that a change in shape occurs at the third generation. [12] This transitional behaviour has even been observed in a completely different class of dendrimers. [13] It was reported that phenylacetylene dendrimers, in non-polar hydrocarbon solvents, display an anomalous spectral shift that is very dependent on generation number. This suggests a change in size and shape beyond the fifth generation, which could be consistent with a transition to a globular structure. [13]

The morphology of polyether dendrimers has also been investigated. [8] This class of dendrimers is found to congest far more quickly than the PAMAM system, due to the higher branching multiplicities, with the result that there are little or no interior cavities. [8]

**Dendrimer hosting capability**

To explore the ability of the dense PAMAM dendrimers to act as hosts, an NMR study was carried out in the presence of small guest compounds. [14] The $T_1$ relaxation times of the guest molecules seemed to indicate that generations four and higher were capable of encapsulation. [14]

More recently, the hosting capabilities of dendrimers have been investigated in a simulation study of the Meijer dendrimer box. [15] This dendritic molecule is formed by the addition of bulky capping groups to a fifth generation poly(propyleneimine) dendrimer. The macromolecule was simulated in solvent and in the presence of Bengal Rose dye molecules. The results agree very closely with experimental work, which found that the dendrimer can encapsulate up to four guests. [15]

**Solvent accessible surface**

The solvent accessible surface (SAS) of a dendrimer can obtained by rolling a "sphere" of radius P (P= effective radius of solvent) around the van der Waals surface of the molecule. [8] By approximating the dendrimers as spherical, the external surface area of both PAMAM and polyether dendrimers were estimated. [8]

It was found that the SAS of PAMAM dendrimers increases rapidly with generation due to the additional internal surface area, so much so that a sixth generation dendrimer has more internal solvent-accessible surface area than external. [8] The more dense polyether system has a much smaller internal surface area. [8]

**Dendrimer dimensions**

Dendrimer diameters have been calculated by a number of methods for both the PAMAM and polyether systems, and generally good agreement with experimental diameters was found. [8] In addition to these two systems, the dimensions of poly(benzyl phenyl ether) dendritic wedges (dendrons) have been measured. [16] In this work the dendrons were attached to a monofunctional core, instead of the traditional trifunctional core molecule 1,1,1-tris(4′-hydroxyphenyl)ethane. By isotopic labelling at the core and surface of these dendrons, the dipolar coupling was measured, and an indication of dimensions obtained. It was found that the average intramolecular distance was approximately the same for generations three to five, which indicates inward folding of the chain ends with increasing generation number. [16]

**Radial density profiles**

The intra- and intermolecular distances obtained from the dipolar coupling measurements, were used as constraints for a molecular dynamics study of the fifth generation dendron in vacuum, and in the solid state as a seven-molecule cluster. [16] This is the first reported example of the use of constraints in a molecular modelling study of dendrimers. A solid-state radial density profile indicated that the density decreases monotonically away from the core, which is similar to the results of the monomer-level simulation studies. [2-6] In the cluster, the area of reduced density at the periphery is filled by the terminal groups of other dendrimers.

These atomic-level calculations provide more detail than the coarse-grained models, and the results are more specific to the particular system under investigation. In addition, the range of properties that can be investigated by atomistic techniques is broader. Encapsulation of guests, solvent accessible surfaces, the transition from an open to a globular structure, are all properties only

predicted with these techniques. Moreover, all of the properties examined in the monomer-level simulations can also be calculated from atomic-level calculations, including relaxation times, dendron segregation and density distributions. The limitation of the technique is the time expense of the calculations, which becomes especially significant when solvent effects are also to be investigated. The monomer level calculations are much faster under these conditions.

## 4.2 Objectives

The review of dendrimer simulation studies provides a background to the research already done in the field of dendrimers, and places this work into perspective. As far as we are aware, no molecular dynamics simulations of the family of poly(benzyl phenyl ether) dendrimers have been reported. Furthermore, no calculations on any organometallic dendrimers have been reported.

The objectives of this study were to simulate the molecular dynamics of generations one through five of the organic poly(benzyl phenyl ether) dendrimers reported by Hawker and Fréchet, [17] and generations one through five of the organochromium dendrimers which were the focus of the synthetic work. Several important properties of the macromolecules, listed below, were targeted for investigation.

- Dimensions
- Density distributions
- Monomer density profiles
- Solvent accessible surface

Analysis of the radial density distributions will provide detailed structural information about these macromolecules currently unavailable by any other technique. In particular, the spatial location of the terminal groups can be determined, and inferences drawn as to the accessibility of the chain ends. This information can be compared to the results of the solvent accessible surface study, to evaluate the potential applicability of the polymers as catalyst supports.

## 4.3 Computer simulation of poly(benzyl phenyl ether) dendrimers

### 4.3.1 Construction of the dendrimers

The general strategy for constructing the dendrimers was based on the strengths of the computational program CHARMm, [18] which was used to construct, energy minimise and simulate the dynamics of the dendrimers under study, as well as performing the analysis of the dynamics trajectories. CHARMm was specifically designed for the study of macromolecules, and so uses repeat units to build up the large structures. In this study, there were several monomer units required to construct the dendrimers *viz.*:

- The "CORE" molecule: 1,1,1-tris(4´-hydroxyphenyl)ethane.
- The main repeat-unit: 3,5-dihydroxybenzyl alcohol.
- The surface functionalities: a benzyl group in the organic dendrimers, and a (benzyl)tricarbonylchromium(0) complex in the organometallic dendrimers.

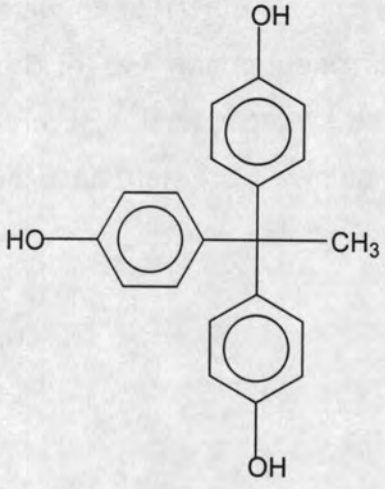


**(a)**

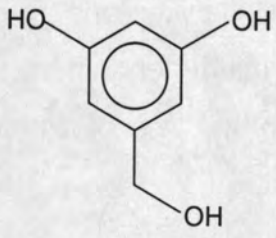


**(b)**

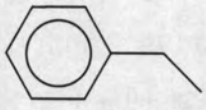

**(c)**

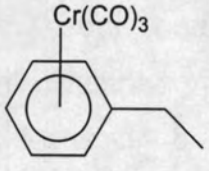


**(d)**

**Figure 4.2**

a) The CORE

b) 3,5-Dihydroxybenzyl alcohol

c) The benzyl surface group

d) The surface complex (benzyl) tricarbonylchromium(0)

These repeat units, depicted in Figure 4.2, were constructed with CHARMm and energy minimised, in order to provide sensible starting structures with which to build the dendrimers.

### 4.3.2 Conformational analysis of the dendrimer repeat unit

Besides the structure of the repeat units, the manner in which they are linked was also considered important. In the synthesis of a dendrimer, two surface groups react with 3,5-dihydroxybenzyl alcohol form a first generation wedge, shown in Figure 4.3.

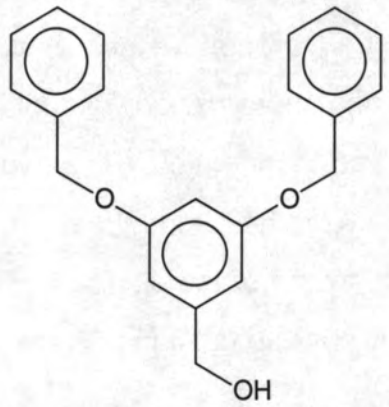


**Figure 4.3:** A first generation organic wedge.

This wedge contains two ether linkages, one between each surface group and what was formerly 3,5-dihydroxybenzyl alcohol. This benzyl phenyl ether linkage is found throughout the dendrimer, not only in connecting surface groups to interior monomers, but also where monomers are linked to each other and to the core. The conformation of the ether link is extremely important, and can be completely defined by three torsion angles: $\Phi$, $\Psi$ and $\Omega$, as shown in Figure 4.4.

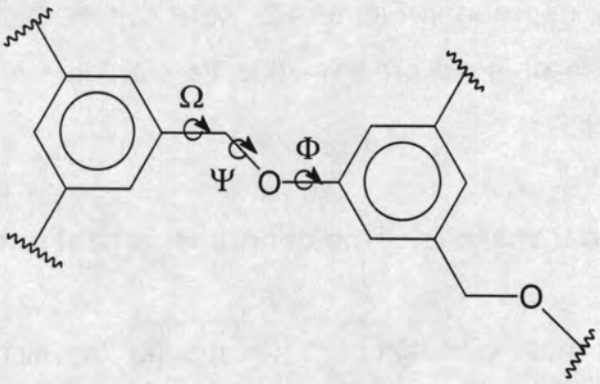


**Figure 4.4:** The general ether linkage and the three torsion angles: Φ, Ψ and Ω.

The central dihedral angle Ψ is the most important. If this torsion angle is 180°, then the ether linkage will be fully extended, and the resulting dendrimer built with this conformation will have a very open, extended structure. Alternatively, if this dihedral angle is 0°, then the molecule will be folded back on itself, and the resulting dendrimer will be very condensed. The two remaining dihedrals Φ and Ω, determine the orientation of the aromatic rings. Thus, together, the three dihedral angles define the topology of the entire dendrimer. This is why the main torsion angle Ψ was carefully parameterised in Chapter 3.

To find the lowest energy conformation of the ether linkage, the energy surface was mapped for a model compound, called the dimer. The dimer, depicted in Figure 4.5, consists of two 3,5-dihydroxybenzyl alcohol monomers connected via an ether linkage, and best represents the interior structure of the dendrimer. Two energy surfaces were calculated, one as a function of the torsion angles Φ,Ψ and the other as a function of the torsion angles Ψ,Ω. These energy surfaces are shown in Figure 4.6.

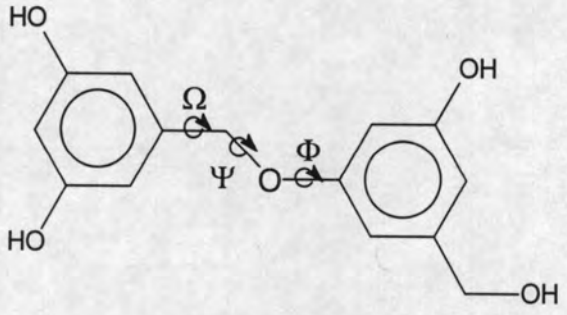


**Figure 4.5:** The "dimer"

The energy surface was mapped as a function of the two torsion angles Φ and Ψ, (or Ψ and Ω) by rigidly rotating through all the Φ/Ψ (or Ψ/Ω) combinations in 360° at 30° intervals. At each interval, the lowest energy local minimum was found by stepping through ninety-six permutations of allowed alcohol group orientations, followed by minimisation.

a)

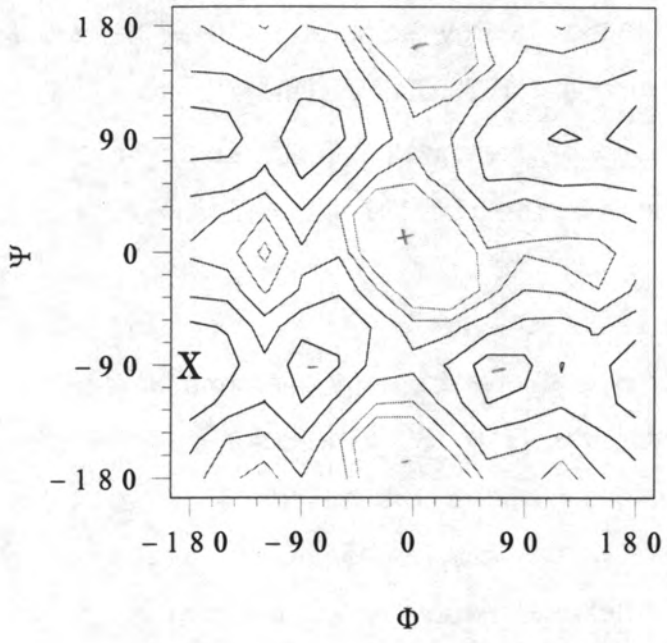


b)

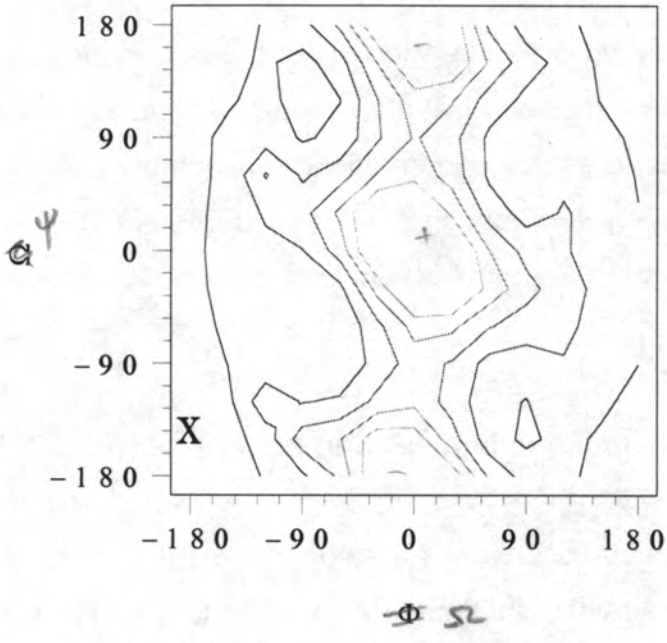


**Figure 4.6:** (a) The Φ,Ψ surface (b) The Ψ,Ω surface
Energy contours are at 2kcal.mol$^{-1}$ above the minimum

From both contour maps, it is clear that the torsion angle Ψ dominates the total energy. There is, in both surfaces, a high energy region for Ψ = 0°, and a low energy trough where Ψ = 180°, irrespective of the values of the other torsion angle. The ether link therefore prefers the extended conformation and dendrimers built with this value (Ψ = 180°) will have an open, extended structure.

In the Φ/Ψ map, there are low energy troughs where Φ = 90° and –90° (due to symmetry) which intersect the high energy region at Ψ = 0°. The global minimum of this energy surface is found at (-180°, -90°). The Ψ/Ω map shows a similar surface, with the preferred value of Ω less well defined. Energy troughs are visible around Ω = 90° and –90°, however the global minimum obtained from this surface, was at (-180°, -150°).

From the two energy surfaces, the lowest energy conformation can be found for the dimer *viz.* Φ = - 90, Ψ= - 180, Ω= - 150. These three torsion angle values, along with the energy minimised monomers described earlier, were used to construct the final dendrimers. In this way, the dendrimers should be relatively low in strain, with fairly open structures - ideal starting conformations for molecular dynamics simulations.

A program written for CHARMm, was used to construct the dendrimers from the monomer units, with the linking topology just described. Generations one to five of the poly(benzyl phenyl ether) organic dendrimers were assembled, along with the corresponding generations of the organochromium dendrimers. The dendrimers were all energy minimised to remove strain, before starting the molecular dynamics simulations.

### 4.3.3 Molecular dynamics simulations of dendrimers

The molecular dynamics simulations were run keeping chemical bonds involving hydrogens fixed via the constraint algorithm SHAKE. The long range interactions were decreased smoothly to zero between 12 Å and 14 Å using the CHARMm switching and smoothing functions on an atom-by-atom basis. The equations of

motion for the dendrimers were integrated in steps of 1fs, using a Verlet algorithm. The simulation period after an initial 15ps heating stage, was 600ps long. During this period, the velocities were periodically rescaled to maintain the correct temperature of 300 K.

## 4.4 Results and analysis

From the data contained in the molecular dynamics trajectories, it is possible to calculate numerous physical properties of the dendrimers, through the use of statistical mechanics. The key areas targeted for analysis, are dimension, density distributions, monomer density profiles and solvent accessible surface.

### Dendrimer dimensions

An indication of the dimensions of the macromolecule can be obtained by calculating the radius of gyration. This is defined as the root-mean-square (RMS) distance of an array of atoms from their common centre of gravity. The time evolution of the instantaneous radius of gyration ($< R_G^2 >$) was calculated for each generation of the organic and organochromium dendrimers, and is displayed in Figure 4.7. The left-hand column contains the time-series for the organic dendrimers, whereas the right-hand column contains the time-series for the organochromium dendrimers. The legend in the top right-hand corner of each plot, indicates the generation of the dendrimer for which that particular time-series was calculated, G1 signifies a first generation dendrimer, G2 a second generation dendrimer and so on. The suffix Cr indicates that the dendrimer is an organochromium dendrimer. For each time series, there is a solid line curve fit.

**Fig. 4.7:** Time evolution of the instantaneous radius of gyration

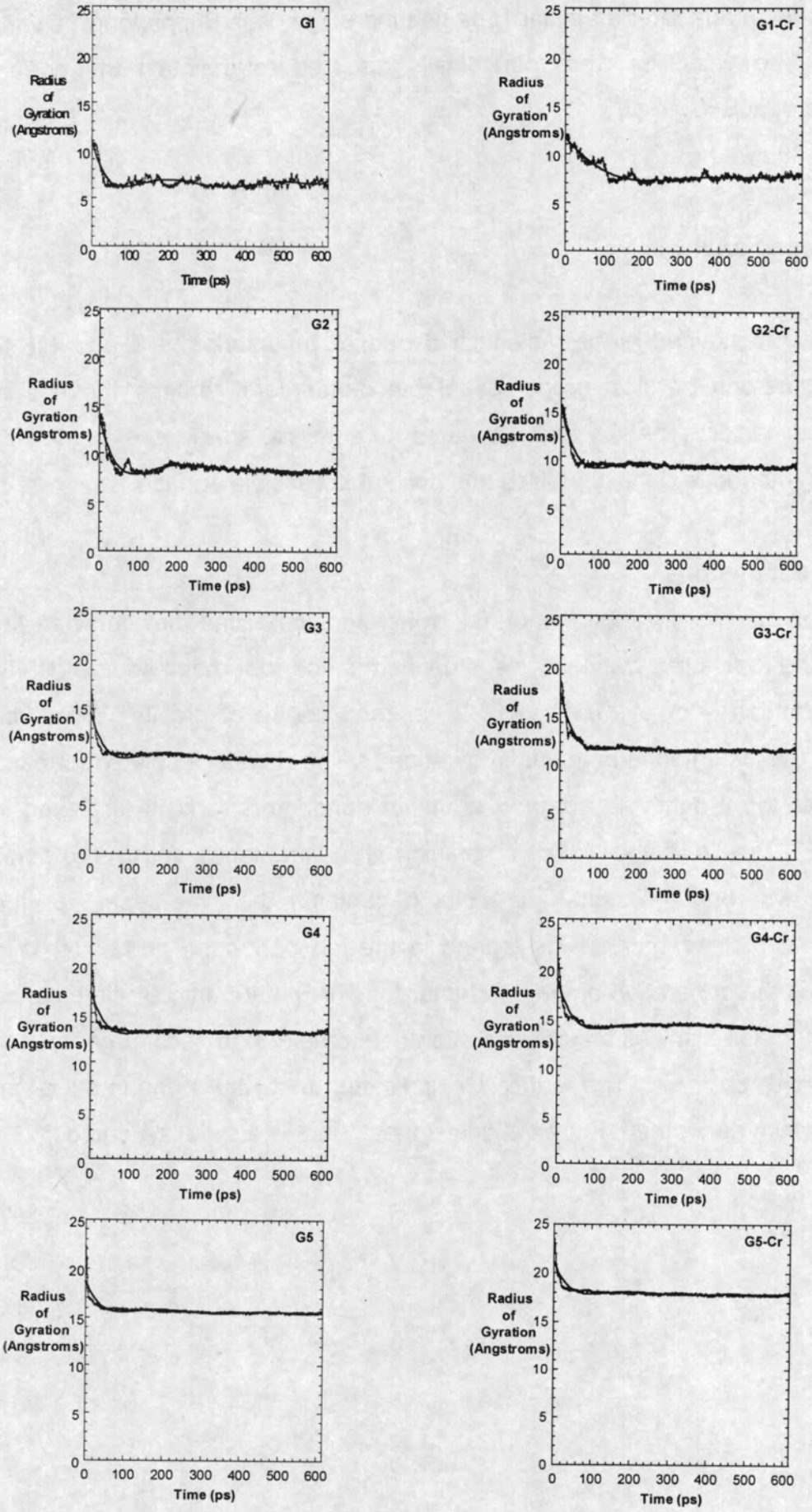

The time series are qualitatively similar, with the same general features. Starting from the initial configuration, whose construction was described above, the dendrimer was equilibrated. The $< R_G^2 >$ rapidly decreases over the first fifty picoseconds and stabilises after this period, to fluctuate around the average value. This indicates that the dendrimer is condensing from the initial extended structure to a far more folded conformation. This is illustrated in Figure 4.8, in which the initial structure of a fourth generation organochromium dendrimer and a corresponding structure which has the lowest energy extracted from the entire dynamics trajectory, are displayed.

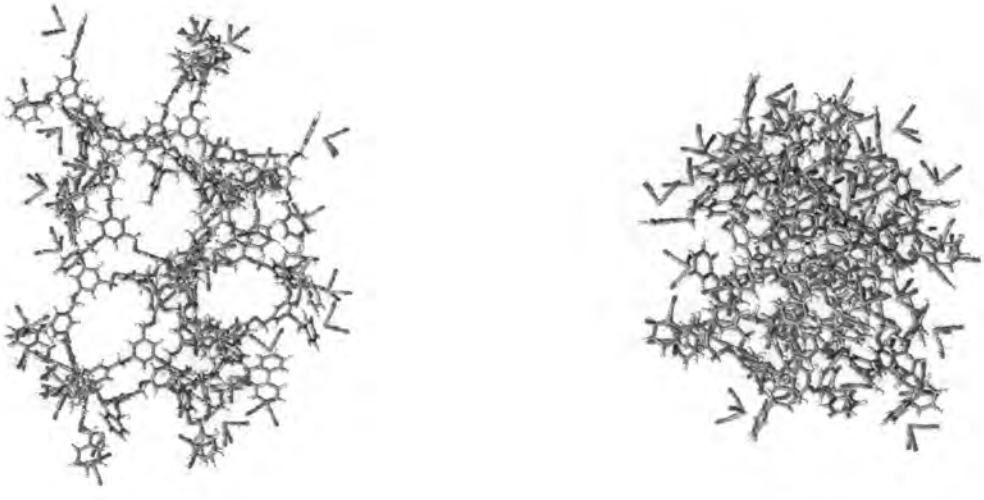

(a) (b)

**Figure 4.8:** (a) The extended structure (b) The folded low-energy conformation

This rapid condensation to a globular, folded structure is a result of the simulation taking place in vacuum. Vacuum simulations are comparable to simulations in a poor solvent. In such a solvent, there are no solute-solvent interactions to compete with the attractive van der Waals and electrostatic solute-solute interactions. Thus the predominant interactions are intra-molecular and attractive, so the molecule folds in upon itself. If the dynamics simulations were run in better solvents it is likely that this condensation behaviour would be observed to a lesser extent, as was observed in a monomer-level study of dendrimers in solvents of varying quality.[6]

The average radius of gyration was calculated as a function of generation, and is illustrated in Figure 4.9. The initial pre-equilibration stages of the simulation are excluded from the calculation of the average properties.

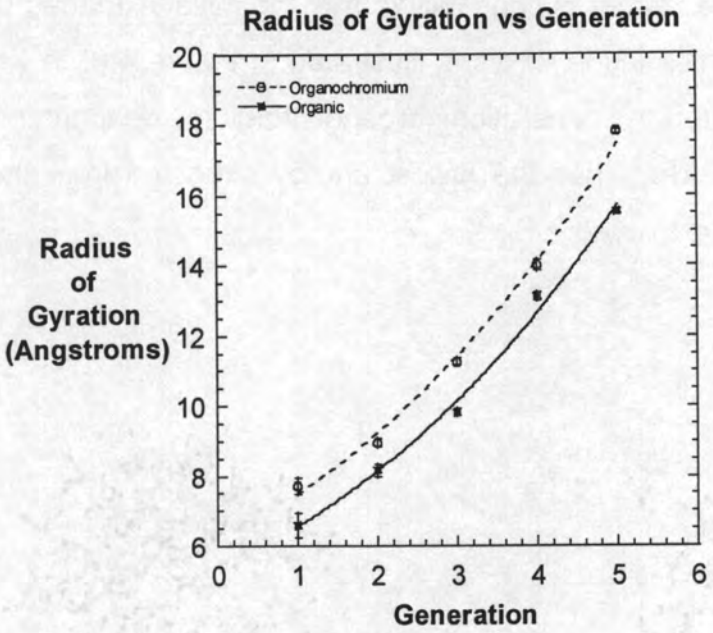


**Figure 4.9:** Average radius of gyration vs. generation for the organochromium and organic dendrimer.

It is clear from Figure 4.9, that the average size of the organochromium dendrimers is larger than that for the corresponding organic dendrimer, as would be expected. The average $< R_G^2 >$ increases exponentially with generation, as shown by the exponential curve-fits in Figure 4.9. Furthermore, the larger errors associated with the earlier generations of both the organic and organochromium dendrimers are a result of the larger fluctuations about the average values observed in Figure 4.7 for these molecules.

The exponential behaviour of this property is unsurprising in light of the fact that the number of monomers, and hence the molecular weight, increases exponentially with generation. A double-logarithmic plot of the average radius of gyration as a function of molecular weight is shown in Figure 4.10.

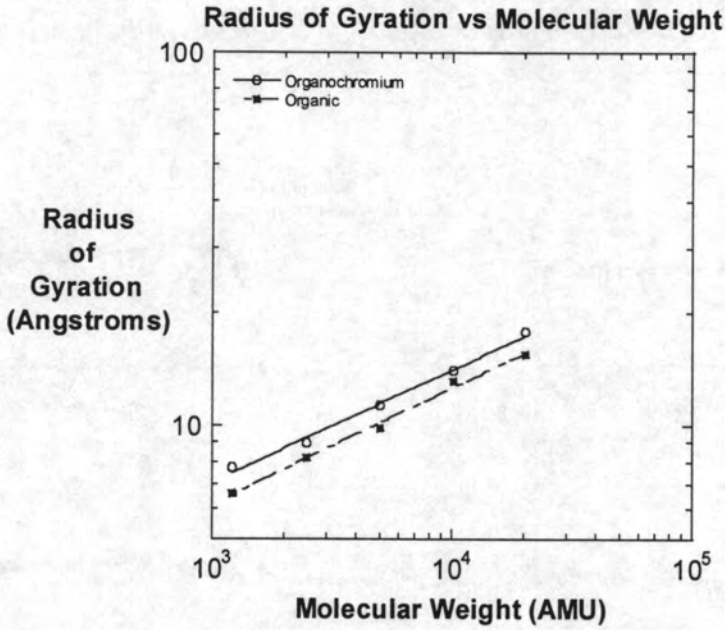


**Figure 4.10**: Average radius of gyration vs. molecular weight on a double-logarithmic scale.

The points correspond to the measured averages, whereas the lines are best fits of the form [$< R_G^2 > = A(MWt)^x$]. The value of x is 0.31 for the organochromium dendrimers and 0.30 for the organic dendrimers.

In addition to the radius of gyration, the instantaneous root-mean-square (RMS) variation of the dendrimers from their initial structures was calculated. This too provides an indication of whether the system has reached equilibrium. The RMS variation for both the organic and organochromium dendrimers are displayed in Figure 4.11. As before, the organic dendrimer data are in the left-hand column and the organochromium dendrimer data in the right-hand column. The legends have the same meanings as previously defined. A solid line curve fit is present in each time series.

**Figure 4.11**: Time evolution of the RMS variation

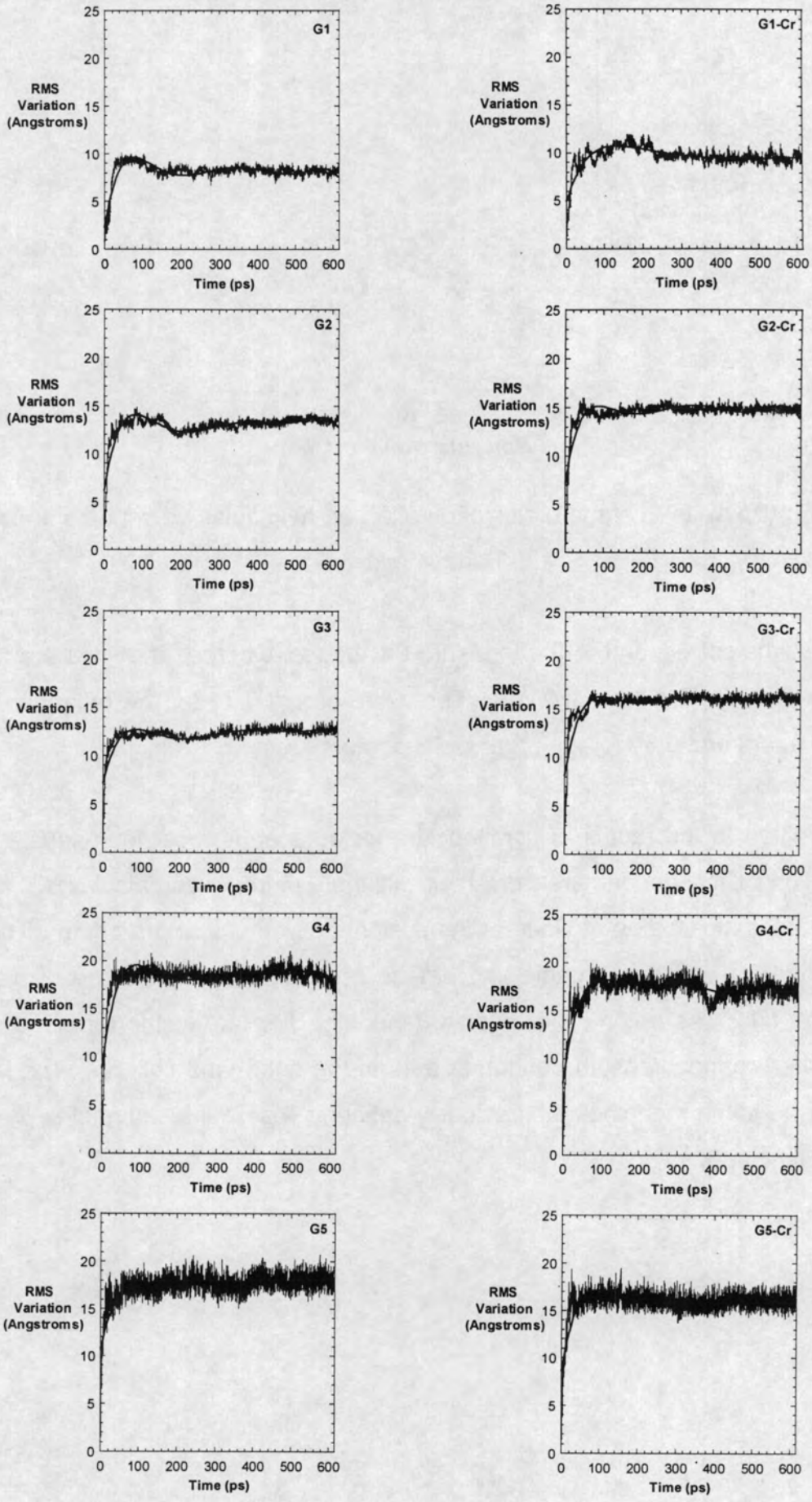

The individual RMS variation time series are qualitatively similar, however substantially more fluctuation is observed in the later generations. As in the radius of gyration time series, the system equilibrates rapidly within the first hundred picoseconds, after which time it stabilises and fluctuates around the average value. The discontinuity present in the time series of the fourth generation organochromium dendrimer has no obvious cause, but might be due to one dendron unfolding, while another folds inward to fill the void.

The relationship between RMS variation and generation, displayed in Figure 4.12, is not as apparent as in the radius of gyration study. The deviation from the mean associated with the RMS variation is larger, due to the increased fluctuation around the average values in Figure 4.11.

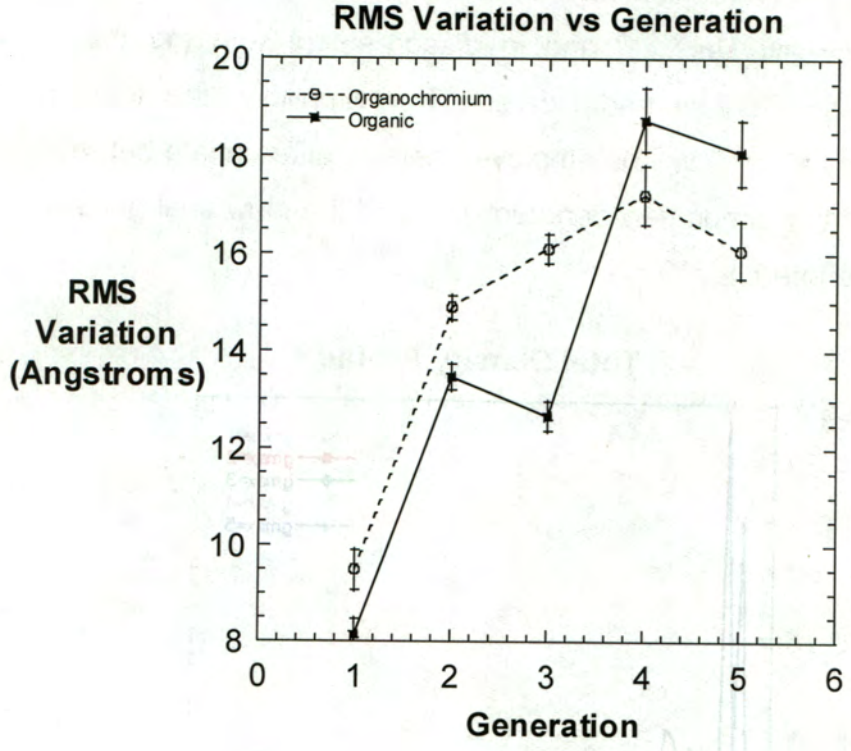


**Figure 4.12**: RMS variation vs. Generation

It is interesting that both the organic and the organochromium dendrimers appear to go through a significant change at some generation, which could be attributed to a transition from a more open structure to a globular condensed structure, as proposed in other studies. [10,11] This behaviour is more apparent for the organochromium dendrimers, where the RMS variation goes through a maximum

at the fourth generation, but is also observed for the organic dendrimers. The latter however is complicated by the apparent minimum in RMS variation that occurs at generation three.

**Density distributions**

The density is calculated as the number of atoms N(r) within a spherical shell of radius r and thickness $\Delta r$, averaged over all of the configurations, divided by the volume of the shell. This is described in equation 1.

$$\rho(r) = N(r)/4\pi r^3 \qquad (1)$$

The density profiles of the organic and organochromium dendrimers, illustrated in Figure 4.13 and Figure 4.14 respectively, were consistent with the findings of all the previous simulation studies, [2,4-6] and in disagreement with the theoretical model proposed by de Gennes and Hervet. For simplicity, the terminology described in a previous study, [6] will be employed here to differentiate between the generation number of the dendrimer, denoted $g_{max}$ and the individual generations within a dendrimer, denoted $g_i$.

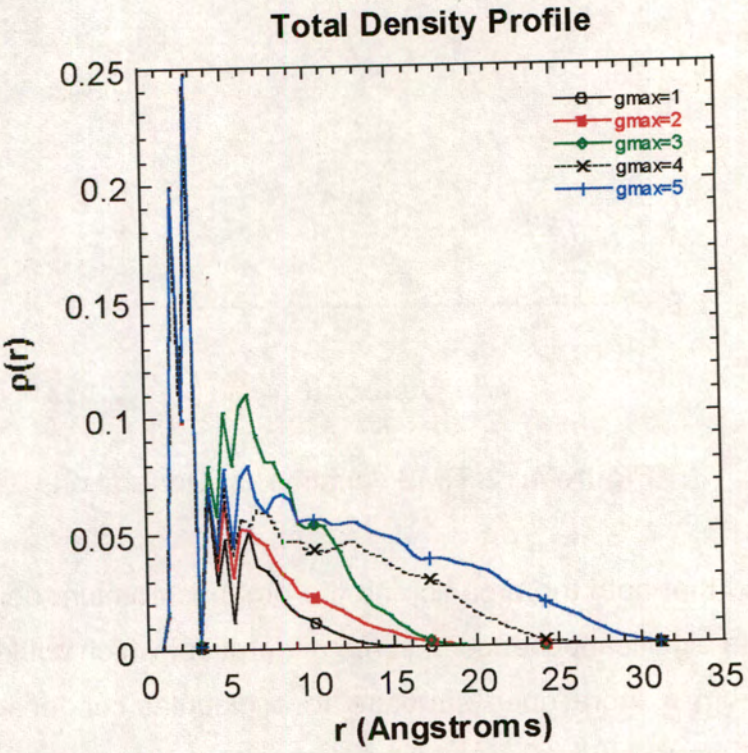


**Figure 4.13:** The density profile of the organic dendrimer series

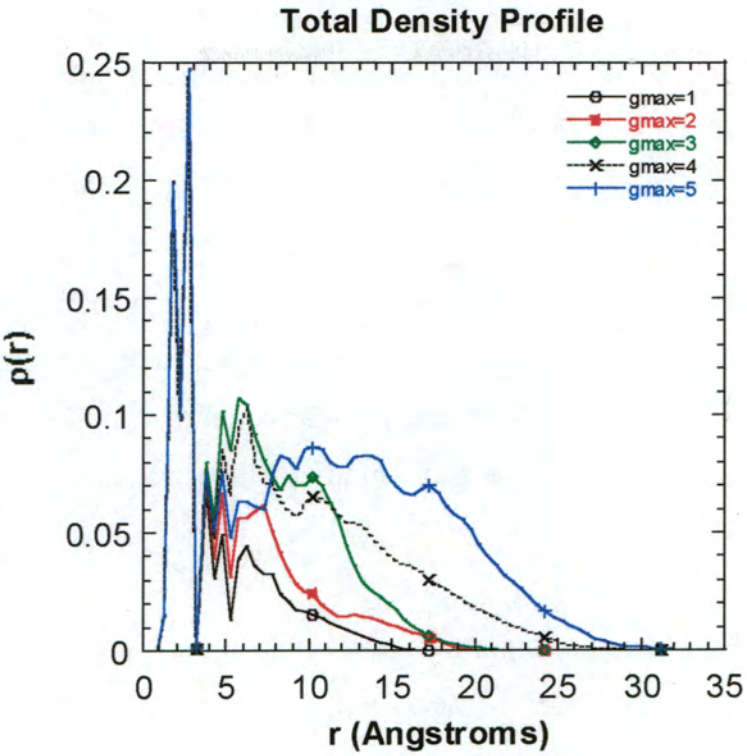


**Figure 4.14:** The density profile of the organochromium dendrimer series

The profiles of each series have common features. After an initial induction distance, the density of each generation $g_{max}$ is at its highest near the centre, and decreases to a minimum at a distance of 3Å away from the core. Beyond this minimum the density increases away from the centre for a period, before tailing off. This is qualitatively consistent with the results of coarse-grained studies except for the induction distance, which was not observed in these calculations.[3-6] The induction distance is probably a result of taking the atomic detail, such as bond lengths, of the core molecule into account.

The region of very high density at the core, which is present in all generations, can be attributed to the atoms belonging to the central core monomer. The remaining density is due to the atoms of the rest of the molecule. As expected for a condensed macromolecule, the density increases and extends further from the core with increasing generation. A region of almost constant density was found in the profile of the fifth generation organometallic dendrimer. This constant density region was observed for the higher generations $5 \leq g_{max} \leq 8$ in one of the monomer-level studies. [6]

A comparison of the density profiles of the organic and organochromium dendrimers highlights some differences between the two systems. The peaks due to each generation occur at approximately the same distance, however the tail zone, where the density decreases gradually, extends slightly further for the organometallic dendrimers, with the exception of the fifth generation which extends to the same distance. The monomers of the fifth generation organochromium dendrimer seem to undergo more backfolding, so that the density is increased at the interior of the molecule, resulting in the region of almost constant density. In general, the density profile findings reported here are in good agreement with all of the previous simulation studies. [2,4-6]

**Monomer density profiles**

An analysis of how the monomers of each generation are distributed within the dendrimer was first performed by Murat and Grest in a coarse–grained simulation study. [6] This calculation allows a detailed structural analysis of the dendrimer, something not currently possible by any other technique. Of particular interest is the distribution of the last generation of monomers. The latter is especially true when these monomers are functionalised by catalysts, as the accessibility of the catalyst might be affected.

Monomer density profiles were calculated for each generation $g_{max}$ of the organic and organochromium dendrimers, and the results are displayed in Figures 4.15 and 4.16. The various contributions to the total density $\rho(r)$ from each generation of growth are clearly illustrated for every generation of dendrimer $1 \leq g_{max} \leq 5$.

It can be seen from these monomer density profiles of the organic dendrimers Figure 4.15(a)-(e), that the peak due to $g$=1 is not localised, and in fact splits into several peaks in the later generations. This is partly a consequence of the monomers for this generation being necessarily selected slightly differently to those of other generations.

**Figure 4.15:** Monomer density profiles of the organic dendrimers

a)

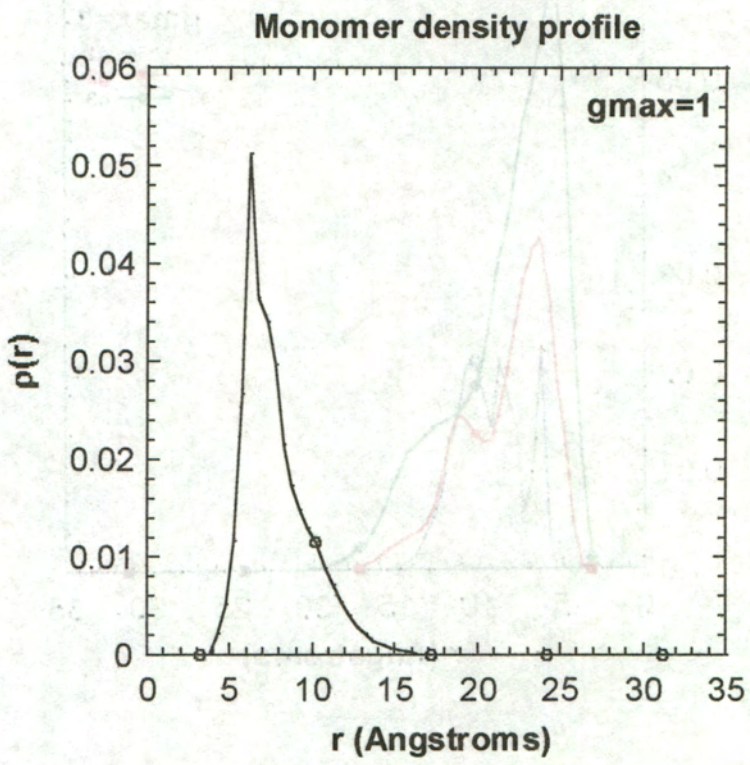


b)

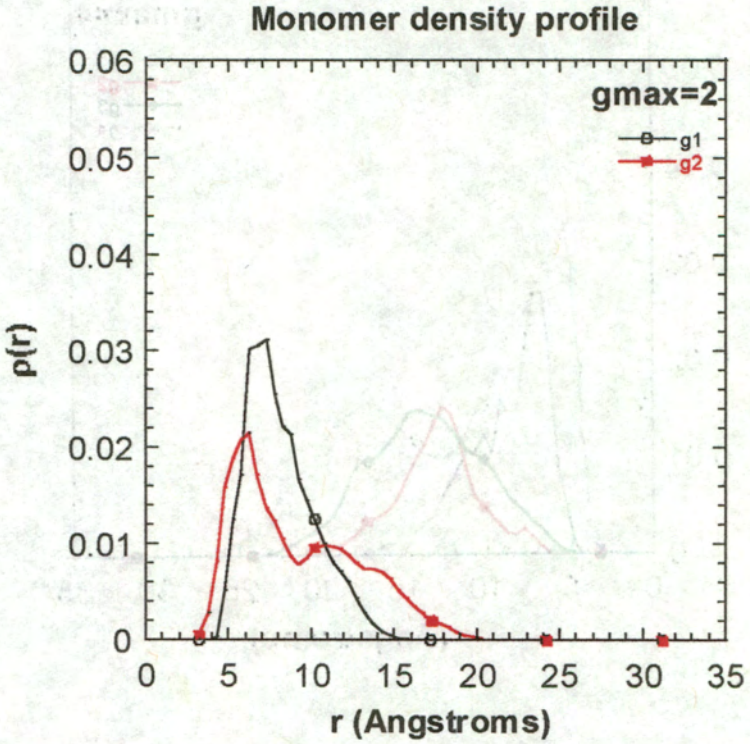

c)

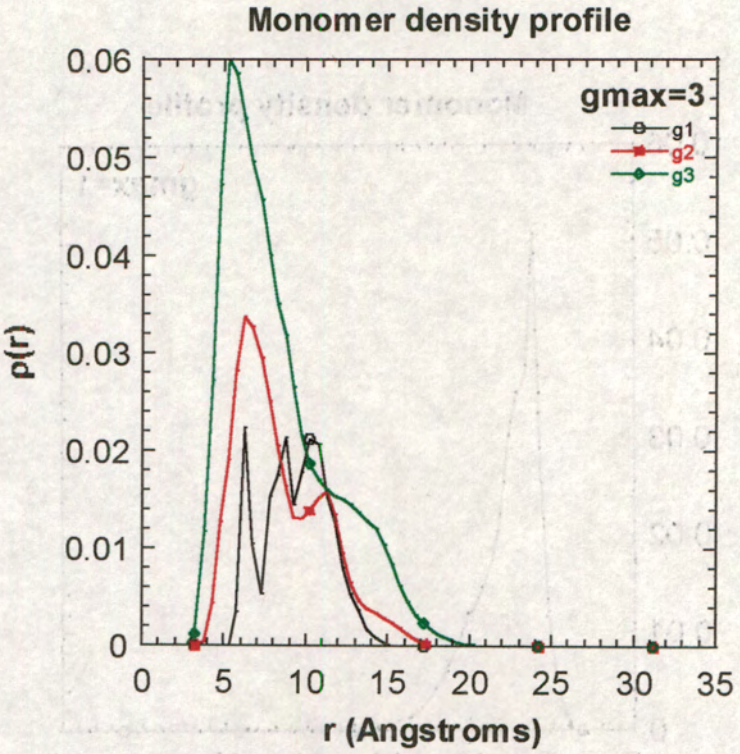
Monomer density profile
gmax=3
g1
g2
g3
p(r)
0.06
0.05
0.04
0.03
0.02
0.01
0
0
5
10
15
20
25
30
35
r (Angstroms)

d)

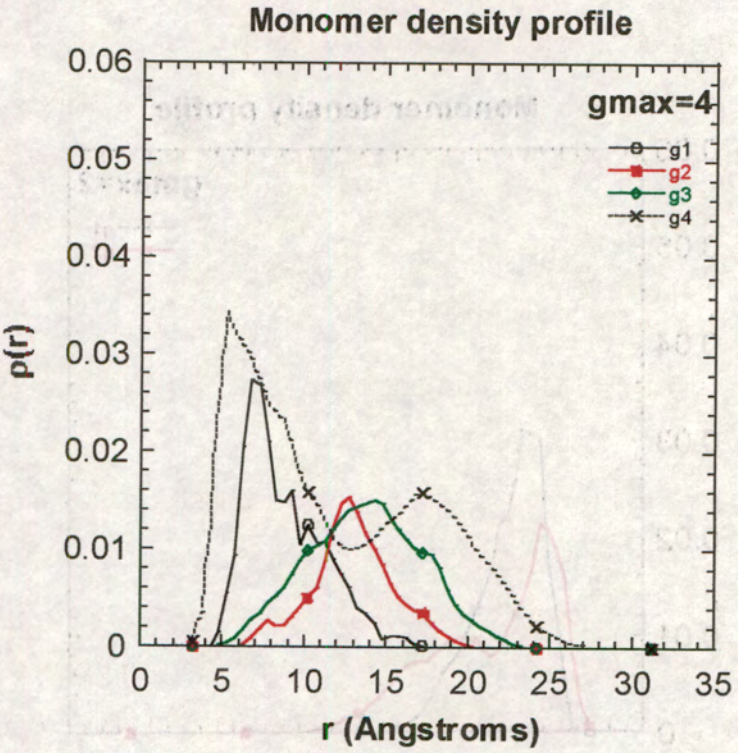
Monomer density profile
gmax=4
g1
g2
g3
g4
p(r)
0.06
0.05
0.04
0.03
0.02
0.01
0
0
5
10
15
20
25
30
35
r (Angstroms)

e)

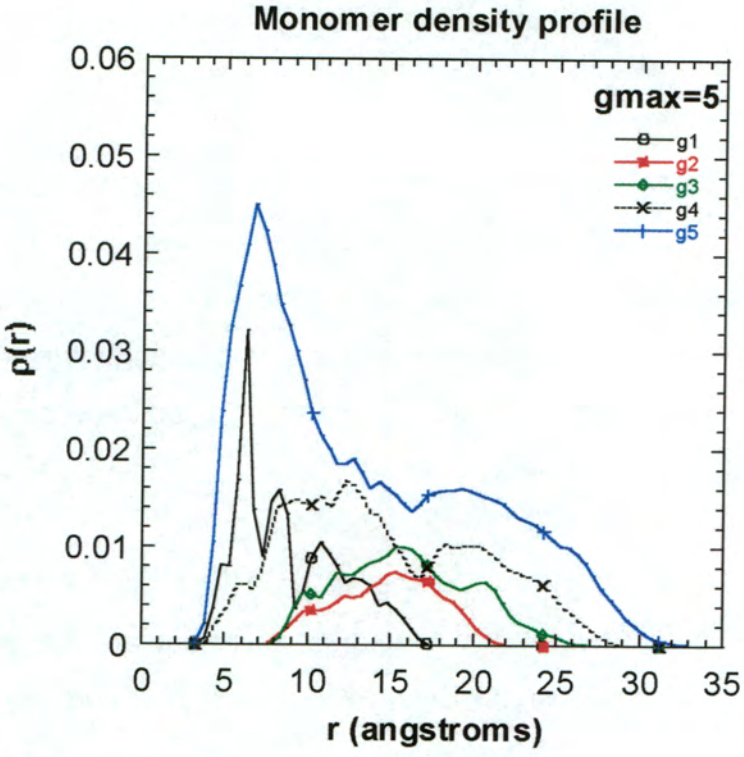


It can be seen from these monomer density profiles (a)-(e), that the peak due to $g$=1 is not localised, and in fact splits into several peaks in the later generations. This is partly a consequence of the monomers for this generation being necessarily selected slightly differently to those of other generations. In the early generation dendrimers ($1 \leq g_{max} \leq 3$ ) there exists significant density due to the second and third generation monomers within the core region. This density extends to a smaller distance from the core than the $g$=1 density, indicating that the monomers of these generations fold back freely into the region of low density.

At $g_{max}$= 4, a marked change occurs. The density peaks due to the monomers of the early generations are shifted to a larger distance from the core according to generation, so that the peak due to the $g$=3 is at a further distance than the peak due to $g$=2. In addition to this, there is no longer any density due to these generations within the core region. This indicates that these monomers have become extended and can no longer fold freely. Only the last generation of monomers are capable of penetrating into the core region of the dendrimer. It is likely that the increased density at the interior as a result of the backward folding of

the chain ends, causes the inner monomers to extend, as has been previously proposed. [6] The picture for $g_{max}$=5 is similar, with the last two generations displaying significant density at the interior, but with only the last generation exhibiting any density within the core region.

In all cases, significant overlap between the peaks due to each generation is observed. Generally, as the generation of the dendrimers increases from $g_{max}$ = 1 to $g_{max}$=5, the peaks and tail zone of each generation shift to a further distance from the core as a result of all generation monomers becoming extended (with the exception of the outer generations). The terminal monomers are found in all regions of the dendrimer, including the core.

This work is qualitatively similar to the previously reported monomer density profiles. The main differences are that the monomers are not as localised for small values of $g_{max}$ as found in the previous study, [6] and that no region of constant density is observed in the density profiles of the generations investigated.

Monomer density profiles for the organochromium system displayed in Figure 4.16(a)-(e), exhibit very similar behaviour to the organic dendrimers for the early generations $1 \leq g_{max} \leq 3$, with the monomers of the early generations free to fold back and penetrate the core region. The profile for $g_{max}$=4 however differs from that for the corresponding organic dendrimer. In the organic molecule, the monomers of $g$=2 and $g$=3 became extended and so the density peaks due to these were localised and shifted away from the core. This behaviour is not observed to the same extent in the organometallic dendrimer, as the peaks due to $g$=2 and $g$=3 are not localised, although they are shifted away from the centre and cannot penetrate the core region. Furthermore, the last generation is not capable of sufficient backfolding to enter the core region either, unlike the organic dendrimer. The diminished density at the interior in comparison with the organic system results in the early generation monomers not being as extended.

**Figure 4.16:** Monomer density profiles of the organochromium dendrimers

a)

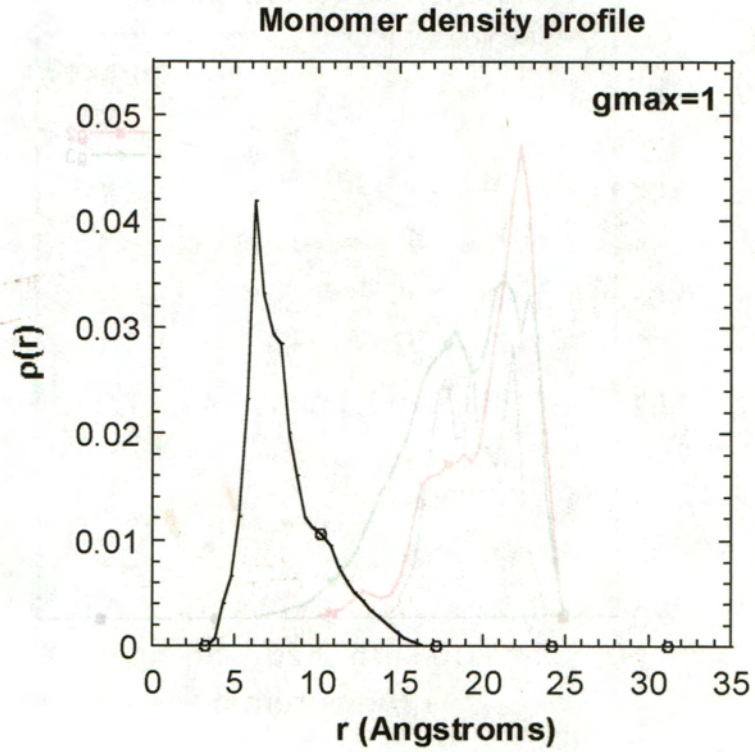


b)

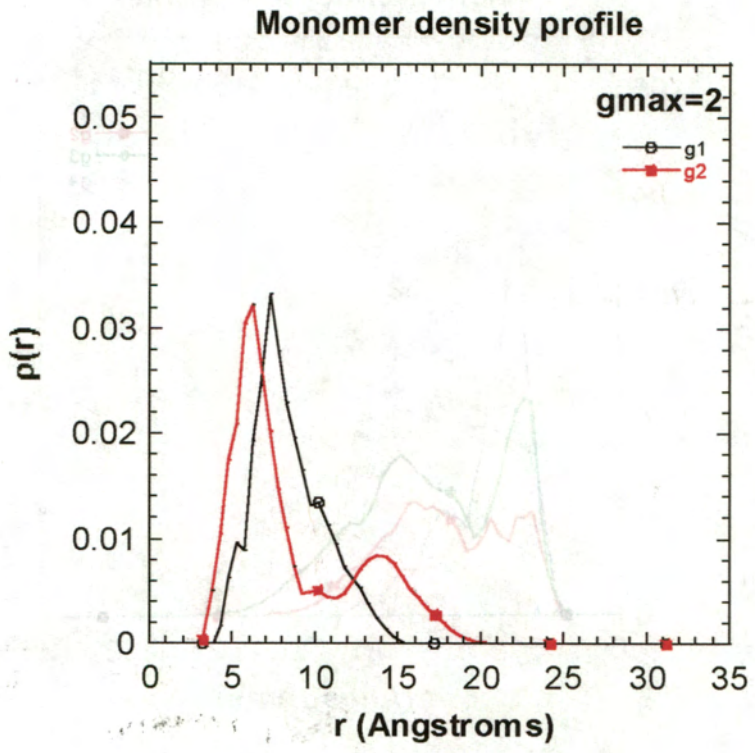

c)

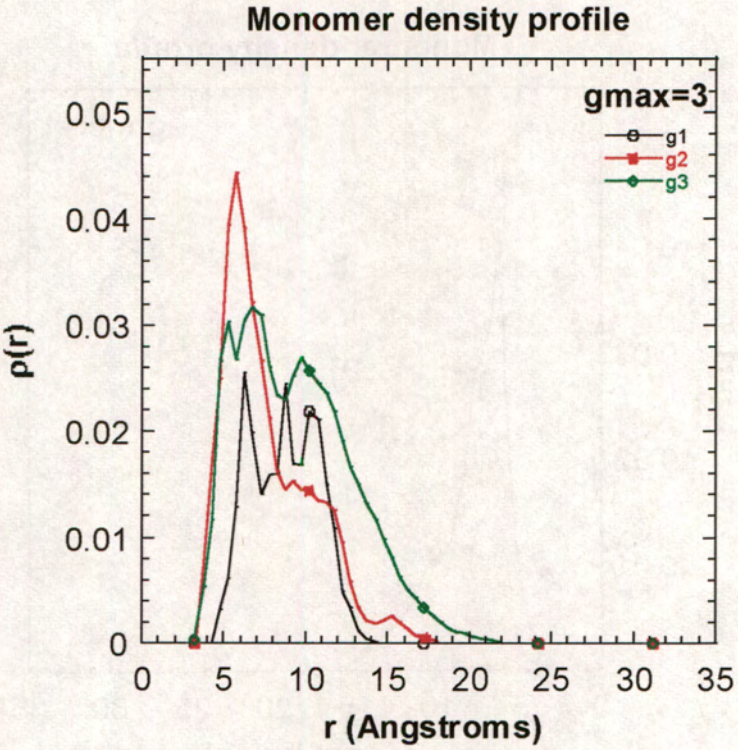
Monomer density profile
gmax=3
g1
g2
g3
ρ(r)
0.05
0.04
0.03
0.02
0.01
0
0
5
10
15
20
25
30
35
r (Angstroms)

d)

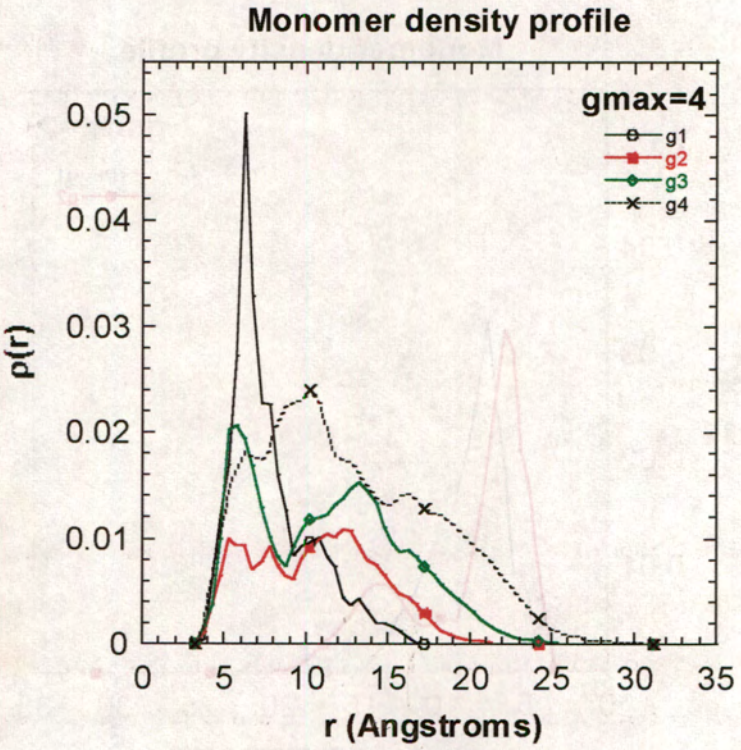
Monomer density profile
gmax=4
g1
g2
g3
g4
ρ(r)
0.05
0.04
0.03
0.02
0.01
0
0
5
10
15
20
25
30
35
r (Angstroms)

e)

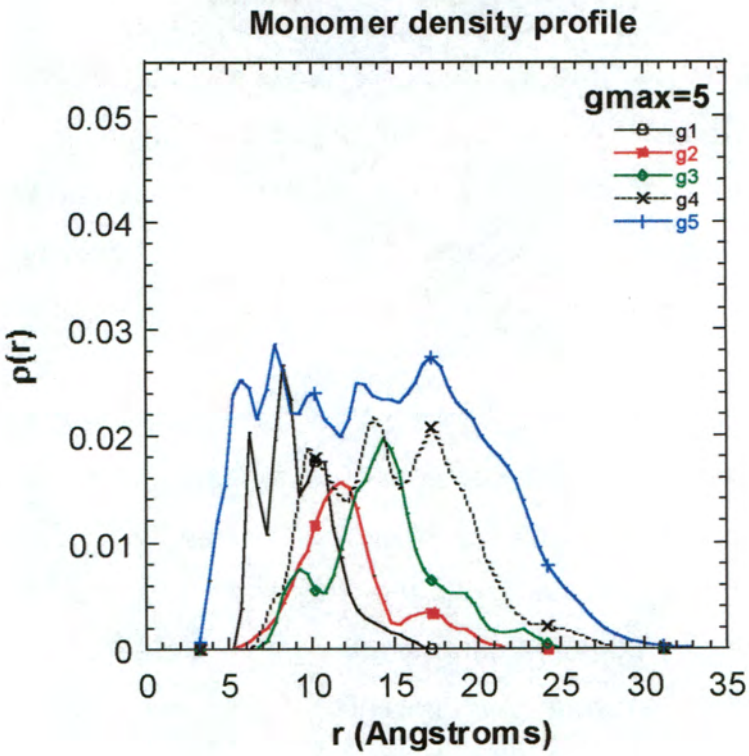


The density profile for the fifth generation dendrimer, shown above, is more similar to the corresponding organic dendrimer. The monomers of the last generation are found in all regions of the dendrimer, including the core, and so the monomers of the early generations become extended. This results in the localisation of the density peaks due to $g$=2 and $g$=3. Once again the fourth generation monomers are capable of backfolding to a large extent, although they are still cannot enter the core region. The profile of $g$=5, which displays a region of almost constant density, is very similar to profiles observed in the previous study, for the higher generation dendrimers $5 \leq g_{max} \leq 8$. [6]

From all of these density profiles, it is clear that the terminal groups are present in the interior of the dendrimer to a significant extent. This indicates that they are mobile and able to penetrate regions of the dendrimer that the other generations cannot. It should be kept in mind however, that although the density due to these monomers may be high near the centre, most of the monomers are still in the outer regions of the molecule (as the number of monomers is obtained by multiplying the density by $4\pi r^3$).

**Solvent accessible surface**

Another measure of the location of the chain ends is available from the solvent accessible surface (SAS) of these groups. This property is calculated by rolling a sphere of radius P (P= effective radius of solvent) around the van der Waals surface of the molecule. [8] If the solvent accessible surface of the outer monomers is measured in this way, an indication of their availability can be obtained. As the SAS of the organometallic moiety was of prime interest in this study, the property was calculated for the tricarbonylchromium group only.

The starting structures for the molecular dynamics simulation were used as reference structures. The open, extended conformation of the dendrimer in this state is taken as having 100% solvent accessible surface. The SAS of these structures were calculated, along with the SAS of the lowest energy configuration of each dendrimer from the dynamics simulation. The SAS of the dendrimer was also calculated as an average over the entire dynamics trajectory. These values are listed in Table 4.1.

**Table 4.1:** The measured values of the solvent accessible surface

| Generation | Initial Configuration | Average Configuration | Lowest energy Configuration | % SAS (Ave/Initial) |
|---|---|---|---|---|
| 1 | 38.39 | 32.68 | 33.21 | 85.13 |
| 2 | 38.39 | 31.85 | 32.00 | 82.96 |
| 3 | 38.42 | 28.52 | 27.61 | 74.23 |
| 4 | 32.45 | 27.38 | 26.21 | 84.37 |
| 5 | 31.84 | 25.85 | 25.35 | 81.19 |

From the table it is clear that the SAS decreases with generation number, although all generations possess a significant SAS (> 70%), which means that the terminal groups are mostly present at the surface of the molecule or in a solvent accessible area.

It is also clear that the third generation dendrimer has the lowest percentage of SAS. This finding can be correlated to the monomer density profile of $g_{max}$=3, where the g=3 monomers are folded back into the core region to a substantial degree. The fourth generation organochromium dendrimer would thus be the best

choice for catalysis, as it contains a relatively large number of chain ends, which do not penetrate too deeply into the interior of the dendrimer and in addition display good solvent accessibility.

## 4.5 Conclusions

The objectives of this computational study of dendritic macromolecules have been successfully achieved. Molecular dynamics simulations were performed on the organic dendrimers of generations one through five, as well as the corresponding organochromium dendrimers. Several properties of these molecules were examined. The radius of gyration and RMS variation of the two dendrimer series were investigated as a function of generation. It was found that the radius of gyration increases exponentially with generation, however the relationship of RMS variation to generation is not as clear-cut. Some evidence for a transition to a globular state was observed in the RMS variation behaviour.

The density distributions of all five generations were calculated for both dendritic systems, and the results agree well with the coarse-grained simulation studies. [3-6] Interestingly, an induction distance was noted in the density distribution profiles of all generation numbers, this phenomenon was not observed in the previous studies. [3-6]

An analysis of how the monomers of each generation are distributed within the dendrimer, was undertaken. The results are in general agreement with previous work, [3] but are far more applicable to the specific system under investigation, as atomic details were taken into consideration in this study. For the first few generations $1 \leq g_{max} \leq 3$ the monomers belonging to the early generations $g$ seem capable of significant backfolding. This behaviour decreases as the generation number $g_{max}$ increases and the interior monomers become more extended. At $g_{max}=4$ and 5, significant density due the outer monomers is found in all regions of the dendrimer, including the core region. This indicates that the chain ends are mobile and are capable of burying deep within the molecule. This backfolding

occurs to such an extent in the fifth generation organochromium dendrimer, that a region of almost constant density is found at the interior.

The results of the monomer density profile study, were compared to those of the solvent accessible surface (SAS) calculation. It was found that the SAS of the organometallic moiety decreases with generation, as more steric crowding and backfolding occurs. In particular, the third generation dendrimer has a low percentage of SAS due to the flexibility of the terminal monomers in this molecule.

It can be concluded for every generation of dendrimer studied, that although the terminal groups are found to some extent in all regions of the dendrimer, the majority of these monomers are still located at the periphery of the molecule, or alternatively in a solvent accessible area. Therefore, it would appear that even though the study was carried out in a poor solvent, the surface groups of the dendrimers are fairly accessible. If however, catalytic reactions were to be performed with these dendrimers in a better solvent, it is likely that the reactivity of the system would be enhanced.

If it is not possible to synthesise the organochromium dendrimers, or they are found to be poor catalysts, the methodology has been well developed in this study, to investigate any other potential catalysts based on poly(benzyl phenyl ether) dendrimers. In particular, dendritic arene complexes of other metals could be easily studied.

### 4.6 References


1. P.G. de Gennes and H. Hervet, *J. Physique Lettres*, 1983, **44**, L351-L360
2. R.L. Lescanec and M. Muthukumar, *Macromolecules*, 1990, **23**, 2280-2288
3. W. Carl, *J. Chem. Soc., Faraday Trans.*, 1996, **92**(21), 4151-4154
4. M.L. Mansfield and L.I. Klushin, *J. Phys. Chem.*, 1992, **96**, 3994-3998
5. M.L. Mansfield and L.I. Klushin, *Macromolecules*, 1993, **26**, 4262-4268
6. M. Murat and G.S. Grest, *Macromolecules*, 1996, **29**, 1278-1285

7. T.H. Mourey, S.R. Turner, M. Rubenstein, J.M.J. Fréchet, C.J. Hawker and K.L. Wooley, *Macromolecules*, 1992, **25**, 2401-2406
8. D.A. Tomalia, A.M. Naylor and W.A. Goddard III, *Angew. Chem. Int. Ed. Engl.*, 1990, **29**, 138-175
9. M.L. Mansfield, *Polymer*, 1994, **35**(9), 1827-1830
10. A.M. Naylor and W.A. Goddard III, *Polym. Prepr.*, 1988, **29**(1), 215-216
11. C.J. Hawker, K.L. Wooley and J.M.J. Frechet, *J.Am. Chem. Soc.*, 1993, **115**, 4375-4376
12. M.F. Ottaviani, S. Bossmann, N.J. Turro and D.A. Tomalia, *J. Am. Chem. Soc.*, 1994, **116**, 661-671
13. C. Devadoss, P. Bharathi and J.S. Moore, *Angew. Chem. Int. Ed. Engl.*, 1997, **36**(15), 1633-1635
14. A.M. Naylor and W.A. Goddard III, G.E. Keifer and D.A. Tomalia, *J. Am. Chem. Soc.*, 1989, **111**, 2339-2341
15. P. Miklis, T. Çağin and W.A. Goddard III, *J. Am. Chem. Soc.*, 1997, **119**, 7458-7462
16. K.L. Wooley, C.A. Klug, K. Tasaki and J. Schaefer, *J. Am. Chem. Soc.*, 1997, **119**, 53-58
17. C.J. Hawker and J.M.J. Fréchet, *J. Am. Chem. Soc.*, 1990, **112**, 7638-7647
18. B.R. Brooks, R.E. Bruccoleri, B.D. Olafson, D.J. States, S. Swaminathan and M. Karplus, *J. Comput. Chem.*, 1983, **4**, 187-217

# Chapter 5 Conclusions and Future work

In this work, organic and organochromium poly(benzyl phenyl ether) dendrimers were investigated by synthetic and computational methods.

The synthetic effort was focused on the preparation of a first generation chromium complexed dendritic wedge, with which it should be possible to build up the complete dendrimer. As starting materials, the first generation organic dendrimer and the first generation benzylic alcohol and bromide wedges were synthesised. Several chromium arene complexes were prepared by different routes, and the halogenation methodology was thoroughly investigated with various reagents.

The synthesis of the first generation chromium complexed wedge was then thoroughly explored by a number of routes. Although it was not possible to prepare this compound by any of the methods investigated, some new and interesting chemistry was discovered. In particular, a previously unreported complex, (dibenzyl ether)bis[tricarbonylchromium(0)] was prepared by two routes. The novel compound was fully characterised and the crystal structure was determined. This crystal structure, and the structure of a second compound (benzyl methyl ether)tricarbonylchromium(0) were used to parameterise the dendrimer force field. Further interesting chemistry was observed with alternative coupling reactions, resulting in the preparation of two complexes: (bibenzyl)tricarbonylchromium(0) and (toluene)tricarbonylchromium(0).

In order to perform the molecular mechanics and molecular dynamics calculations, a dendrimer force field was constructed. The existing CHARMm polymer force field was extended to include parameters for the tricarbonylchromium moiety. The accuracy of the new parameters was assessed by simulation of the crystal structure of (dibenzyl ether)bis[tricarbonylchromium(0)]. Furthermore, the important ether linkage torsion angle parameter, which plays a large role in the topology of the dendrimer, was singled out for refinement. This torsion angle was

parameterised using the model compound benzyl phenyl ether, by fitting the CHARMm results for rotation about the dihedral, to *ab initio* rotational data.

Molecular dynamics simulations were performed on the organic dendrimers of generations one through five, as well as the corresponding organochromium dendrimers. Several properties of interest were successfully examined, and the potential application of these dendrimers as catalyst supports was discussed.

The radius of gyration and RMS variation of the two dendrimer series were investigated as a function of generation. The radius of gyration was found to increase exponentially with generation, however the relationship of the RMS variation to generation is not as clear-cut. Some evidence for a transition to a globular state was observed in the RMS behaviour.

Density distributions were calculated for all five generations of both dendritic systems, and the results were consistent with previous coarse-grained simulation studies. An analysis of the distribution of monomers from each generation within the dendrimer, was performed. The monomers of the smaller dendrimers seem to be capable of significant backfolding. In the fourth and fifth generation dendrimers, monomers associated with the earlier generations are fairly extended, while the terminal groups are mobile and found in all regions of the dendrimer, including the core.

Solvent accessible surface studies showed that a large percentage of the organometallic species are in solvent accessible areas, and thus available for catalysis. The third generation organometallic dendrimer exhibited the lowest percentage of solvent accessible surface and was thus identified as a relatively poor choice as a polymer supported catalyst.

It was concluded for every generation of dendrimer studied, that although the terminal groups are found to some extent in all regions of the dendrimer, the majority of these monomers are still located at the periphery of the molecule, or alternatively in a solvent accessible area. Consequently, it would appear that

these dendrimers would be good catalysts. Furthermore, the availability of these groups could be enhanced by the use of a better solvent.

The computational methodology developed in this work, can be extended to include any other organometallic dendrimer based on the poly(benzyl phenyl ether) dendritic system. In particular, dendritic arene complexes of other metals could be easily investigated. Further simulation studies of these dendrimers could include the effects of solvent on the physical properties of the macromolecules.

# APPENDIX 1

| Bond Parameters: $E_b = k_b (r - r_0)^2$ | | |
|---|---|---|
| **Bond** | $k_b$ **(kcal.mol$^{-1}$Å$^{-2}$)** | $r_0$ **(Å)** |
| CA - OE | 334.300 | 1.411 |
| CT2 – OE | 340.000 | 1.4300 |
| CT3 – OE | 390.000 | 1.407 |
| CA – DUM | 305.000 | 1.4130 |
| CA1 – DUM | 305.000 | 1.4110 |
| CA – CA | 305.000 | 1.3750 |
| CA - CA1 | 305.000 | 1.3750 |
| CA – CT | 345.000 | 1.500 |
| CT - CT3 | 268.000 | 1.522 |
| CT2 – CA | 230.000 | 1.4900 |
| CT2 - CA1 | 230.000 | 1.4900 |
| CT3 - CT2 | 222.500 | 1.5280 |
| HA – CA | 340.000 | 1.0830 |
| HA - CT2 | 309.000 | 1.1110 |
| HA - CT3 | 322.000 | 1.1110 |
| HP – CA | 340.000 | 1.0800 |
| HP - CA1 | 340.000 | 1.0800 |
| MCR – CM | 300.000 | 1.8400 |
| MCR – DUM | 210.000 | 1.728 |
| OH1 – CA | 334.300 | 1.4110 |
| OH1 - CT2 | 428.000 | 1.4200 |
| OH1 - H | 545.000 | 0.9600 |
| OM - CM | 1115.00 | 1.138 |

| Angle Parameters: $E_\theta = k_\theta (\theta - \theta_0)^2$ | | | | |
|---|---|---|---|---|
| **Angle** | $k_\theta$ **(kcal.mol$^{-1}$radian$^{-2}$)** | $\theta_0$ **(degrees)** | **Urey-Bradley** $k_\theta$ **(kcal.mol$^{-1}$radian$^{-2}$)** | **Urey-Bradley** $\theta_0$ **(degrees)** |
| CT2 - OE - CA | 40.000 | 109.60 | 30.00 | 2.26510 |
| CT3 - OE - CT2 | 58.0 | 112.4 | | |
| CT2 - OE - CT2 | 58.0 | 112.4 | | |
| CA - DUM - CA | 40.000 | 120.00 | 35.00 | 2.41620 |
| CA1 - DUM - CA | 40.000 | 60.00 | 35.00 | 2.41620 |
| CA1 – DUM - CA1 | 40.000 | 120.00 | 35.00 | 2.41620 |
| CA - CA - CA | 40.000 | 120.00 | 35.00 | 2.41620 |
| CA1 - CA - CA1 | 40.000 | 120.00 | 35.00 | 2.41620 |
| CA - CA1 - CA | 40.000 | 120.00 | 35.00 | 2.41620 |
| CA - CT2 - CA | 70.000 | 109.47 | | |
| CA - CT2 - OE | 80.00 | 109.47 | | |
| CA1 - CT2 - OE | 80.00 | 109.47 | | |
| CA - CA - CT | 70.0 | 122.0 | | |
| CA - CT - CA | 70.0 | 109.47 | | |
| CA - CT - CT3 | 70.0 | 111.6 | | |
| HA - CT3 - CT | 37.5 | 110.70 | | |
| CA – DUM - MCR | 50.000 | 90.0000 | | |
| CA1 – DUM - MCR | 50.000 | 89.4300 | | |
| CM - MCR - CM | 5.0 | 90.00 | | |
| CM – MCR - DUM | 5.0 | 126.25 | | |
| CT2 - CA - CA | 45.800 | 122.3000 | | |
| CT2 - CA1 - CA | 45.800 | 122.3000 | | |

| Continued: Angle Parameters: $E_\theta = k_\theta (\theta - \theta_0)^2$ | | | | |
|---|---|---|---|---|
| **Angle** | **$k_\theta$ (kcal.mol$^{-1}$radian$^{-2}$)** | **$\theta_0$ (degrees)** | **Urey-Bradley $k_\theta$ (kcal.mol$^{-1}$radian$^{-2}$)** | **Urey-Bradley $\theta_0$ (degrees)** |
| CT3 - CT2 - OE | 57.0 | 110.0 | | |
| H – OH1 - CA | 65.000 | 108.0000 | | |
| H – OH1 - CT2 | 57.500 | 106.0000 | | |
| HA - CA - CA | 29.000 | 120.00 | 25.00 | 2.15250 |
| HA - CT2 - CA | 49.300 | 107.5000 | | |
| HA - CT2 - CA1 | 49.300 | 107.5000 | | |
| HA - CT2 - CT3 | 34.600 | 110.10 | 22.53 | 2.17900 |
| HA - CT2 - OE | 55.50 | 109.4700 | | |
| HA - CT3 - OE | 55.50 | 109.4700 | | |
| HA - CT2 - HA | 35.500 | 109.00 | 5.40 | 1.80200 |
| HA - CT3 - CT2 | 34.600 | 110.10 | 22.53 | 2.17900 |
| HA - CT3 - HA | 35.500 | 108.40 | 5.40 | 1.80200 |
| HP - CA - CA | 30.000 | 120.00 | 22.00 | 2.15250 |
| HP - CA - CA1 | 30.000 | 120.00 | 22.00 | 2.15250 |
| HP - CA1 - CA | 30.000 | 120.00 | 22.00 | 2.15250 |
| MCR - CM - OM | 25.0 | 179.0 | | |
| OH1 - CA - CA | 45.200 | 120.0000 | | |
| OE - CA - CA | 45.200 | 120.0000 | | |
| OH1 - CT2 - CA | 75.700 | 110.1000 | | |
| OH1 - CT2 - HA | 45.900 | 108.8900 | | |

| Improper Torsion Parameters: $E_\omega = k_\omega (\omega - \omega_0)^2$ | | | |
|---|---|---|---|
| **Improper Torsion** | **$k_\omega$ (kcal.mol$^{-1}$radian$^2$)** | **Periodicity** | **Phase(degrees)** |
| DUM - X - X - CA | 15.0 | 0 | 0.0 |
| DUM - X - X - CA1 | 15.0 | 0 | 0.0 |
| OE - X - X - CA | 150.0000 | 0 | 0.0 |

| Nonbonded Parameters | | | | | | |
|---|---|---|---|---|---|---|
| **Atom** | **Polarizability** | **e** | **van der Waals Radius** | **1-4 Polarizability** | **e** | **van der Waals radius** |
| MCR | 0.01 | -0.020 | 1.465 | | | |
| OE | 0.00 | -0.1591 | 1.6 | | | |
| CA | 0.000000 | -0.070000 | 1.992400 | | | |
| CA1 | 0.000000 | -0.070000 | 1.992400 | | | |
| CM | 1.650000 | -0.0262 | 2. | | | |
| CT2 | 0.000000 | -0.055000 | 2.175000 | 0.000000 | -0.010000 | 1.900000 |
| CT3 | 0.000000 | -0.080000 | 2.060000 | 0.000000 | -0.010000 | 1.900000 |
| H | 0.000000 | -0.046000 | 0.224500 | | | |
| HA | 0.000000 | -0.022000 | 1.320000 | | | |
| HP | 0.000000 | -0.030000 | 1.358200 | 0.000000 | -0.030000 | 1.358200 |
| OH1 | 0.000000 | -0.152100 | 1.770000 | | | |
| OM | 0.84000 | -0.1591 | 1.540 | | | |
| DUM | 0.000000 | -0.000000 | 0.000000 | | | |

| Hydrogen Bond Parameters | | |
|---|---|---|
| **Donor-Acceptor** | $E_{min}$ | $R_{min}$ |
| H* - O* | -0.00 | 2.0 |
| OH* - O* | 0.000 | 2.7500 |

| Dihedral Parameters: $E_\phi = \|k_\phi\| - k_\phi \cos(n\phi)$ | | | |
|---|---|---|---|
| **Dihedral** | $k_\phi$ **(kcal.mol$^{-1}$radian$^{-2}$)** | **Periodicity** | **Phase(degrees)** |
| X - CT2 - OE - X | 0.2700 | 3 | 0.0 |
| CA - CT2 - OE - CA | 0.1500 | 3 | 0.0 |
| X - CT3 - OE - X | 0.2700 | 3 | 0.0 |
| X - CA - CA - X | 3.1 | 2 | 180.0 |
| X - CA - OE - X | 0.2700 | 2 | 0.0 |
| X - CT - CA - X | 0.01 | 6 | 0.0 |
| X - CT - CT3 - X | 0.15 | 3 | 0.0 |
| CA - CA - CA - CA | 3.1000 | 2 | 180.00 |
| CA - CA1 - CA - CA1 | 3.1000 | 2 | 180.00 |
| CA - DUM - MCR - CM | 0.0 | 6 | 180.00 |
| CA1 - DUM - MCR - CM | 0.0 | 6 | 180.00 |
| CT2 - CA - CA - CA | 3.1000 | 2 | 180.00 |
| CT2 - CA1 - CA - CA1 | 3.1000 | 2 | 180.00 |
| CT3 - CT2 - CA - CA | 0.2300 | 2 | 180.00 |
| OE - CT2 - CA - CA | 0.2300 | 2 | 180.00 |
| OE - CT2 - CA1 - CA | 0.2300 | 2 | 180.00 |
| H - OH1 - CA - CA | 0.9900 | 2 | 180.00 |
| HA - CA - CA - CA | 3.5000 | 2 | 180.00 |
| HA - CA - CA - HA | 2.5000 | 2 | 180.00 |
| HA - CT3 - CT2 - CA | 0.0400 | 3 | 0.00 |
| HP - CA - CA - CA | 4.2000 | 2 | 180.00 |
| HP - CA - CA1 - CA | 4.2000 | 2 | 180.00 |
| HP - CA1 - CA - CA1 | 4.2000 | 2 | 180.00 |
| HP - CA - CA - CT2 | 4.2000 | 2 | 180.00 |
| HP - CA - CA1 - CT2 | 4.2000 | 2 | 180.00 |
| HP - CA - CA - HP | 2.4000 | 2 | 180.00 |
| HP - CA1 - CA - HP | 2.4000 | 2 | 180.00 |
| OH1 - CA - CA - CA | 3.1000 | 2 | 180.00 |
| OH1 - CA - CA - HP | 4.2000 | 2 | 180.00 |
| X - CT2 - CA - X | 0.0000 | 6 | 0.00 |
| X - CT2 - CA1 - X | 0.0000 | 6 | 0.00 |
| X - CT2 - OH1 - X | 0.1400 | 3 | 0.00 |
| X - CT3 - CA - X | 0.0000 | 6 | 0.00 |
| X - MCR - CM - X | 0.0500 | 4 | 0.00 |